Escola de Camins
Escola Tècnica Superior d'Enginyeria de Camins, Canals i Ports
UPC BARCELONATECH

TREBALL FINAL DE GRAU

# Development of self-heating concrete for urban furniture by means of electrically conductive concrete

Project made by:
**Joan Mas Soldevilla**

Directed by:
**Antonio Aguado De Cea**
**Ignacio Segura Pérez**
**Gerard Faneca Llesera**

Bachelor in:
**Civil Engineering**

Barcelona, 10th of June 2019

Civil and Environmental Engineering Department

# ABSTRACT

In recent years, conductive cementitious materials have gained immense attention as they are seen as an alternative for achieving multifunctional materials. This research is focused on the analysis, characterization and modelling of a self-heating conductive concrete.

This project has been developed as part of a series of experimental studies aiming at developing self-heating and de-icing urban furniture concrete elements, suitable for industrial production. It is based on an experimental point of view of the heating caused by the flow of electric current through a cement paste containing carbonaceous materials carbon fibre and graphite flakes, which reduce the electrical resistance of the resulting composite.

The usual approach used in previous studies has been to incorporate carbonaceous nanomaterials and/or virgin carbon fibers into cementitious matrices. However, this paper presents a research devoted to the development of electrically conductive cementitious materials using recycled carbon fibers (rCFs) to add value to the material, meeting with sustainable standards and the zero-waste philosophy.

After a wide literature study and taking the results of previous researches in this topic, an ultra-high-performance concrete (UHPC) conductive concrete with different carbon fibre additions was manufactured. Different samples were produced and submitted to several electrical behaviour and thermal behaviour test series.

The main interest was devoted to the study of the thermal behaviour. For this reason, the samples were submitted to different test scenarios changing the heating cycles, the voltage applied, the moisture content, the electrodes disposal and the geometry and dosage of the samples.

Straightaway, the tests' results were analysed and compared to previous observations. After the analysis and the characterization of the material, the data collected was post-processed and, the behaviour of the material for heating and cooling cycles and the correlation between different magnitudes were modelled using different programs, such as Matlab, Rstudio and Excel.

High conductivities up to 2 S/m were reached with high frequencies, for additions of conductive carbonaceous materials just below the percolation threshold, i.e. without having a fully connected path of fibres throughout the sample. Furthermore, the correlation between conductivity and frequency was modelled a logarithmic law.

Significant temperature variations were achieved, developing temperatures that reaches up to 60°C. From the two different carbonaceous materials used as conductive additions, the recycled chopped carbon fibre was the best, both for electrical and thermal behaviour. Moreover, only with 0.4-0.5% vol. just below the percolation threshold mixed with a UHPC was able to develop very significant temperature variations up to 25°C in cycles of 8 hours for relatively low voltages, confirming the possibility of using this material for self-heating systems embedded to buildings or de-icing systems for outdoor urban furniture and concrete pavements, for cold environments.

In some experiences the room temperature was increased by 4°C and for some sample average heating rate for the left end of 0.172°C/min were developed, increasing 1°C every 5.8 min.

# ACKNOWLEDGEMENTS

First and foremost, special appreciation to my tutors Ignacio Segura Perez, Antonio Aguado de Cea and Gerard Faneca Llesera for their support, their direction and their knowledge, which have helped me enormously throughout this project. Furthermore, I think that all I learned from them will help me in my future and in the professional world.

I would like to express my gratitude to Gerard Faneca and the company Escofet 1886 S.A. who have provided me all the test results and information collected during the last year, making my research project possible.

I would like to thank Enric Pericas for putting me in touch with Gerard, introducing me to such an amazing opportunity and mentoring me for the last few years.

Finally, I would like to express also very special appreciation to my family and my partner for the unconditional support, especially, in such a hard year for the family. They are capable of doing anything for me and never letting me down, putting all their trust in me.

# INDEX

# INDEX OF FIGURES

# INDEX OF TABLES

# INDEX OF EQUATIONS

# 1. INTRODUCTION

## 1.1. INTRODUCTION AND MOTIVATION

Nowadays, we are living in the era of the constant technological innovation. Each day, new technologies and engineering innovations appear to make our life easier and create a response to problem that has never been considered before. But, when it comes to the need of human beings of dealing with climate effects and adversities, there is still a long way to go.

In many areas of north America, Nordic countries and Russia, the snow and ice that covers these places for long periods entails a daily challenge for citizens in terms of mobility, security, and comfort; for companies, which loose big quantities of money if transportation trucks do not reach their destination, if workers can not arrive at their job place, etc.; and for administrations, which spend a lot of money in removal techniques, in replacing damaged facilities, etc.


*Figure 1.1 Newark Liberty International Airport is the airport with more weather-delayed flights in the US and mainly due to snow (www.cnbc.com)*

For example, in the United States of America, the Bureau of Transportation Statistics/U.S. Department of Transportation estimates that more than one third of the flight delays in all the US airports, adding from September 2016 to August 2017 a total amount of 22 million minutes. Besides, the list of the most weather-delays major airports, shows that form the five more affected airports, four of them stem their weather-delays from snow storms (see Figure 1.1.). But, aside from an inconvenience, it represents a huge economical toll [1].

Therefore, at the moment, there is an important demand of smart materials and structure, capable of controlling their temperature, developing a heating system, self-sensing the loads and deformations on structures, etc. For this reason, the research of

cementitious materials used for civil and building construction is no longer focused on the study of the mechanical properties and durability for the structural function. But, on the development of new properties in these materials that can generate non-structural functionalities that can complement the main structural function. In this manner, a conventional cementitious material becomes a multifunctional conductive cementitious material.

Multifunctionality consists of taking advantage of the structural material itself to develop non-structural functionalities, without the need of any type of external device. Multifunctionality is achieved by combining a cementitious material with different additions that provide the resulting material a new range of applications [2 – 21], keeping or even improving its structural characteristics [22 – 36]. Thus, cost is reduced, design is simplified, durability is enhanced increasing the surface volume and the decrease of the mechanical properties due to the use of embedded devices is minimized. Functional properties include: anode for electrochemical chloride extraction [15, 16, 37-39], electromagnetic wave shielding [13,40], strain/stress sensor self-sensor [19, 20, 41], dynamic monitoring and damage detection, electrical and thermal conductivity enhancer, temperature sensor, heating and thermal control [4-7, 11-14, 21, 32-36, 42-45], among others.

This research is focused on one of these properties. A study from the experimental point of view of the heating caused by the flow of electric current through a cement paste containing carbonaceous materials carbon fibre and graphite flakes, which reduce the electrical resistance of the resulting composite. This study may serve as a base for the many applications that a cementitious material capable of increasing its temperature in a controlled manner would have such as evaporating the rainwater of a sports court, heating a room through walls and/or floor or melting ice of a road or a runway of an airport, without the use of salt.

The electrically conductive cementitious materials are one of the main categories within multifunctional cementitious materials. The increase in conductivity, or reduction of the electrical resistivity, of these materials is accomplished by adding conductive materials to the cement paste. The greater the fractional volume of conductive additive the greater the conductivity of the resulting material. Carbonaceous materials have a high thermal conductivity, although not as high as metals, a low coefficient of thermal expansion, lower than metals, and are highly resistant to corrosion. All this makes these materials good candidates for thermal applications in multifunctional cementitious composites such as heating of buildings or pavement de-icing, among others.

*Figure 1.2 Steel bridge highly damaged due to the use of salts to remove ice from the road (blogs.ei.columbia.edu)*

Thus, with the application as ice controller on different transportation infrastructures, such as highways, interchanges, bridges, airport runways, the safety for the drivers would be increased, while not compromising the durability of the structures with the use of substances that can damage it (see Figure 1.2.).

The technique of snow removal by mechanical ways is the most used but it is an intensive, costly and time-consuming labour [46]. Furthermore, not all the snow is completely cleaned from the driveway by the snowploughs, leaving a small layer to be eliminated (see Figure 1.3.). Many of the methods currently used to remove ice from roads are based on the use of chemicals [47]. Most of them are harmful to both reinforced concrete and steel structures, e.g. viaducts, tunnels, airport runways, and for the environment.

*Figure 1.3 A fleet of snowploughs operating in Utah during a snowstorm (www.government-fleet.com)*

Compared to these methods discussed, there is the possibility of using heating systems of conductive concrete layers. Several researchers have analysed the feasibility of using conductive multifunctional concrete, with different additions, for pavement de-icing. Since the late 90s, steel fibres, steel shavings, carbon fibres, and graphite products have been added into concrete as conductive materials to greatly improve the electrical

conductivity. Some drawbacks about using steel shavings in the mixtures were noticed, and thus carbon products were used to replace the steel shavings in the conductive concrete mixture design.

With the purpose of studying the thermal function, this research is focused on the heating effect produced by the electric current passing through a cement that has been added with various carbonaceous materials such as recycled carbon fibres and graphite flakes, all with high electrical conductivities and capable of reducing the electrical resistance of the resulting cementitious material.

But the usage of carbon fibres entails a problem of availability and economic costs. Consequently, in this research project recycled carbon fibres have been used, which makes it not only more affordable, but also more sustainable and environmentally friendly, adding to it an extra value. In this manner is born the possibility of turning a concrete with additions from industrial residues into a material adequate to the concept of a smart city.

This new concept city is spreading among society. The concept of a smart city where infrastructures, buildings, new technologies, sustainability and people converges, leading to a sustainable economic development and a more efficient management of the natural resources. In this scenario, infrastructures are provided with advanced technological solutions. Along these lines, combining structural and lining materials with additional functional properties is an advance towards the aim of achieving multifunctional materials that can fulfil diverse requirements, apart from the strictly structural one.

Considering the aforementioned ideas and thanks to the cooperation between the Civil and Environmental Engineering Department of the UPC and the company Escofet 1886 S.A., arises the wish of elaborating a project focused on the characterization, analysis and modelling of heating urban furniture and pavements from electrically conductive concrete, based on an experimental study.

## 1.2. OBJECTIVES

This project is embraced in a series of experimental studies performed by the Escofet 1886 S.A. company together with the Civil and Environmental Engineering Department of the UPC, with the final goal of developing self-heating and thermal control urban furniture concrete elements.

The main objective of this research project consists in analysing, characterising and modelling an electrically and thermal conductive concrete using recycled carbon fibres, comparing its behaviour with previous models and analysing its applications with.

The main focus of the research lies in the heating and thermal control function, for which there is already a specific demand in northern countries' market. Once this material is developed, the work consists in designing structural elements, pavements and urban furniture with it.

In order to achieve this main objective, different smaller and more specific goals are set:

- Review the historical evolution of conductive concrete, understanding how it has been studied in previous researches and which functionalities has been developed.

- Characterise the recycled carbon fibres, studying the obtaining of the material its properties and compering its characteristics with a normal fibre carbon.

- Featuring the manufacture of samples of recycled carbon fibre reinforced concrete performed by Escofet 1886 S.A. together with the Civil and Environmental Engineering Department of the, taking into account advices and previous knowledge from the analysis of precedent researches.

- Presenting and analysing the results from the tests developed during the experimental campaign and extracting conclusions on the development of the heating function, the performance of the recycled carbon fibres, the electrical conductivity reliability, and obtaining an optimal dosage of the components of the material for its industrialization.

- Understand and make a critical assessment of the obtained results, comparing them with previous researches.

- Contributing with these conclusions to further researches and projects.

## 1.3. METHODOLOGY

This research has been conducted by the Civil and Environmental Engineering Department of the UPC from the ETSECCPB in cooperation with the company Escofet 1886 S.A. dedicated to the design, development and manufacturing of pavements,

architectonic façades and urban furniture, using concrete as the principal production component.

The preparation of the models, manufacturing of samples and fresh state tests were carried out at the industrial unit of the company in Martorell. The electrical characterisation was carried in the Laboratorio de Instrumentación y Bioingeniería of the UPC.Whereas, the thermal characterisation tests were performed in the company's headquarters, in Martorell.

Initially, it was considered to achieve the conductivity of the concrete by the addition of conductive fibres, verifying at the same time the most convenient matrix type. It was convenient to characterise it by means of tests, aiming at understanding its behaviour facing the different functionalities that it was supposed to carry out.

Previously, a literature study was conducted in order to have a better understanding of the conductive cementitious materials and the heating and temperature control functionalities. All this information is organized in the chapter 2, where a historical review of the conductive concrete is presented, together with an explanation of different functionalities that have been developed, a description of, a characterisation of the recycled carbon fibres and the recycling fibres and a definition of the heating and thermal control functionality with some examples of application.

In order study the behaviour of the samples with electrical current flow, different dosages of carbonaceous materials were employed, either with an addition of two different types of recycled carbon fibres or putting in an extra addition of graphite flakes. These percentages were chosen according to the electrical properties of the materials. The dosages are expressed in terms of the amount of cement used. Moreover, Ultra-High-Performance Concrete (UHPC) was used the concrete.

The tests were distributed in two campaigns. A first round of samples of 40 x 40 x 160mm testing the electrical properties of the material. A second round of heating tests in plates of 300 x 600 x40mm and beams of 10 x 10 x 400mm, with different electrodes combinations.

The samples were submitted to different tests, depending on the state of the matrix and the type and percentage of fibre addition, in order to characterise the material properties in different functionalities.

Firstly, for the electrical conductivity characterisation, the samples where submitted to different voltages, in order to know the conductivity and the resistivity of

the material, which indicates the functionality of the material and the variation of its conductive properties.

Then, in order to characterise the heating behaviour of the material, the samples were submitted to a series of heating test, changing form each the voltage, the time of the cycles and the moisture of the samples. Due to the fact that the heating degree of the samples depend on the exposure time, the temperature reached and the amount of water present in the sample. Different tests were performed for cycles of 1h, 3h, 4h, 8h and 48h, the last one alternating connected and disconnected periods, to analyse the heating and the cooling behaviour.

After the heating tests were performed, all data was collected and analysed by means of the Joule effect, considering impedance, power, effective voltage and effective current.

Subsequently, the results obtained from the analysis and characterisation of the heating functionality were compared with an existing model of the heat and thermal control behaviour, so as to see if the test results and the modelling results coincided.

Finally, the most significative conclusions were extracted from the obtained results to use them as a base for new projects and researches on the composite material developed and its applications.

# 2. STATE OF THE ART

## 2.1. INTRODUCTION

Following the objectives set and the course determined, in this chapter an analysis of the key points and major concepts on which the research is based is presented. The bibliographic research has focused on the definition of conductive concrete and revision of previous approaches, on the possibilities the recycled carbon fibres are conductive and economically sustainable and, finally, on the analysis of the functionalities that can be extracted from its addition and the presentation of the heating and control temperature functionality and some of its applications. Besides, this previous analysis was intended also to compile useful data for analysing critically the design of the manufactured conductive concrete by means of previous experiences conducted, analysing the different approaches that other authors have used to achieve a conductive cementitious material and its characterization, as well as reviewing a little bit the concept of fibre reinforced concrete.

## 2.2. CARBON FIBRE

The carbon fibre is a synthetic composite material formed by a fabric of carbon ribbons generated by the union of the polymeric chains join together forming cylindric filaments, that acts like the reinforcement or core of the composite material, providing to it flexibility and resistance, together with a thermostable resin, generally epoxy, that solidifies thanks to a hardening agent, acting like the matrix of the material binding together the fibres , protecting them and transferring the loads along all the material. For his part, a curing agent helps to turn the resin in a hard plastic.

From the combination of these compounds, the mechanical properties of the new material are obtained, since, although, the mesh of carbon fibres forms by itself a resistant element, it needs to be combined with the resins to be protected from external factors and physical efforts.

### 2.2.1. Mechanical Properties

Carbon fibres are flexible fibres that can be manageable and transformable. They have a high Young modulus that characterize them as a material with high resistance and low density, which implies that their specific mechanical properties or by unit weight are exceptionally high (see Table 2.1.).

It is a very adequate material for structural applications submitted to repetitive loading and fatigue, since it is the only known material whose mechanical properties are barely sensitive to the application of cyclic loads and its wear resistance is very low. In normal conditions of temperature, carbon fibres are elastic, thereby, they are more resistant to fracture and unsensitive to fatigue. Proportionally, it has ten times much ultimate limit strength than steel, but without plasticity, so that the ultimate strength coincides with the yielding strength. In this manner, it is a very brittle material. Furthermore, it has excellent acoustic dumping properties [48].

| Properties | Values |
|---|---|
| ***Diameter (μm)*** | $7 \pm 0.2$ |
| ***Density (g/cm³)*** | 1.6 |
| ***Tensile resistance (MPa)*** | 3000 - 4127 |
| ***Elasticity modulus (GPa)*** | 220 - 240 |
| ***Electrical conductivity (s·cm$^{-1}$)*** | 100 - 1000 |
| ***Thermal conductivity (W/(m·K))*** | 21 - 500 |

*Table 2.1 Carbon fibre standard properties*

### 2.2.2. Electrical and termal properties

Carbon fibres have high electrical and thermal conductivity, even higher than metals and three times the thermal conductivity of coper, thanks to its composition of oriented graphitic crystals, preferably, following the fibres axis direction. The orientation degree of its graphitic structure determines the magnitude of these properties, hence, the higher the orientation and organization of its internal structure the better the electrical and thermal conductivity. Along these lines, the higher the temperature of the treatments the lower the electrical resistivity that the carbon fibres present, and so higher conductivity, due to the better order of the graphitic sheets at high temperatures.

One of its indubitable advantages is the evolution of the mechanical properties with temperature, which are not only maintained but even improved unlike many other materials that deteriorate at high temperatures, limiting their performance [48, 49].

### 2.2.3. Environmental impact

The production of carbon fibre implies a high energetic consumption, such that if the cycle of associated pollutant emissions, like the $CO_2$ cycle, is evaluated, results in high contaminant levels. For this reason, recycling or reusing it is very useful and important. Moreover, the recycling of this material has both, environmental and commercial benefits. In order to illustrate the magnitude of this problem and its

economic and environmental relevance, some important data from the material's production and disuse is presented. The estimated level of this type of residues in USA and Europe add up to 3000 tonnes per year. Furthermore, until 2030, it is expected that between 6000 and 8000 commercial aircrafts are going to be demolished, whereas the production of virgin carbon fibre in 2018 has risen to 100000 tonnes annually [50].

Besides, none of the current residues treatments is optimal for the elimination of CFRP, neither the dumping sites nor the incineration, and the environmental regulations can come to the ban of these processes in the near future.

Consequently, the potential of the recycling of this product is very appealing and both small and big companies are looking for its reuse by means of compatible processes with the environment. Nevertheless, the development of an industry of recycling of CFRP is still in his early stages and the processes developed so far are very expensive and complex, principally, regarding the fact that it is an engineering high performance material. Moreover, many current recycling techniques weaken the fibres, reducing their utility.

## 2.3. RECYCLING OF REINFORCED MATERIALS WITH CARBON FIBRES

The carbon fibre is used as a reinforcement element only in applications with high mechanical demand and big budgets. Consequently, in order to avoid the use of such expensive materials other alternative have been evaluated in the recycling field.

By means of the development of the research projects presented below, it is demonstrated that chemical techniques as much as thermal techniques can be applied for the recycling of composite materials form the aerospace field, obtaining a carbon fibre that can be used as an addition in new high-performance materials. The fact of providing an alternative to the carbon fibre obtained as a product of a recycling process justifies its use and, moreover, it has been proven that it can be combined with concrete supplying high-graded mechanical properties, at a very similar price from the currently used materials.

### 2.3.1. Origin of the carbon fibres residues

The composite materials with carbon fibre (CFRP) have many applications and a constant increase of usage in various fields, such as aerospace, transportation and wind energy production. They use this type of compounds because of their durability, lightness and the ability of making complex shapes. For example, taking data from 2007 in the United Kingdom, a total amount of more than 2000 Tm products were produced

using composite materials reinforced with carbon fibres, absorbing the aerospace industry and military industry a 36% and the wind energy production industry a 33%, as the most important sectors. As reflected in the illustration below presenting all the components of a commercial aircraft made out of CFRP (see Figure 2.1.).

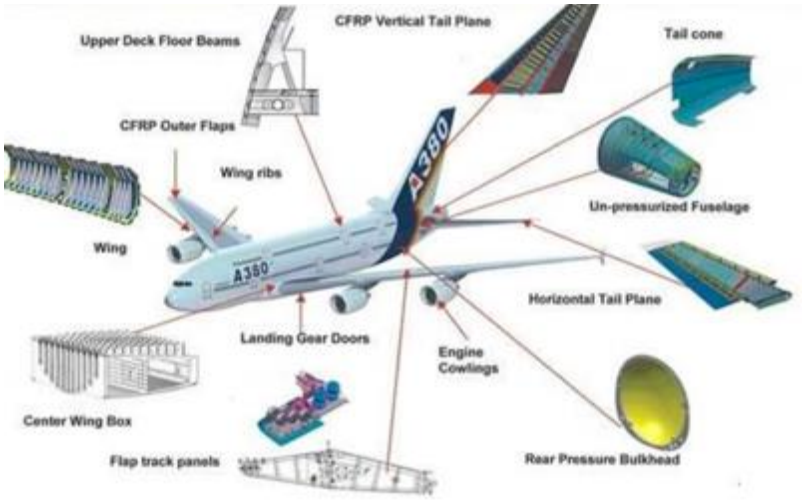


*Figure 2.1 Illustration of all the components of an aircraft made out of CFRP (www.airbus.com)*

The recycling process of this type of material is complex, as the majority of them use matrices of thermostable resins, which are not easily recyclable due to their high chemical cross-linking, since it does not allow them to be melted again and subsequently moulded, as it is done with the thermoplastic materials.

As aforementioned, a high amount of residues of CFRP are expected in the following years, coming mainly from the aerospace field, and neither using dumping sites nor the incineration are sustainable ways to treat this type of residues. Therefore, different alternatives have been developed and studied for their recycling and subsequent use or treatment.

Even though, the production of composite materials with carbon fibres only symbolises the 2% in volume of this materials family and the majority of the volume corresponds to composite materials with glass fibres, the residue of carbon fibre generated has 10 times more value. If this factor is added to the short life cycles of the products generated, between 2 to 8 years, and the visibility of the sustainability politics, promote the research in this field.

The carbon fibre residues can be generated from the manufacturing process until the end of the service like of the manufactured product, presenting three different types of residues:

- Dry fibre, leftovers or fibre residues, generated during the manufacturing process, fabric or set of bobbins from carbon fibre.

- Coated fibre, pre-coated fibre residues with resins coming from out of use row material due to resins' degradation.

- Laminated products, fibre residues from monolithic pieces, manufacturing cuttings, excess and pieces at the end of its service life.

### 2.3.2. Recycling mechanisms for carbon fibre

Principally, there are two main categories of processes for the recycling of thermostable composite materials reinforced with fibres, in this particular case carbon fibres. On the one hand, the mechanical recycling process and, in the other hand, the thermal and chemical recycling process (see Figure 2.2.). Depending on which recycling process is used, the resulting fibres can be reused in different applications (see Figure 2.3.).

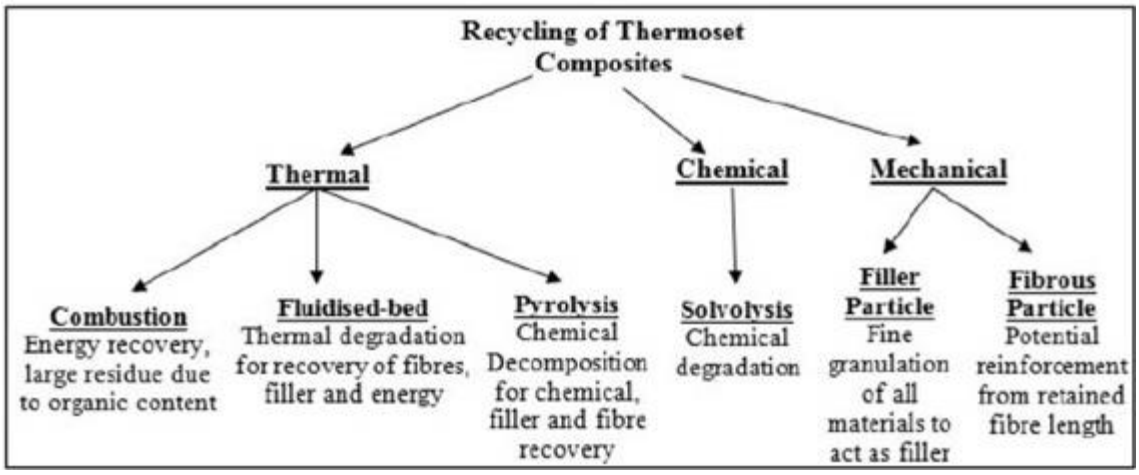


*Figure 2.2 Diagram of the categories of recycling processes of CFRP*

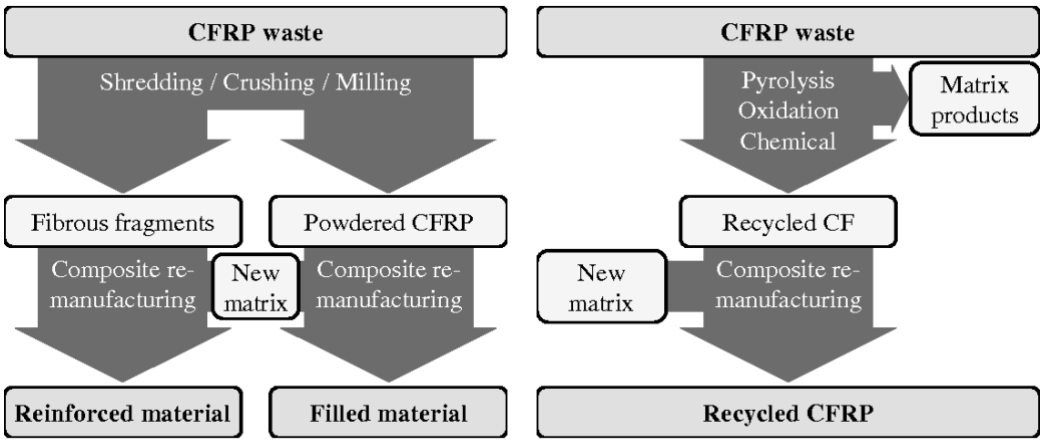


*Figure 2.3 CFRP waste treatment processes and reuse alternatives of the recycling products*

#### 2.3.2.1. Mechanical recycling

The mechanical recycling process consists in reducing the residues size, by means of successive stages of shredding, crushing and milling. The larger the residue's size the slower the process, increasing the velocity in subsequent stages, as the particles size reduces.

In the first stage the size of the residues is reduced up to 50-100 mm, making possible the separation of metals and other compounds of different material nature, achieving a certain compaction that reduces the costs in transportation, due to the decrease of volume.

Afterwards, the material undergoes another process where the milling velocity is increased and, therefore, the residue's size decreases up to 10 mm – 50 μm. The finest fractions are formed mainly of polymer powder and mineral charges, whereas the fractions with bigger size are formed of more fibrous materials and longer particles.

#### 2.3.2.2. Energy and material recovery by combustion (incineration)

By means of a combustion process, calorific energy is extracted from the polymeric matrix at a ratio of 30000 KJ per Kg of residue [51], whereas the carbon fibres, even so they do not break down, they suffer such a deterioration level that they are no longer capable for a subsequent use.

The deterioration of the fibres from the combustion of the composite material is higher, the less controlled the oxidation process is carried out. Consequently, for this alternative, the recovery of the incombustible material, the fibres, it only has a certain value if the combustion takes place in cement production kilns. In this manner, the incombustible materials from the composite material incorporate to the cement, including fibres and inorganic charge minerals.

### 2.3.2.3. Fluidised bed system

The recycled reinforcement fibres, especially the carbon ones, have higher value if they are suitable to be reused again in composite materials of high added value. In order to do so, the fibre properties need to be maintained after the recycling process and remain free of impurities.

Aiming at meeting these requirements recycling processes have been developed using a fluidised bed of silica sand, where the residues are introduced with a size around 25 mm. the sand fluidises by means of an air jet at 450ºC-550ºC that volatizes the polymeric resins and suspends the fibres in the resulting gas, allowing to separate them in a secondary process where the polymer leftovers are completely eliminated (see Figure 2.4.).

The glass fibres obtained throughout this process maintain 50% of their initial tensile resistance, whereas the carbon fibres maintain up to 80% of their properties. The initial rigidity and elasticity of fibres is preserved after the process.

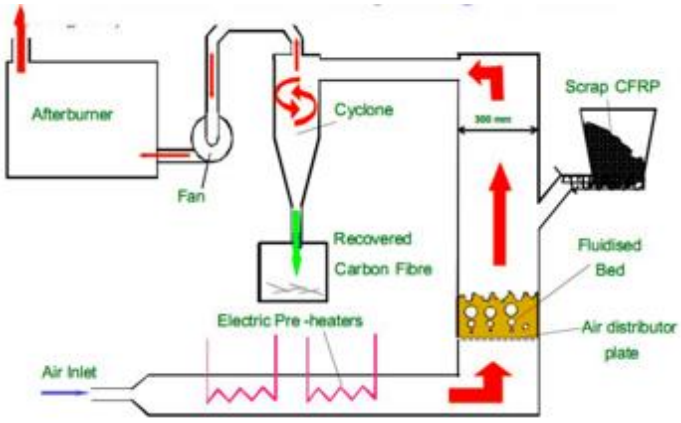


*Figure 2.4 Fluidised bed recycling process illustration*

### 2.3.2.4. Pyrolysis in inert atmosphere

In a pyrolysis process the composite material is heated in absence of oxygen or in very limited quantities. In these conditions, the organic compounds that form the resin decompose in new organic compounds with less molecular weight, like gases and liquids, which are simpler to separate from fibres (see Figure 2.5.).

The lower the temperature at which the pyrolysis process takes place, the less the degradation of the mechanical characteristics of the carbon fibres. Although, the longer the cycle time needed in the reactor. As a consequence, catalyser agents are needed in order to accelerate the decomposition process of the resin.

The carbon fibres obtained with this process can preserve up to 90% of their initial mechanical properties, as well as obtaining fibres with surface practically free of resin, making possible their use in applications of high-performance reinforcement, with uses very similar from the original fibre.

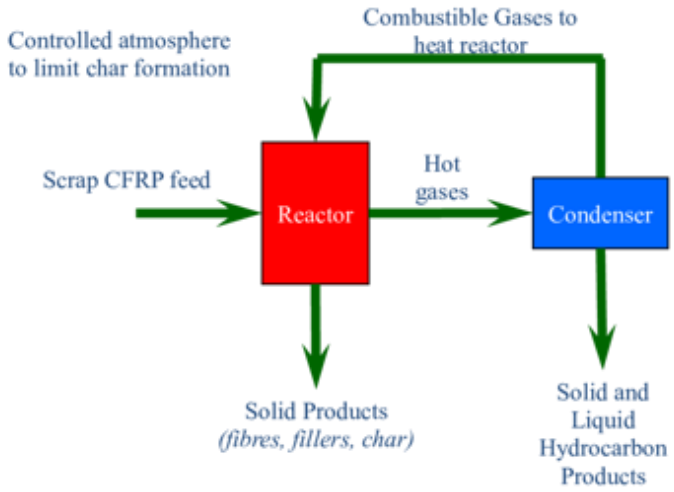


*Figure 2.5 Pyrolysis recycling process diagram*

#### 2.3.2.5. Solvolysis

Solvolysis is a recycling process based on the chemical degradation of the resin, in order to release the fibres without affecting them. Solvolysis itself is a chemical reaction in which the solvent, such as water or alcohol, is one of the reagents and is present in great excess of that required for the reaction. Solvolytic reactions are usually substitution reactions, i.e. reactions in which an atom or a group of atoms in a molecule is replaced by another atom or group of atoms. The solvents act as or produce electron-rich atoms or groups of atoms (nucleophiles) that displace an atom or group in the substrate molecule. At high temperatures or in the presence of strong bases, some solvents act as eliminating agents, producing alkenes from alkyl halides. It is common practice to name solvolysis reactions after the specific solvent, such as “hydrolysis” when water is the reagent. Since the recycling process is based on this chemical reaction, it takes its name.

At low temperature and pressure (LTP), catalysts and acidic or alkaline solutions must be used to achieve complete degradation. However; the resulting solutions are often a significant hazard with respect to health, safety and the environment. At near- or supercritical conditions, even the hardest, most stable thermoset, e.g. epoxies, and thermoplastic, e.g. PEEK, resins can be fully degraded using solvents such as water, methanol, ethanol, propanol and acetone without the need for additional catalysts (see Figure 2.6.).

After the treatment, fibres are separated from the liquid residue, dried and can be directly reused for new applications. The carbon fibres obtained with this process can preserve up to 90-95% of their initial mechanical properties, with very similar results to pyrolysis or even a little bit better. Besides, the obtained fibres' surface is practically free of resin, making possible their use in applications of high-performance reinforcement, with uses very similar from the original fibre.

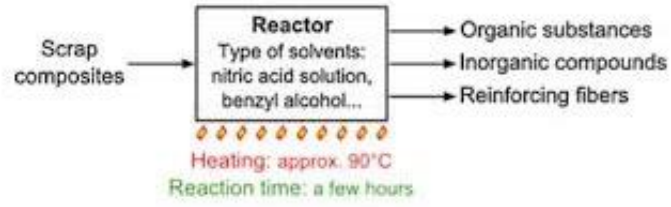


*Figure 2.6 Solvolysis recycling process diagram*

### 2.3.3. Properties of the recycled carbon fibres

During the recycling processes, the carbon fibres deteriorate due to the high temperatures at which they are submitted, suffering burns that weaken their initial characteristics, even though they preserve an important magnitude of their mechanical and electrical properties and they are similar to the original fibres (see Table 2.2.). Furthermore, their use is very recommendable from the economic point of view.

| Properties | Values |
|---|---|
| ***Diameter (μm)*** | 7.5 |
| ***Density (g/cm$^3$)*** | 1.8 |
| ***Tensile resistance (MPa)*** | 3150 |
| ***Elasticity modulus (GPa)*** | 200 |
| ***Electrical conductivity (s·cm$^{-1}$)*** | 100 - 1000 |
| ***Thermal conductivity (W/(m·K))*** | 21 - 150 |

*Table 2.2 Example of properties of recycled carbon fibres from ELG Carbon Fibre recycling company (www.elgcf.com)*

Taking this particular case as an example of the remarkable performance of these recycling processes and how promising this alternative is, the ELG Carbon Fibre recycling company states that the company's recycled carbon fibre (RCF) products can offer from 30 to 40% cost savings compared to the virgin carbon fibre (VCF). Moreover, they describe the RCF properties as basically the same as VCF (≥ 90%), though they say tensile strength is 10 to 20% lower [52].

Various researches have been conducted about the recycling of carbon fibre and one of them emerged after its publication in the Water manage magazine for its accuracy and results [53]. Some results from this paper are presented below (see Figure

2.7.). It can be seen that there are very few differences between the virgin carbon fibre and the recycled carbon fibre mechanical properties. From these results, the chemical recycling procedure or solvolysis emerges as the alternative with better results.

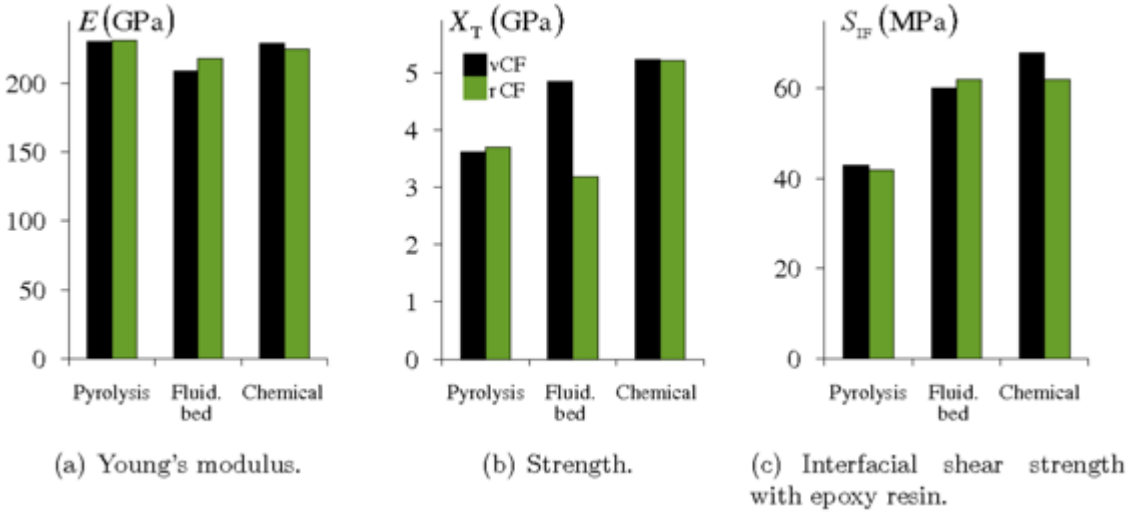


*Figure 2.7 Mechanical properties of recycled carbon–fibres and their virgin precursors (Jiang et al. 2009, 2008, Panesar 2009)*

## 2.4. CONDUCTIVE CONCRETE

### 2.4.1. Description of the conductive concrete

Electrically conductive cement-based materials are one of the main categories of the multifunctional cementitious materials. These materials are increasingly recognized, since they are structural materials with imbedded new non-structural properties and the modern building construction materials, require more and more functional properties that can provide new possibilities, widening the boundaries of the multifunctionality of cementitious materials.

Standard concrete, formed out of a Portland cement mix, fine aggregates and coarse mineral aggregates, water and chemical additives, is a dielectric material, i.e. that very few or insignificant electrical conductivity. Therefore, it does not contribute with any different functional characteristic from the ones strictly of structural nature.

Resistivity for saturated and dry concrete ranges between $10^6$ Ω·cm and $10^9$ Ω·cm, respectively. Concrete electrical resistivity lies at the border between insulators and poor semiconductors. It is theoretically feasible to improve the conductivity of concrete matrix by the addition of well dispersed electrically conductive components inside the concrete matrix to attain stable and good electrical conductivity. However, the content of the conductive component should be within certain limits to avoid degradation of other related physical and mechanical properties of the concrete mixture [10, 54].

Conductive concrete has been investigated using different types of conductive fillers or phases in the form of particles or fibres which are included into the cement matrix. Examples of the conductive fillers or phases used are graphite and carbon fibres and microfibres, steel fibres and micro fibres, steel shavings, graphite powder, steel wool, carbon black powder and carbon black nanoparticles and carbon nano-fibres and nanotubes [23, 55].

Furthermore, an electrically conductive admixture can enhance the conductivity of the composite material even when the volume fraction of the admixture is below the percolation threshold, i.e. the volume faction above which the admixture units inside the cementitious materials touch to form a continuous conduction path.

The percolation threshold is determined from the variation of the electrical resistivity with the volume fraction of the conductive admixture. The electrical resistivity abruptly decreases by orders of magnitude at the percolation threshold and, in most cases, the percolation threshold decreases with increasing the aspect ratio and decreasing the unit size of the admixture. Besides, the conductivity of concrete has been proven to be dependent on the distribution and orientation of these admixtures. However, the percolation threshold it also depends on the unit size of the non-conductive or less conductive components in the composite [54].

Along these lines, several investigations found that the electrical resistivity of concrete is greatly affected by its constituent's parameters, mainly, the type and content of aggregate, w/c ratio and sand to cement ratio. Emphasising the significant effect of aggregate content on concrete conductivity especially the sand content volume fraction.

Moreover, the aggregate type, the grain size distribution, the w/c ratio and the sand to cement ration have a direct influence on the workability of the mix and the voids ratio inside the composite material. Some researchers have proven the adversely effect of these voids in the conductive properties of concrete. So that, in order to obtain better conductivity very dense concrete mix without interruptions in the grain skeleton are more suitable, since electric current cannot pass through the air voids. In case the voids are filled with ionised water the effect is not as significant, but it does not conduct as well as the solid skeleton [2, 10].

The curing age has relatively minor influence on the electrical resistivity, although it has a major influence on mechanical properties.

Conductive concrete has been proposed for several applications, such as self-heating and overlay snow melting system of highway bridge decks, parking

garages, sidewalks, driveways and airport runways [2, 4-12, 32-36, 43-45, 54] , cathodic protection (CP) systems of steel reinforcement in concrete structures [15, 16, 37, 39], structural health monitoring systems and self-sensing for smart structures [17, 19, 20, 25, 54], antistatic flooring and electromagnetic pulse shielding [18, 54]. Also, electrically conductive concrete (ECC) has good potentials to be used in grounding systems.

Grounding is crucial in structures especially those which require good grounding such as central offices, electrical power stations, residential buildings, etc. Conventional grounding systems could be in some cases ineffective and could cause great deal of damage. Besides, traditional grounding systems are prone to damage due to natural processes and human behaviour, i.e. cutting or theft. Using ECC to replace or enhance foundations and buried ground grid systems will allow for integral above and below grade ground connections that are efficient, low maintenance, easy to test and resilient to damage [18, 54]. Recently, conductive concrete was proposed to be used in electrochemical extraction of chloride from reinforced concrete structures and in the developing battery in the form of cement- matrix composite [15, 16, 39].

Nevertheless, the application of ECC has been limited because the earlier conductive concrete mixtures did not meet structural requirements, i.e. mainly strength, and/or were too expensive to produce. Vipulanandan and Garas highlighted that previous studies have focused on getting the percolation thresholds and the critical percolation exponents for the different composites and to assess the nature of conductivity, while the correlations between the electrical properties and the physical and mechanical properties of cement-based materials have received little attention. Several researches included the measurement of some mechanical properties of produced conductive concrete such as compressive, tensile and flexural strengths and modulus of elasticity. But, almost no research reported the effect and correlation of using different conductive fillers on fresh concrete properties and durability characteristics. Fresh concrete properties are important during the construction of structural concrete. While durability characteristics are important for producing structural.

In order to make these materials much more affordable several researches have focused on using recycled materials as electrically conductive admixtures, in the last few years. In such a way, not only the price from using recycled material instead of a virgin one decreases, but it also represents a sustainable and environmental added value.

### 2.4.2. Typologies of conductive concrete

There are different ways to achieve conductive concrete, depending on the additions or the different natures of the phases. But, at the moment, there is not a strict classification of conductive concrete types, since it is a very new investigation field and every research uses its own combination of admixtures, combining materials of different natures, trying to develop new properties. Therefore, after the literature study, different researches have been group depending on the combination of admixtures used and the patterns followed in their experimental campaigns.

The most commonly used admixtures are graphite and carbon fibres and microfibres, steel fibres and micro fibres, steel shavings, graphite powder, steel wool, carbon black powder and carbon black nanoparticles, carbon nano-fibres and nanotubes, carbon fibre wires and slags and basalt aggregates.

However, due to certain drawbacks of conventional conductive fillers, heat generation capability and mechanical properties of the electrically conductive concrete may decrease over a longer period of time.

#### 2.4.2.1. Steel fibres, microfibres and shavings.

It is a very suitable admixture due to its high electrical and thermal conductivity and Its low thermal expansion coefficient. However, it presents some problems dealing with corrosion compared to other admixture materials. Although, this is not so problematic if it is stainless steel.

It was one of the first types of admixtures for conductive concrete and it is widely used due to its high accessibility and low price, compared to other alternatives. However, barely never is used alone.

Generally, it is used combined with graphite powder, or silica fume or carbon black powder. Sometimes, it is used together with carbon powder and graphite powder, forming what is called three-phase composite conductive concrete which has been used many times for the generation of self-heating and de-icing pavements in recent years.

Normally, steel fibres and micro-fibres present angular shaped profiles, whereas steel shavings have a rough texture (see Figure 2.8.). Consequently, they are particularly good in anchoring to the cementitious matrix, providing significant bond stresses. Taking this together with the excellent mechanical properties of steel, it provides a very resistant material.

*Figure 2.8 Special steel shavings for conductive concrete mix (www.omaha.com)*

The use of steel fibres and/or shavings reinforced concrete for the purpose of de-icing has been proven effective in lab and field tests. However, there still exist some questions on the risk of tire punctuation in long-term service due to the expo- sure of steel fibres on the pavement surface. Extra shielding of the pavement may prevent the exposure of steel fibres, but it may impede the heat conduction to the pavement surface. Layered steel fibre reinforced concrete is a new development in the field of road engineering in recent years. Instead of using steel fibres in the whole body of concrete, fibres are layered in the pavement with a horizontal orientation in one or multiple layers. However, understanding of the performance of this new type of electrically conductive concrete with layered steel fibres is still limited.

Moreover, steel fibres and steel shavings can cause corrosion problems, increasing the electrical resistivity and degrading the durability of the composites [44].

For these reasons, a type of electrically conductive concrete with double-layered stainless steel fibre (DSSF) for the de-icing of pavement has been actively developed and tested in some researches which presented satisfactory performance in regard to its resistivity and ice-removing capability [43].

#### 2.4.2.2. Carbon fibres, micro fibres, carbon black powder and graphite flakes and powder

It is the most used admixture material at the moment, due to its excellent properties, not only mechanical, but also electrical and thermal. Carbonaceous materials have a high thermal conductivity, although not as high as metals, a low coefficient of thermal expansion, lower than metals, and are highly resistant to corrosion. Besides, its mechanical properties are improved with temperature are improved and it is a light admixture material. It can be used individually, only using carbonaceous materials admixtures or combined with steel fibres, nano-fibres and nanotubes, among others.

In many other researches, the addition of carbon fibre has been indexed, either in form of short fibre, or studying the conductivity as a function of the size and the appearance ratio, or even in a carbon fibre mesh form, also for the construction of thawing pavements.

However, if it is used as a virgin material, it is very expensive, which is one of the reasons why at the beginning conductive concrete was that expensive. However, in recent years, researches and companies has seen in recycled carbon fibre admixtures a perfect alternative for developing much cheaper conductive concrete.

It performs very well in all the functionalities that have been developed with conductive concrete due to its electrically conductive characteristic, but it stands out when used for thermal applications like self-heating concretes, temperature control systems, etc.

This type of materials can be added directly to the mixing process or, in some cases, can form by themselves a semi-dry mix with water and by means of a palletisation process create conductive aggregates [31].

Other types of conductive concretes have been developed using fines and conductive powders additions, like graphite powder, with the objective of creating a material that auto-monitored its stresses with the change in conductivity associated to the geometric deformation of the material and its microstructure.

#### 2.4.2.3. Slags and basalt

Some conductive concretes have been developed by using slag from steel production furnaces as conductive phase [56]. Slags are chemically formed by CaO, FeO, $Fe_2O_3$, $SiO_2$ and MgO so that thanks to the presence of iron compounds, conductive concrete can be developed. Furthermore, this type of addition has many advantages, such as being a material of low economical cost and environmentally sustainable, since an industrial residue is being reused. However, a thorough control needs to be performed on the calcium oxide and magnesium oxide unstable compounds that can affect hydration reactions of concrete.

Following the same lines, there are conductive concretes that have been created adding basalt as a conductive aggregate, aiming at stablishing a conductive web by contact between the different phases.

#### 2.4.2.4. Carbon nano-fibres and nanotubes

This type of admixture is very new and it has only been used in tests and researches. It stands out by an excellent performance in multifunctional cement-based materials. Some researchers have adventured in the use of carbon nano-fibres and nanotubes for the development of self-heating and de-icing conductive concrete [55], but with an economical restriction due to the high cost of this type of material (see Figure 2.9.).

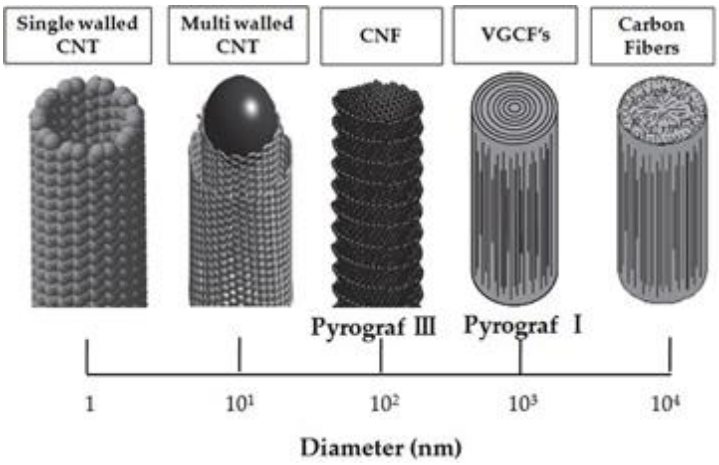


*Figure 2.9 Comparizon between carbon fibres, nano-fibres and nanotubes (www.intechopen.com)*

### 2.4.3. Functionalities of a conductive concrete

A multifunctional cement-based concrete with the ability of conducting the electrical current, as a functional material, can fulfil many new requirements of future new applications. The main applications are anode for electrochemical chloride extraction, electromagnetic wave shielding, strain/stress sensor, dynamic monitoring and damage detection, electrical grounding, electrical and thermal conductivity enhancer, temperature sensor, self-heating and thermal control.

In this section of the project, conductive concrete applications and properties developed so far in previous researches are reviewed, in order to set a context for our study.

#### 2.4.3.1. Anode for electrochemical chloride extraction

The electrochemical extraction of chlorides (EEC) is a non-destructive methodology to prevent corrosion of steel rebar, a principle problem in structural concrete. There is an extensive bibliography on this technique beginning with its initial utilization in the 1970s. The method basically consists in applying an electric field between the steel rebar (the negative pole or cathode) and an externally deposited

electrode at the concrete surface (the positive pole or anode). Since chlorides ($Cl^-$) are negatively charged ions, the imposed force field causes them to migrate from the rebar to the exterior electrode through the concrete pores. Nevertheless, some doubts have been expressed concerning features such as end-point determination, side effects and durability of structures submitted to EEC trials [38].

Cementitious conductors have been used as anodes for cathodic protection in research [37]. A commercial conductive, polymer-modified, cementitious mortar has been successfully used as the anode for applying cathodic protection to more than 40,000 $m^2$ of reinforced concrete [39].

Other researches have focused on the viability of the application of a conductive cement paste (CCP) as an anode for the EEC technique because of the potential advantages it has when compared to the usual anodic systems. Some of these advantages include the possibility of the application as a fine layer, the adaptation to various types of surfaces, and the possibility of reutilization for repeated EEC treatments, which may be necessary for certain structures and conditions.

A single EEC trial may be unable to eliminate enough $Cl^-$ ions, in cases of heavy or progressive chloride contamination of concrete, to reduce permanently the steel corrosion rate below its threshold value of about 0.1–0.2 $\mu A/cm^2$.

Another interesting possibility is the combination of an initial EEC treatment, followed eventually by cathodic protection applied using the same CCP anode. The second of these actions may be deemed necessary or convenient when analysing the corrosion state of the structure after the EEC trial. Furthermore, the current density needed for the effective cathodic protection of steel, may be significantly lowered as a consequence of the reduction of $Cl^-$ content of concrete near the steel, produced by the initial EEC treatment.

However, a disadvantage of using CCP anodes is the impossibility of using the half-cell potential mapping technique for assessing the corrosion state of reinforcement after the EEC treatments, since the conductive character of the overlay homogenizes the potential values [15].

#### 2.4.3.2. Electromagnetic shielding

The electromagnetic shielding of a material is defined as its capacity of protection from the electromagnetic waves, either avoiding them completely to pass through the material or attenuating their power [55].

The rapid development of modern electronic equipment and wireless devices has resulted in severe electromagnetic (EM) radiation pollution, which has implications in human health and the normal functioning of electronics. Thus, the design and exploration of effective EM wave absorption materials is of basic scientific importance. Especially, in subterranean constructions of electrical use that contain transformers and other electronic compounds that are important for power plants and telecommunications [13].

In the same manner, but in a different level, this type of protection can be necessary in constructions destined to be the home of strategic electronic systems in nuclear plants, airports or military bases. In these cases, the protection would be against the electromagnetic waves generated by nuclear detonations in altitude or systems of weapons similar in terms of the effect.

The primary mechanism of EM shielding is usually reflection. For reflection of the radiation by the shield, the shield must have mobile charge carriers (electrons or holes) which interact with the electromagnetic fields in the radiation. As a result, the shield tends to be electrically conducting, although a high conductivity is not required. For example, a volume resistivity of the order of 1 V cm is typically sufficient [18].

However, electrical conductivity is not the scientific criterion for shielding, as conduction requires connectivity in the conduction path (percolation in case of a composite material containing a conductive filler), whereas shielding does not. Although shielding does not require connectivity, it is enhanced by connectivity.

Metals are by far the most common materials for EMI shielding. They function mainly by reflection due to the free electrons in them. Metal sheets are bulky, so metal coatings made by electroplating, electroless plating or vacuum deposition are commonly used for shielding. The coating may be on bulk materials, fibers or particles. Coatings tend to suffer from their poor wear or scratch resistance.

A secondary mechanism of EM shielding is usually absorption. For significant absorption of the radiation by the shield, the shield should have electric and/or magnetic dipoles which interact with the electromagnetic fields in the radiation. The electric dipoles may be provided by $BaTiO_3$ or other materials having a high value of the dielectric constant. The magnetic dipoles may be provided by $Fe_3O_4$ or other materials having a high value of the magnetic permeability, which may be enhanced by reducing the number of magnetic domain walls through the use of a multilayer of magnetic films [54].

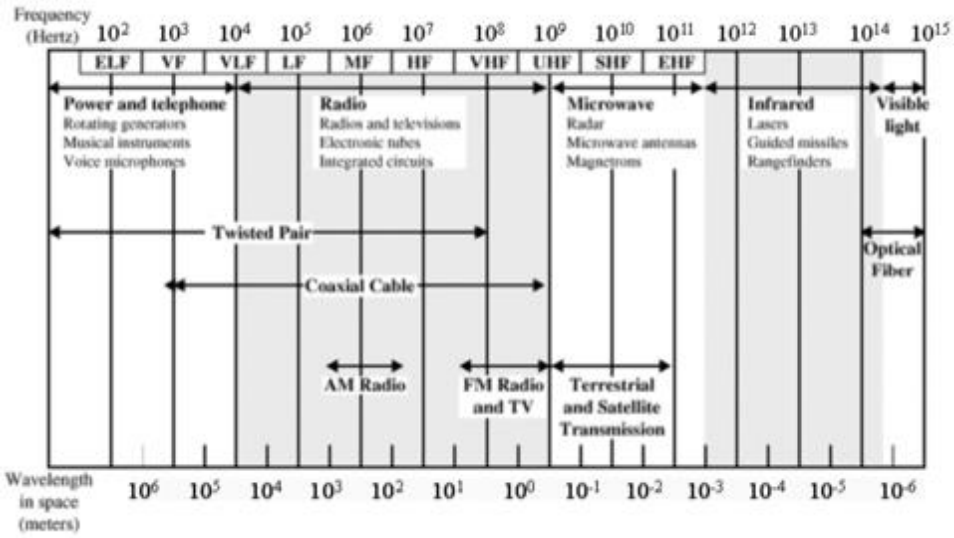


*Figure 2.10 Electromagnetic spectrum for telecommunications*

EM waves consist of a time-varying electric and magnetic field, and EM wave absorption is achieved by the attenuation of EM wave energy through dielectric loss and magnetic loss as well as electromagnetic impedance match, which can minimize the reflection of the incident EM wave (see Figure 2.10.). Therefore, dielectric loss and magnetic loss are the main factors determining absorption capability. Good impedance matching between the specimen and free space is necessary for enhancing EM wave absorption capability.

Carbon nanotubes (CNTs) offer the unique potential to be excellent EM wave absorbents. Besides their superior mechanical and thermal properties, they have very high carrier mobility and current carrying capacity. Most of the research effort to date has focused on CNTs decorated with magnetic metal or metal oxide particles for enhancing magnetic attenuation.

However, the anticipated improvement in EM wave absorption performance has often been hindered by the poor dispersion of CNTs and their impedance mismatch with free space. CNT films, on the other hand, not only retain the high permittivity of individual CNTs in an isotropic network structure but also greatly facilitate the dispersion of CNTs in the matrix. Furthermore, the dispersion of $Fe_3O_4$ nanoparticles on the surface of CNTs can effectively improve permeability and impedance matching. Thus, the CNT film- $Fe_3O_4$ absorber provides a highly desirable combination to enhance dielectric and magnetic loss and impedance matching as well as facilitate ease in composites processing [40].

The effect of EM shielding achieved by reflection can be used in an automatic lateral guidance system for automatic highways, which refer to highways that provide

fully automated control of vehicles, so that safety and mobility are enhanced. In this manner the vehicle will go automatically, with both lateral and longitudinal control.

There are different types of composites materials with useful shielding functions at different electromagnetic frequencies. The use of a material for this functionality, requires an electromagnetic characterization apart from an electrical conductivity characterization.

#### 2.4.3.3. Strain/stress self-sensing and damage detection

Conductive concrete provides a new alternative of structural self-sensing in such a way that stresses and deformations can be controlled and monitored without needing internal sensors added to the material. This can be achieved thanks to the variation of the conductivity when a load is applied, so that, it is possible to perceive the deformation of the structure and, in elastic regime, the corresponding stress.

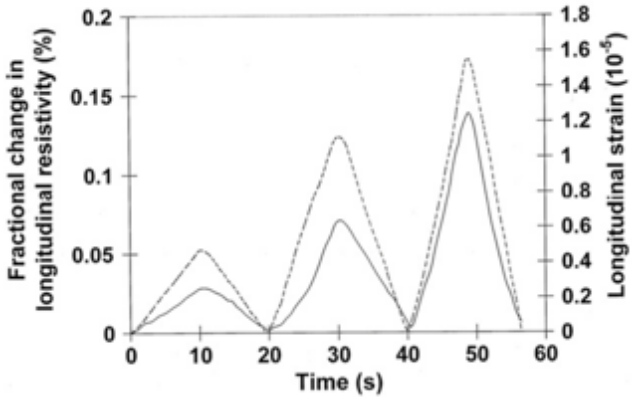


*Figure 2.11 Variation of the fractional change in longitudinal electrical resistivity with time (solid curve) and of the strain with time (dashed curve) during dynamic uniaxial tensile loading at increasing stress amplitudes within the elastic regime for carbon fibre silica fume cement paste [54]*

This perception of the deformation of the material is achieved thanks to the fact that the unit variation of the electrical resistivity in volume is proportional and reversible, within the elastic regime, to the stress at which it is submitted and, therefore, to its unit deformation (see Figure 2.11.). Thereby, if a longitudinal compressive stress is applied, the electrical resistance on that direction is reduced. Whereas, if there is upon tension stress, the resistance increases in a similar way. Within the elastic regime of the studied material, both responses are reversible, thus the electrical resistance recovers its initial value when the applied stress ceases (see Figures 2.12. and 2.13.).

This effect, in the case of cementitious materials, is interesting for structural service state monitoring, room occupancy control, load control or vehicle weighing. Nevertheless, the perception of a structural damage is related to the material's plastic behaviour and implies non-reversible changes of the unit variation of the electrical resistivity [17].

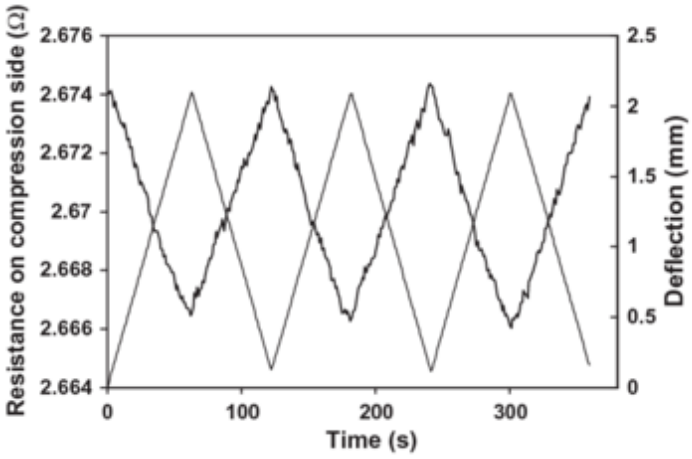


*Figure 2.12 Compression surface resistance (thick curve) during deflection (thin curve) cycling at a maximum deflection of 2.098 mm (stress amplitude of 392.3 MPa) for a 24-lamina quasi-isotropic continuous carbon fiber epoxy-matrix composite [29]*

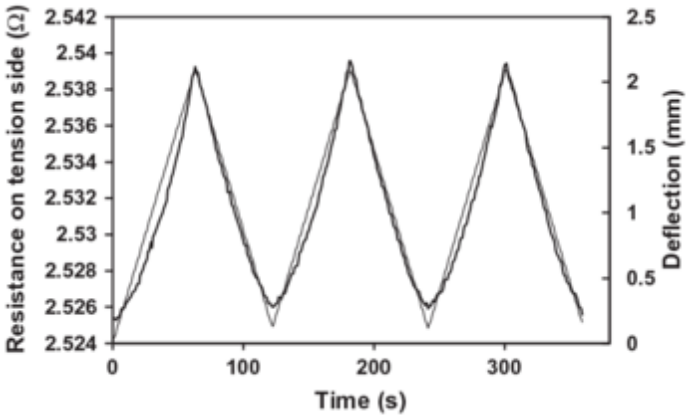


*Figure 2.13 Tension surface resistance (thick curve) during deflection (thin curve) cycling at a maximum deflection of 2.098 mm (stress amplitude of 392.3 MPa) for a 24-lamina quasi-isotropic continuous carbon fiber epoxy-matrix composite [29]*

In order to quantify the deformation perception, the gauge factor is used, which consist in a dimensionless parameter represented by the unit variation of the electrical resistivity over the unit deformation (see Equation 2.1.). It is the same parameter than the one used for strain gauges of common use.

$$FG = \frac{\frac{\Delta\rho}{\rho_o}}{\frac{\Delta l}{l_o}} = \frac{\frac{\Delta\rho}{\rho_o}}{\varepsilon} \tag{2.1}$$

Where:
$\Delta\rho$ : Variation of the electrical resistivity
$\rho_o$ : Initial electrical resistivity
$\Delta l$ : Variation of length
$l_o$ : Initial length
$\varepsilon$ : Unit deformation

For a perception of the deformation with enough magnitude and reversible, the addition of electrically conductive particles in the cementitious matrix is needed. Even though, it is not needed to reach the percolation limit, i.e. it is not needed that the addition's material forms a continuous path through the concrete, so that the perception of the deformation is effective. This implies that very low electrical resistivities are not needed to perceive the deformation [19].

For this application carbonaceous materials perform very well and are very suitable, such as carbon nanotubes and carbon fibres.

The sensibility of the deformation perception in electrically conductive concretes is very high with an FG value higher than 700, compared to the FG value of 2 for the strain gauges of common use [54]. This is due to variation of the electrical resistance of an element. This is not only caused by the dimensional changes generated by the application of loads, nut also the variation of the electrical resistivity intrinsic of the material. Modifications because of variation in the microstructure type and interaction of the phases that form the material, i.e. matrix-fibre.

The functionality of the deformation perception, is applicable in the control of the deformations in service structures, the control of loads and the monitorization of the traffic in road infrastructures [41].

#### 2.4.3.4. Electrical grounding

Electrical grounding is needed for buildings, transmission towers and other structures which involve electrical power, as well as lightning protection in tall buildings. Metals, such as steel are commonly used in these applications. However, the use of electrically conductive concrete diminishes the volume of metal required and so, is attractive for cost reduction, durability improvement and installation simplification.

In the grounding engineering of the power network, metallic materials, such as copper or stainless steel, were the main grounding materials at present. Unfortunately, the metallic grounding materials had poor corrosion resistance and fell into dis- repair

easily due to the stray current in transmission towers. Therefore, conductive concrete became a focus of the study of grounding materials, due to its good mechanical properties, electrical conductivity and corrosion resistance.

The resistivity of conductive concrete was lower than that of soil. The contact area between the electrode and soil could be enlarged by laying conductive concrete around the metal grounding electrodes and the grounding resistance could be reduced. Currently, conductive concrete was mainly used as auxiliary grounding material in grounding engineering by casting around the vertical grounding body through mechanical press or directly casting around the level ground. However, researches about the grounding characteristics and model of conductive concrete are notably lacking.

Carbon fibre is a good candidate to modify electrically conductive concrete for engineering application because of its high conductivity and tensile stress. Meanwhile, carbon black particles can effectively improve the conductivity of cement matrix. Combining carbon fibre and carbon black provides conductive concrete materials both high conductive performance and excellent mechanical properties.

In some researches, the carbon fibre-carbon black composite electrically conductive concrete has been used as a new grounding material, and its basic grounding characteristics such as conductivity, temperature stability and mechanical properties were studied. The concrete has been used to made rod grounding electrodes which were laid in parallel on the bottom and side walls of the foundation ditch of transmission tower to build new type of stereo grounding grid. Considering parallel grounding effect, some computational models of grounding resistance of conductive concrete stereo grounding have been established based on the calculation of grounding resistance of the metal electrodes [3].

#### 2.4.3.5. Heating function

The capacity of conductive concrete to develop thermal functionalities, such as self-heating and temperature control, is directly related with the improvement of its electrical conductivity. Along these lines, a conductive cementitious material acts like an electric resistance, transforming part of the electrical energy into heat, increasing the temperature of the material. This behaviour is called Joule effect and allows concrete to develop the capacity of warming up systems, constructions, buildings or urban furniture which constitutes [2, 4-7, 9-12, 14, 21, 29, 44]

At the moment, one of the most used alternatives in order to generate this functionality in concrete, is the addition of carbon-based materials to the cementitious matrix. The carbon-based material, such as the carbon fibres addition to concrete, are ideal for this use, since they have high electrical and thermal conductivity, a low thermal expansion coefficient and a high resistance to corrosion. All this makes these materials

good candidates for thermal applications in multifunctional cementitious composites such as heating of buildings or pavement deicing, among others [2].

A cementitious material capable of increasing its temperature in a controlled manner can develop many applications such as evaporating the rainwater of a sports court, heating a room through walls and/or floor, melting ice of a road or a runway of an airport, without the use of salt or heating urban furniture, widening its use during all the year and avoiding damages due to snow and ice, among others.

Due to the environmental issues associated with the use of fossil fuels and its ephemeral nature, electrical heating is increasingly important. Although electric heat pumps are widely used for the electrical heating of buildings, resistance heating is a complementary method which is receiving increasing attention due to the low cost of its implementation and control, its adaptability to localised heating, e.g. the heating of a particular room in a building, its nearly 100% efficiency of conversion of electrical energy to heat energy and the increasing demand of safety and quality of life.

The herald application of resistance heating systems and, self-heating and temperature control conductive concrete is the de-icing of driveways, bridge decks and airport runaways functionality. he technique of snow removal by mechanical ways is the most used but it is a labour intensive, costly and time-consuming task. Furthermore, not all the snow is completely cleaned from the driveway by the snowplows, leaving a small layer to be eliminated. Many of the methods currently used to remove ice from roads are based on the use of chemicals. Most of them are harmful to both reinforced concrete and steel structures (viaducts, tunnels, airport runways) and for the environment. Furthermore, it is a matter that affects directly the safety of the road users, the mobility of people and the production and economy of companies and administrations, creating traffic jumps as the one shown below (see Figure 2.14.).

*Figure 2.14 Traffic chaos in Atlanta due to a snowstorm ( www.bbc.com)*

Compared to the aforementioned methods, there is the possibility of using heating systems of conductive concrete layers. Several researchers have analyzed the feasibility of using conductive multifunctional concrete, with different additions, for pavement deicing (see Figure 2.15.).

*Figure 2.15 Illustration of the ice melting process by means of conductive concrete*

Since the late 90s, steel fibers, steel shavings, virgin carbon fibers, and graphite products have been added into concrete as conductive materials to greatly improve the electrical conductivity. However, the use of such materials, like virgin carbon fibre, made it very expensive at that time and, even if the results were very satisfactory, they were not implemented due to the high cost. Besides, in some cases, some drawbacks about using steel shavings in the mixtures were noticed, not only in terms of properties and performance, but also due to some puncture cases.

But, in recent years, the study and development of new carbonaceous materials and new mechanisms have improved the performance of these systems. Consequently, the researches on this topic are increasing significantly and in some places of the US and china it has already been implemented successively in reality.

In some researches about de-icing pavements by heating system, estimated the electrical resistivity needed for generating a thawing effect in pavements of this functionality in values around 10 $\Omega$·m [57].

In order to use concrete as a resistance, in the heating system by means of the Joule effect, the electrical resistance cannot be very high, otherwise, the electrical current intensity passing through the material would be very low, making the system inefficient. Although, it cannot be too high, as a very high electrical current intensity would be needed to reach the sufficient power.

A heating system based on underfloor heating or embedded to the structure implies passing current through the metallic heating elements as a unifying thread

inserted in the structural material or between the layers constituting the building. However, this type of systems that get the warming up through electrical resistance have some important disadvantages: a loss of mechanical capacity of the structure, due to the decrease of the cross section, by difficulties in substituting and repairing the conductive elements and by the lack of uniformity of the heat generated along space.

Unlike this type of systems, a conductive concrete that works as a resistance thanks to the Joule effect does not have these limitations, since with the addition of carbon fibres the mechanical capacity is improve and there is no need to embed wires and unifying threads inside the elements, which would simplify the installation and maintenance. Furthermore, as the concrete element is an electrically conductive material in its totality, the thermal effect generated is much more uniform.

If it is possible to optimize economically the dosage, in terms of the infrastructure cost, and limit the energetic consumption, in terms of operational cost, the conductive cementitious materials can be an excellent alternative thanks to their durability and structural performance. Different approximations of associated costs of various thawing systems for pavements have been computed, illustrating the viability of the introduction of this innovative system compared to other already existing alternatives.

In the following section of the project different applications developed using self-heating and thermal control materials are presented, aiming at setting up a base knowledge for our experimental campaign, which is developed in this field.

#### *2.4.3.5.1. Smart and radiant heating floor using conductive concrete screeds and tiles*

Screed is an indispensable part of the modern interior design for height adjustment and has to withstand different static and dynamic loads. Common floor screeds are cement-based composites consisting of Portland cement, sand and aggregates, and in most cases, they are fabricated as a free-floating structure. Heating elements are placed in floor heating screeds between the screed plate and the underlying insulation. To be able to withstand shrinkage and temperature stresses, fibre reinforcement is often added to the composite mixture.

But, if fibre reinforcement would be included as admixture of electrically conductive fibres, in-situ electrical heating of the screed would be feasible without installing heating elements below the floor plate, assuming that the admixed conductive fibres can provide good conductivity of the composite on the one hand and provide high flexural strength on the other hand [11].

This reasoning was very similar to the idea used for designing de-icing road pavements in previous projects. Therefore, some researchers concluded that the same principal used for ice melting outdoor pavements could be implemented for indoor tiles, changing the thickness of the slabs and with electrodes arranged in parallel from top to bottom [14].

Since electrical heating is more expensive than conventional heating with gas or fuel oil, developing smart heating systems for saving energy is essential to reduce costs. This concept is implemented, for instance, in heating only selected areas of the floor heating screed in order to save energy for those areas where heating is typically not required.

Accordingly, in a research conducted by the German cementitious materials company Schwenk Zement KG together with the University of Ausburg of Solid State and Materials Chemistry a prototypic modular floor heating plate was designed, which allows individual heating of different areas by using a grid of embedded electrodes [11]. By screening matrix properties, they could empirically show that carbon fibre reinforced cement-based screed exhibits the best conductivity using carbon fibres with approximate aspect ratios around 400. Based on percolation theory, the fibre volume content suitable for electrical resistance heating was found to be 1 to 2% vol. of carbon fibres. Graphite or silver electrode were used. A permanent heating of carbon fibre reinforced composite at 60ºC for 4 weeks caused no measurable loss of strength. using graphite or silver electrodes for contacting purposes.

Furthermore, it was shown that embedding a grid of electrodes into fibre reinforced cement plate opens up the possibility to heat selected areas of the plate up to 100ºC by applying an AC voltage of 12 V [11].

On the other hand, another research proved the feasibility of creating conductive concrete tiles by experiment, energy consumption analysis, and numerical simulation. Nine conductive concrete tiles were fabricated to test an indoor radiant heating system (see Figure 2.16.). Thermal sensors and an auto-power control switch were integrated into the system. The electrical circuit developed for the heating system combined a number of parallel and series connections to minimize the risk of overload, caused by the high current of the household AC, and to facilitate detection and repair if the system malfunctions.

A 2m high room thermally insulated was built to investigate the temperature distribution in the room under radiant heating.

It was concluded that using 20mm thick conductive concrete tiles using a steel wire mesh exhibited excellent electrical heating characteristics, increasing 52ºC in one hour under a 36V AC power. Moreover, the results also shown that the floor system was also effective for radiant heating applications increasing 4.5ºC in 10 minutes [14] (see Figure 2.17.).


*Figure 2.16 Radiant heating floor system [14]*

*Figure 2.17 Finished radiant heating floor [14]*

#### *2.4.3.5.2. De-icing concrete pavements*

The application of conductive concrete as ice controller on different transportation infrastructures, such as highways, interchanges, bridges, airport runways, increase the drivers' safety, while not compromising the durability of the structures with the use of substances that can damage it.

De-icing concrete pavements has been the most widely studied heating functionality of conductive concrete. Consequently, is the application in which more admixture materials have been tested and so, with a higher variety of characterisations.

Some researchers have chosen carbon fibre heating wires to develop self-heating concrete pavement. The advantage of this addition is that its disposal and orientation is made separately from the concrete mix, so that it is much easier to control its dispersion and so the homogeneity of heat production in the final product. This embedded method inside concrete slabs has also been verified, showing that, with an input power of 1134 W/m$^2$, the temperature on the slab surface rises from -25 °C to above 0 °C in 2.5 h at an approximate rate of 0.17 °C/min [45].

Others have focused on the heating effect produced by the electric current passing through a cement that has been added with carbonaceous materials such as carbon nano-fibres (CNF), carbon nanotubes (CNT), carbon fibre powder (CFP) and

graphite powder (GP), all with high electrical conductivities and capable of reducing the electrical resistance of the resulting cementitious material.

For this type of model, the concrete element acts like a resistance transforming electrical into heat due to the Joule effect. It such a way, the reduction obtained with the use of nanotubes is very high, achieving electrical resistances which are even 100 times smaller than the material without additions. Whereas, the addition of materials such as graphite powder or carbon fibre powder produces small reductions in the electrical resistance, which are normally added in smaller amounts.

The performance of these materials depends on the temperature reached and the amount of water present in the sample, whose influence is large since it can be evaporated during heating, the type of carbonaceous materials used influences the electrical resistance of the sample and the electric power that can be applied.

The moisture content of the samples is an important factor to be considered. The higher the moisture content of the sample the more conductivity, the more power can be applied and higher surface temperatures can be achieved [10].

But the most commonly used admixture is the carbon fibre and micro-fibre and, carbon powder [4]. These materials enhance the performance of self-heating concrete pavements with their excellent properties.

Researchers from the University of Arkansas, US, have developed an anti-icing airfield pavement using conductive concrete and renewable solar energy for airport runaways [21]. This approach maintains the concrete slab surface at an above- freezing temperature using direct current energy supplied by a photovoltaic and battery system (see Figure 2.18.).

*Figure 2.18 Thawing system test in a local airport [21]*

To test this approach, the University of Arkansas Engineering Research Centre constructed a series of conductive concrete overlay test sections. The thermal mass properties of concrete were used in this work to minimize energy demands. Energy was continually supplied to the concrete mass to maintain a uniform temperature and, therefore, to negate the need of an energy surge to remove snow.

Although the conductive concrete test sections showed some heat gain from the photovoltaic energy system, the overall heat gain was not sufficient to ensure reliable snow-melting capabilities during cold and windy conditions. Additionally, the costs for additional photovoltaic cells and batteries necessary to supply the energy needed for the system would result in poor cost-to-benefit ratios.

Also in the US, the Federal Aviation Administration (FAA) The Federal Aviation Administration (FAA) has been searching for a cost-effective and durable heated pavement technology for large-scale implementation for snow and ice removal at main hubs. The asphalt around the gates at a terminal is always congested due to activities by the ground crew, unloading and loading the passengers, luggage, waste disposal, fuelling, meals and other services. Snow and ice accumulation on the asphalt slows down these operations and causes delay of flights.

Therefore, they are currently funding a project to develop a cost-effective conductive concrete that yields the lowest cost, while providing adequate mechanical strength, long-term durability and de-icing performance. The scope of work includes selecting conductive materials, conducting mechanical and accelerated durability tests on CC test specimens, and evaluating the heating characteristics of the various mix designs in a laboratory freezer. The CC developed has met or exceeded the required mechanical strengths for highway and airfield concrete pavements. It has also showed good durability and should provide an anticipated service life of 25–30 years.

A 3 × 6m and 150mm thick test pad was constructed outdoors using the most cost-effective mix developed and it was energised during the 2015–16 snowstorms. The result presented in the illustration below shows the excellent de-icing performance of the test pad (see Figure 2.19.). The operating costs range from \$0.02 to \$0.04/$ft^2$ and is maintenance free. The conductive concrete de-icing technology is far superior to its peer technologies. The cost of the concrete is approximately \$400/$m^3$.

*Figure 2.19 Heated test pad after a snowstorm on 27-28 December 2015 [57]*

This project demonstrates that CC technology is affordable for large-scale implementation. The project will run through September 2016. If the FAA is satisfied with the findings from this study, the Administration would implement a 46 × 12m test asphalt section at its Technical Centre at the Atlantic City International Airport, New Jersey.

Although the cost of CC is about twice that of regular concrete, there is tremendous life-cycle cost savings compared to the use of regular concrete with other de-icing means. The additional cost is justified by its superior strength (about 1.5 times that of regular concrete), its low operating cost and being maintenance free. Conductive concrete also offers intangible benefits such as saving time, saving money and saving lives.

However, the development of this application for steel bridge decks is quite different from the previous ones. Generally, it is carried out using conductive gussasphalt concrete. Gussasphalt is a paving mixture which can be poured or cast in place that can be described as a special mastic type paving mixture. Its behaviour depends on the properties and relative proportions of asphalt cement and mineral filler. It forms a practically void less pavement surface that can be achieved without the use of rollers or any other compaction equipment. It is composed of crushed stone, sand, mineral filler and asphalt cement, and its softness or hardness is controlled by either the use of asphalt cement of different consistencies or by slight adjustment in the asphalt content [42].

A group of researchers from the Chang'an University, China, have developed a steel bridge deck that act as a heat conductor using conductive gussasphalt concrete pavement, for snow- and ice-melting [7].

They stated that the snow- and ice-melting effect and energy usage of steel bridge deck pavement are affected by the heat-transfer rate and temperature change in the middle of the combination structure when using conductive gussasphalt concrete (CGA). To determine the heat conduction effect and the snow melting time of conductive gussasphalt concrete pavement, they derived a particular heat conduction estimation method and a theoretical equation of the CGA combination structure.

Afterwards, they prepared a CGA combination structure with spreading carbon fibre in the middle of the CGA layer and evaluated the heat conduction effect and the time required to reach and maintain the temperature above 0ºC of different CGA combination structures. In this manner, with the estimation results and weather conditions, they could turn on or off the power ahead of time to improve the de-icing efficiency and save energy.

#### *2.4.3.5.3. Heated deck of the Roca Spur Bridge, Nebraska*

It is considered the mother of all conductive concrete applications. The heated deck of Roca Spur Bridge is the first implementation in the world using conductive concrete for de-icing. The three-span highway bridge over Salt Creek at Roca, Nebraska, USA, is 46m long and 11m wide and located near Highway 77 South. The Bridge construction was completed in November 2002 and the heated deck control system was finished in March 2003.

The technology provided an environmentally friendly solution to the looming crisis of water supply contamination by road salts, especially from bridge run-off over streams and rivers. It is also beneficial to rural communities and residents that are at a great distance from plough truck dispatch centres.

Conductive concrete mixed developed contained 1.5% vol. of steel fibre, micro-fibre and steel shavings and around 15% vol. of carbon powder for the bridge deck cover, aiming at providing an adequate resistance and an adequate thermal power density to melt ice at very low temperatures.

For each slab, two 9x9x0.6cm iron angles with 1m space in between which act an electrode, as shown in the Illustration above (see Figure 2.20.), and coiled sleeves welded at one of the extremes of the iron angles producing the electrical connection.

*Figure 2.20 Iron angles electrodes and wiring disposal*

The de-icing performance of the heated deck was monitored from 2003 to 2008 by the Nebraska Department of Roads. Powered by a 3-phase, 208V AC source, the de-icing system performed exceedingly well. One of the corresponding temperature–time histories during the de-icing operation is presented below (see Figure 2.21.). On average, the energy cost for the heated deck was about US$85/day (£60) during a major winter storm [57].

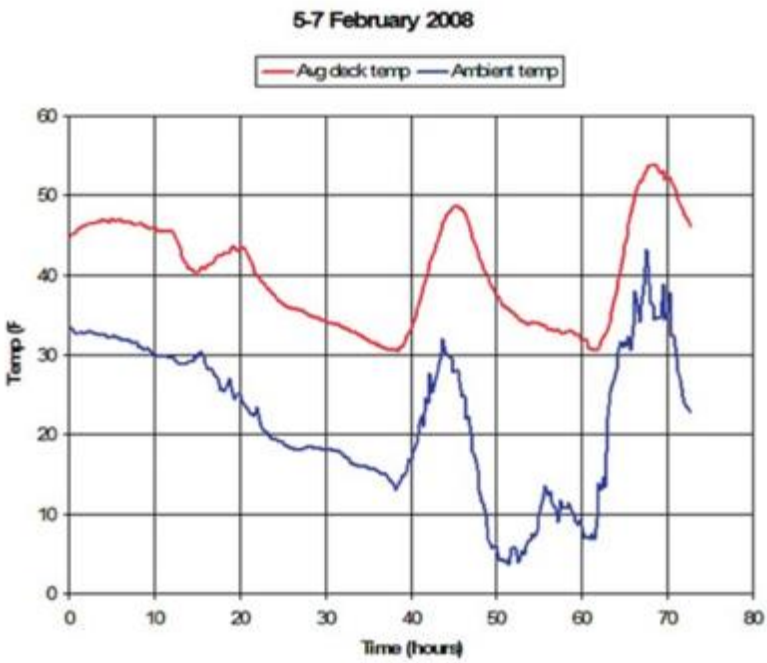


*Figure 2.21 Average deck temperature vs air temperature – 6 February 2008 [57]*

Analysing the construction costs, the total construction cost of the de-icing system of the bridge was 193,175 $, a cost per conductive unit of 59$/$m^2$.

In the table below, a comparison of the costs of installing and running between different de-icing systems deducted from this project is presented (see Table 2.3.).

It is expected that the construction costs of conductive concrete infrastructure will drop significantly, when this type of technology is widely accepted, which constitutes the main disadvantage of the system, nowadays. However, it can be seen that the costs for running the system are significantly smaller than any other type.

| De-icing system | Initial cost | Annual operational cost | Power consumption |
|---|---|---|---|
| **Automated spray system** | $600,000 | $12,000 | Not applicable |
| **Electric heating cable** | $54/$m^2$ | $4.8/$m^2$ | 323-430 W/$m^2$ |
| **Hot water** | $161/$m^2$ | $250/storm (76mm snow) | 473 W/$m^2$ |
| **Heated gas** | $378/$m^2$ | $2.1/$m^2$ | Not available |
| **Conductive concrete** | $635/$m^2$ | $0.81/$m^2$/storm | 350 W/$m^2$ |

*Table 2.3 Comparison between different de-icing systems [57]*

# 3. EXPERIMENTAL CAMPAIGN

## 3.1. INTRODUCTION

This section presents a detailed work plan on the testing, analysis, characterization and modelling of the material developed in this project. However, in order to present a background for the analysis of the material, the manufacturing process will also be presented and evaluated, even though it was previously performed. The main objective of this chapter consists in the experimental evaluation and characterization of the manufactured samples with only one type of cementitious concrete material combined with two types of fibres and different additions, in order to compare them. So as to perform an electrical and thermal characterisation of the composite materials and verifying the viability of using recycled carbon fibres for the development of multifunctionality.

For the experimental production of the mortar samples with carbon fibre, many of the aspects reflected in the state of art section were considered. However, within the framework of this technical research several determinant factors intervened.

On the one hand, the materials used for the concrete matrix, where materials available at Escofet 1886 S.A., initially diverting as little as possible from the most frequently used raw materials. In this manner, it allowed us a quick access to the raw material, equipment and facilities available for conducting the first experimental campaigns.

On the other hand, the recycled carbon fibres used in the project, were initially selected following economical and maximum availability criteria, permitting us to ensure a regular supply of fibres during all the process, with economical determinants affordable since the beginning of the tests.

Besides, observing some of the quoted researches about the obtaining of recycled carbon fibres by means of the pyrolysis method and how satisfactory where the results, obtaining almost unchanged fibres, provided the department enough confidence to use it in previous reaches. So that after the promising results obtained previously, it was used also in this project.

In order to study the behaviour of the samples with electrical current flow, different dosages of carbonaceous materials were employed, either with an addition of two different sizes of recycled carbon fibres or putting in an extra addition of natural

graphite flakes. These percentages were chosen according to the electrical properties of the materials. The dosages are expressed in terms of the amount of cement used.

The tests were distributed in two different campaigns as explained subsequently:

- 1st Campaign: which consisted in testing the electrical properties and the consistency of the material, using samples of 40x40x160mm

- 2nd Campaign: which consisted in several heating tests, using plates of 300x600x40mm and beams of 10x10x400mm, with different electrodes combinations.

The samples were submitted to different tests, depending on the state of the matrix and the type and percentage of fibre addition, in order to characterise the material properties in different functionalities.

As it has been described before, the basic idea of using multifunctional conductive cementitious materials lies in structural implantation embedded to new non-structural functionalities. Therefore, after manufacturing a set of samples of mortar with recycled carbon fibre and natural graphite flakes admixtures, they were submitted not only to compression and flexural tests, following the UNE-EN 196-1. But also, to electrical tests, so as to study the conductivity and resistivity of the material, and thermal tests, in order to estimate the thermal properties of the material and see if a self-heating system could be developed.

The chapter is organized as follows. First, the work plan will be presented and straightaway the manufacturing of the samples will be introduced, where different production aspects will be described, together with a short description of the materials used. Second, the materials and the different dosages that were used for different kinds of sample will be analysed and characterised. Third, the characterisation process of the samples of each of the different behaviours will be defined, following the Spanish regulations of mortar manufacture UNE-EN 196-1, with some variants due to the novelty of adding recycled carbon fibre and graphite powder and, because special characteristics need to be adopted in the samples for the electrical and thermal characterisation.

## 3.2. WORK PLAN

The operations of the experimental process were designed aiming at reproducing the industrial conditions, so as to make possible that the final result of the project could be easily implemented afterwards on a production scale. Therefore, apart

from a previous selection of accessible materials and compounds, all the manufacturing processes were conducted using the means available in the factory, focussing on the lab only for the most specific characterization of the materials.

The production process started with concrete matrix dosages typically used in the manufacturing process of urban furniture and architectonic façades. With two different dosages of admixture, either recycled carbon fibres in two different sizes or putting in an extra addition of natural graphite flakes. These percentages were chosen according to the electrical properties of the materials. The dosages are expressed in terms of the amount of cement used.

The samples were submitted to different tests, depending on the state of the matrix and the type and percentage of fibre addition, in order to characterise the material properties in different functionalities.

Firstly, for the electrical conductivity characterisation, the samples where submitted to different voltages, in order to know the conductivity and the resistivity of the material, which indicates the functionality of the material and the variation of its conductive properties.

Then, in order to characterise the heating behaviour of the material, the samples were submitted to a series of heating test, changing form each the voltage, the time of the cycles and the moisture of the samples. Due to the fact that the heating degree of the samples depend on the exposure time, the temperature reached and the amount of water present in the sample. Different tests were performed for cycles of 1h, 3h, 4h, 8h and 48h, the last one alternating connected and disconnected periods, to analyse the heating and the cooling behaviour.

After the heating tests were performed, all data was collected and analysed by means of the Joule effect, considering impedance, power, effective voltage and effective current.

Subsequently, the results obtained from the analysis and characterisation of the heating functionality were compared with an existing model of the heat and thermal control behaviour, so as to see if the test results and the modelling results coincided.

This experimental campaign was designed aiming at fulfilling the following specific objectives:

- Analysing and characterizing the electrically conductive behaviour, and the resistivity of the composite material.
- Analysing and characterizing the thermal conductive behaviour and its performance as a self-heating material.

- Modelling the heating performance of the conductive concrete.

- Studying the influence of the different admixtures in the overall performance of the composite cementitious material.

## 3.3. COMPOSITION OF THE COMPOSITE CEMENT-BASED MATERIAL

### 3.3.1. Concrete matrix

The cementitious nature matrix used is presented in the following table (see Table 3.1.), together with the dosage of aggregates, additions and additives.

For this project, ultra high performance concrete was used. A CEM I 52,5 R cement was used in big proportions. The aggregates used were a siliceous sand with maximum particle size of 0,5mm (see Figure 3.1.) and a limestone fine aggregate, called Betoflow, with maximum particle size of around 1mm. By the same token, superplasticizer additive, called MasterGlenium ACE 425, based on carboxylate was used and viscosity modulator additive based on siliceous nano-particles, called Meyco ms 685.

| UHPC CONCRETE DOSAGE | | | |
|---|---|---|---|
| **Materials** | | UHPC | |
| | | Compound | Content (kg/m$^3$) |
| **Cement** | | CEM I 52,5 R | 800 |
| **Siliceous sand** | | Siliceous sand 60/70 | 1161 |
| **Limestone fines** | | Betoflow | 200 |
| **Additives** | **Superplasticizer** | Glenium ACE 425 | 30 |
| | **Nano-silica** | Meyco ms 685 | 57 |
| **Water** | | | 110 |

*Table 3.1 UHPC Concrete matrix dosage*

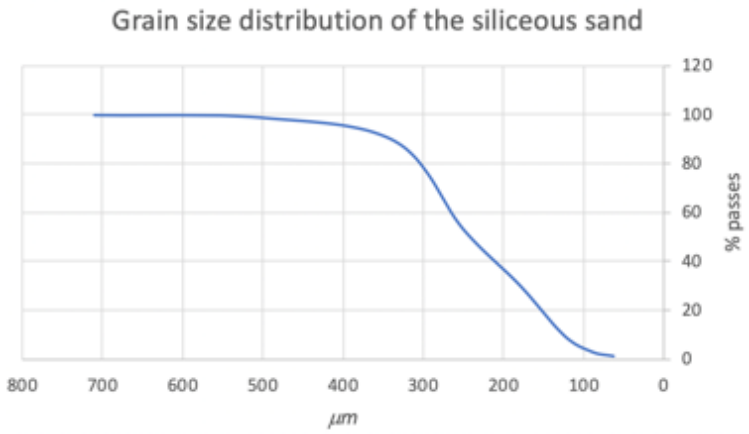


*Figure 3.1 Siliceous sand grain size distribution*

### 3.3.2. Recycled carbon fibre

The carbon fibre used in this conductive concrete has been supplied by the company "ELG Carbon Fibre LTD", located in the United Kingdom. It comes from a primary recycling process of rests of carbon fibre reinforced composite materials' compounds. They can be either trimmings or defective pieces or raw material with deteriorated resin pre-coated, etc. The main origin of these residues are companies dedicated to the manufacture of compounds for the aerospace, automotive and similar industries.

For this specific case, the carbon fibre is obtained by shredding and subsequent pyrolysis process in order to eliminate the polymeric resins impregnated to the fibre. The resulting fibre is presented as chopped carbon fibre tow in two different sizes, 6mm and 12mm lengths (see Figure 3.2.). The precision of the chopped fibres offers higher structural and electrical properties compared to milled fibres and are defined as ideal as reinforcing material for thermoplastic injection moulding compounds, cement reinforcement, coatings and elastomers (see Table 3.2.).

| Properties | Values |
|---|---|
| **Carbon fibre content (%)** | 100 |
| **Fibre diameter (µm)** | 7 |
| **Fibre density (kg/m$^3$)** | 1800 |
| **Fibre length (mm)** | 6 (±1) / 12 (±1) |
| **Sizing content (%)** | < 1.5 |
| **Metal contamination** | < 0.1g / 1000g |
| **Packaging (kg)** | 15 |
| **Tensile strength (MPa)** | 4150 |
| **Young modulus (GPa)** | 252 |
| **Electrical conductivity (S · cm$^{-1}$)** | 100-1000 |

*Table 3.2 Carbiso$^{TM}$ CT6/12 recycled carbon fibres properties (ELG Carbon Fibre LTD)*

*Figure 3.2 CarbisoTM CT6/12 chopped recycled carbon fibre(ELG Carbon Fibre LTD)*

### 3.3.3. Natural graphite flakes addition

An addition of natural graphite flakes 9580L is added in 1.65% vol. to the samples which already contain recycled carbon fibres to boost the electrical and thermal conductivity, and compare the results with the ones from the material that only contains recycled carbon fibres. Throughput the project this addition treated as micronized carbon fibre.

The particle size distribution of this material is defined by a minimum percentage of material retained at sieve 0.425mm of 10-30% and at sieve 0.300mm of 80%. Moreover, its main properties are presented in the table below (see Table 3.3.).

| Properties | Values |
|---|---|
| **Carbon content** | Min 95% |
| **Density** | 0.65-0.85 g/ml |
| **Ash** | Max 6% |
| **Moisture** | Max 0.5% |
| **Specific weight** | 2.1-2.3 g/cm$^3$ |

*Table 3.3 Natural graphite 9580L addition properties (Minerals I Derivats, S.A.)*

### 3.3.4. Carbon fibre reinforced concrete dosages

The carbon fibre reinforced concrete, can be considered as the combination of a matrix and a reinforcement fibre, in order to form a composite material.

Both phases and proportions used, had an influence in the final properties of the resulting cement-based composite material as much in mechanical characteristics as electrical and thermal.

The obtaining of the dosages of the cement matrix (see Table 3.4.) and the proportions of additions were obtained from previous dosages of conductive concrete tested by the department in previous researches.

| | UHPC CONCRETE DOSAGE | | | | |
|---|---|---|---|---|---|
| | **Materials** | | UHPC | | |
| | | | Compound | Content (kg/m$^3$) | For 40L |
| **M** | **Cement** | | CEM I 52,5 R | 800 | 36 |
| | **Siliceous sand** | | Siliceous sand 60/70 | 1161 | 52.245 |
| | **Limestone fines** | | Betoflow | 200 | 9 |
| | Additives | **Superplasticizer** | Glenium ACE 425 | 30 | 1.35 |
| | | **Nano-silica** | Meyco ms 685 | 57 | 2.565 |
| | **Water** | | | 110 | 4.95 |
| | ***Total*** | | | 2358 | 106.11 |

*Table 3.4 Detailed dosage of the UJPC concrete for the samples*

Two different types of carbonaceous fibre additions were added to the cement matrix, with a corrected volume percentage 0.407% vol. of chopped recycled fibre Carbiso CT6/CT12 and 1.65% vol. of natural graphite flakes (see Table 3.5.).

| | Fibre additions content | | | |
|---|---|---|---|---|
| | **Materials** | UHPC | | |
| | | Compound | Content (kg/m$^3$) | For 40L |
| **A** | **Natural graphite flakes** | FCM-20 | 36 | 1.65 |
| **F** | **Chopped recycled carbon fibre** | FC-CT-05 | 9 | 0.407 |

*Table 3.5 Fibre additions content for both types*

Three dosage combinations were performed for the different samples of material as shown in the table below (see Table 3.6.), in order to be able to compare them and the effect of each of its addition for the characterisation of the material.

| **Dosage combinations performed for the different samples** | |
|---|---|
| **M** | Matrix |
| **M + F** | Matrix + Fibre |
| **M + A + F** | Matrix + Fibre + Addition |

*Table 3.6 Dosage combinations performed for the different samples*

## 3.4. MANUFACTURING AND MOULDING OF THE SAMPLES

### 3.4.1. Mixing process of all the compounds

For the production of the concrete sand the moulding of the samples, a reduced scale kneading station with capacity for 150L was used (see Figure 3.3.), with 3 rotating paddles hanging from a central axis. One of the paddles is equipped with an agitator the provides a better kneading energy.

*Figure 3.3 Kneading station and mixing rotating paddles*

In the kneading station the components of the dosage were added together with the fibres, following the specified order and mixing time (see Figure 3.5.) in the usual production process in factories. Generally, these standards stablish a mixing of the compounds from higher to smaller particle size, adding at the end of the process the water, the additives and, finally, the fibres (see Figure 3.4.). With these standards, all the dosages were performed in the same way, only changing the percentage of fibre content.

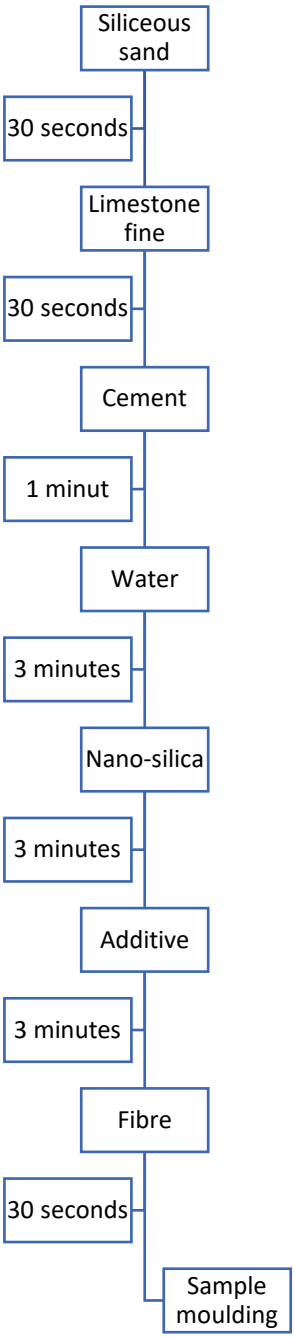


*Figure 3.5 UHPC concrete kneading sequence*

*Figure 3.4 Addition of the recycled carbon fibres to the mix*

### 3.4.2. Sample moulding system

#### 3.4.2.1. 1st Campaign

For the characterisations corresponding to the 1st campaign prismatic samples of 40x40x160mm dimensions were produced, of two different typologies depending whether they were used for electrical conductivity testing. I order to do this, several three samples production moulds for 40x40x160mm samples as the one presented below were used (see Figure 3.6.).

*Figure 3.6 Three samples production mould of 40x40160mm*

Moreover, the samples for the electrical properties' characterisation were kitted out with several connectors as shown in the illustration below (see Figure 3.7.), so that, afterwards, acted as electrodes for the electrical testing.

For the conductive electrodes stainless steel threaded shanks of 6mm diameter and 30mm length were used. They were placed in a plastic template in order to ensure its correct geometric siting and identification. The placing of these connectors was carried out after the filling and compaction of the concrete in the moulds, with concrete in a fresh state.

The curing process in the chamber of moisture was determinant for the selection of stainless steel connector, aiming at avoiding the corrosion of the steel elements during the curing process.

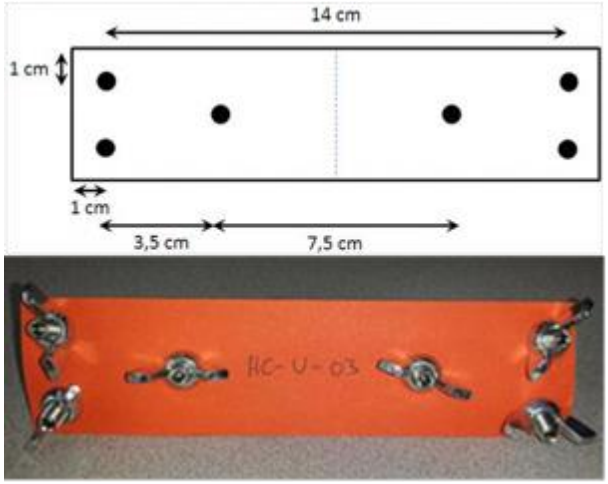


*Figure 3.7 Stainlees steel connectors placing in the prismatic samples*

For the 1st campaign, in order to make easier the identification of the samples, the following notation was implemented, which has been used in previous researches with this type of samples:

$$HC – U - C_f$$

Where:
HC: General reference to indicate the conductive concrete
U: Reference to the UHPC concrete type used
$C_f$: Numerical reference to the carbon fibre content in % vol.

#### 3.4.2.2. 2nd Campaign

In the 2nd campaign, two sets of samples are produced. On the one hand, prismatic beams (V) of 10x10x400mm and, on the other hand, slabs (P) of 300x600x40mm. The moulds used are presented below (see Figure 3.8. and 3.9.).

*Figure 3.9 Beam mould of 10x10x400mm*

*Figure 3.8 Slab mould of 300x600x40mm*

Besides, for every type of sample two different electrode disposal were used, A and B. The disposal A consisted in steel deployé sheets, whereas, the disposal B consisted of conductive electrodes of stainless steel threaded shanks of 6mm diameter and 30mm length.

Equally to the 1st campaign, the placing of these connectors was carried out after the filling and compaction of the concrete in the moulds, with concrete in a fresh state.

In this case, in order to make the identification of the sample easier, the following notation was used.

{V/P} – {A/B} – {M/MF/MAF}

Where:
{V/P}: Reference to the type of sample; V=Beam (Viga) and P=Slab (Placa)
{A/B}: Reference to the type of connector; A= steel deployé sheets and, B= conductive electrodes of stainless steel threaded shanks of 6mm diameter
{M/MF/MAF}: Indicates the presence and the type of addition; M=cement matrix, MF=cement matrix + recycled carbon fibre and, MAF=cement matrix + recycled carbon fibre + addition of natural graphite flakes

## 3.5. ELECTRICAL PROPERTIES

The electrical characterisation test was performed, in order to compute the conductivity and resistivity derived from the addition of recycled carbon fibre and natural graphite flakes. Following the literature study previously conducted, many researches coincided in defining the influence of fibres in the electrical conductivity with the following curve (see Figure 3.10.).

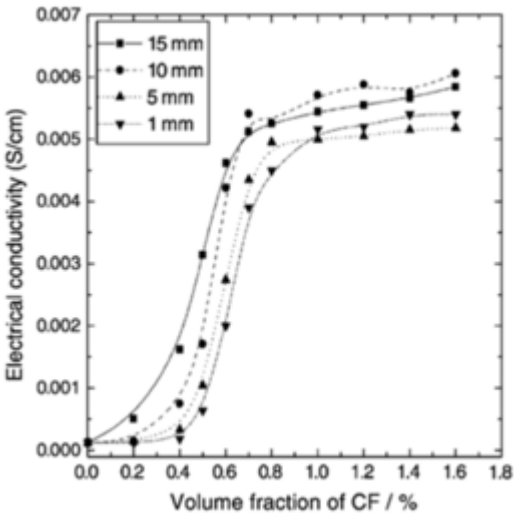


*Figure 3.10 Evolution of the conductivity with respect to the carbon fibre content and the fibre length*

It can be seen that in the section the increase of the conductivity is very slow and, suddenly, it increases drastically in a very short section from 0.4% vol. to 0.6% vol. This fibre content value is the so-called percolation threshold, in which a very significant increase of the conductivity occurs.

In order to determine the electrical resistance of the samples, different tests were conducted in the Laboratorio de Instrumentación y Bioingeniería of the UPC. The measurements were performed with an impedance analyst system called Hewlet Packard HP4192A, together with an amplification instrument that allowed to perform measurements at 4wires. Therefore, the impedances measurements were performed using the 4 wires configuration (4w), as well as the 2 wires configuration (2w). In such a way, the possible presence of parasitic resistances, caused by the introduction of electrical current through the electrodes, could be determined (see Figure 3.11.).

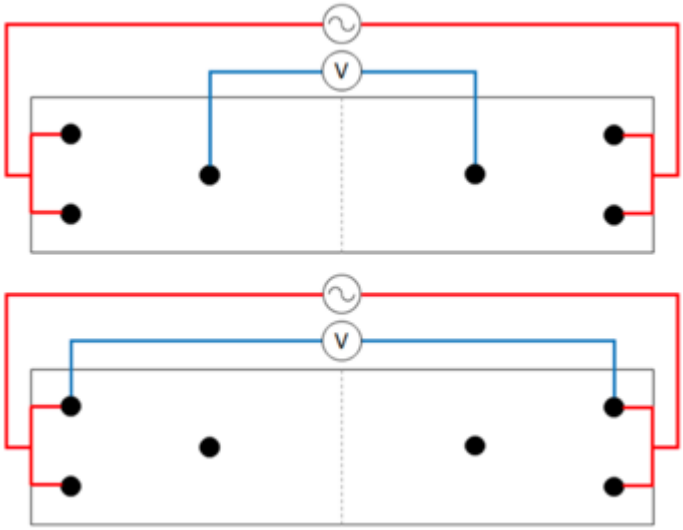


*Figure 3.11 Experimental assembly of the electrical resistance measurements, the upper diagram in 4 wires configuration and the lower in 2 wires configuration*

In the illustration bellow, the measurement equipment, as well as the experimental assembly performed, so as to make the extremes to act as a flat front. In this manner, it is possible to ensure a better homogeneity of the electrical resistance measurements (see Figure 3.12.).

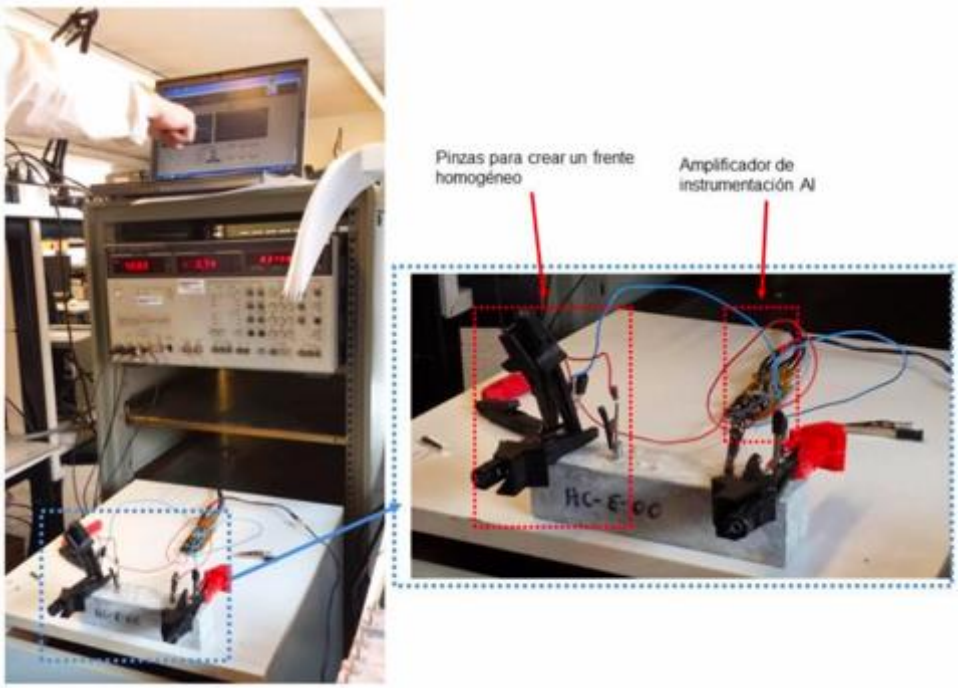


*Figure 3.12 Experimental assembly and equipment for the electrical resistance measurement*

The tests for the electrical characterisation of the conductive cementitious material consisted in fixing a voltage and evaluating the impedance, the phase, the resistivity, the conductivity and the frequency, along time. This process was performed 7 times, increasing the voltage fixed, starting from 0.9V, 1.4V, 7.4V, 14.5V, 30.5V, 60.7V and 90.4V, for each of the different composite materials.

The values obtained in the measurements are the electrical impedance Z [Ω] and the phase α [°]. The impedance is a relation between the electric voltage applied on the samples [V] and the electrical current that passes through them [A]. The impedance is defined as the sum of the resistance R [Ω] and the reactance X [Ω], when the voltage and the current are in phase difference, which normally occurs in alternating current circuits (see Equations 3.1., 3.2. and 3.3.), where j is the imaginary unit. However, when direct current is used or the alternating current circuit is very simple, the voltage and the tension are almost in phase. Therefore, the reactance is very low, so that we get only resistance. In this case, the Ohm's law applies.

$$Z = R + j \cdot X \tag{3.1}$$

$$R = Z \cdot \cos\left(\frac{\alpha \cdot \pi}{180}\right) \tag{3.2}$$

$$X = -Z \cdot \sin\left(\frac{\alpha \cdot \pi}{180}\right) \tag{3.3}$$

Once the material electrical resistance is obtained, from the measurements of the impedance, it is possible to compute the electrical resistivity of the material ρ [Ω·m]. The resistivity is the specific electrical resistance of each material to oppose to the passage of the electrical current and can be computed as shown in the equation below (see Equation 3.4.), where S is the cross-section [$m^2$] and l the length [m]. In this project, the magnitude l can vary being wither 0.07m for 4 wires configuration or 0.14m for 2 wires configuration.

$$\rho = R \cdot \frac{S}{L} \tag{3.4}$$

Hence, once the resistivity is obtained, the conductivity [S/m] can be computed, as it is the inverse of the resistivity (see Equation 3.5.).

$$\sigma = \frac{1}{\rho} \tag{3.5}$$

The first data obtained from the measurements performed, is represented by means of Bode's Diagrams, which is a type of plot used to characterise the answer of a system in frequency. In this specific case, it presents the impedance variation with respect to the variation of the applied alternating current frequency.

These diagrams are intended to relate, not only the variation of the impedances with respect to the increase of the electrical current frequency, but also, how the fibre content and its variation modify tis relation.

Another useful analysis, consists in obtaining the diagrams that relate the reactance with the resistance, called Nquist diagrams, which is interpreted as the variation of the impedance modulus with the variation of the fibre content.

## 3.6. THERMAL PROPERTIES

Once the electrical characterisation is completed and, having set a working framework with previous analysis of the mechanical properties, the thermal evolution characterisation is carried out. The characterization of these properties, had an initial objective, the evaluation of the thermal behaviour against a given electrical current. So as to verify the initial assumption, that the materials developed in this research would behave as low efficiency electrical conductors and, therefore, the major part of the electrical energy applied, would transform into head, as it had been proven in previous researches.

The main aim of this section of the project was characterising the thermal properties of this conductive cement-based material, in order to use it for self-heating and de-icing applications in urban furniture.

The thermal tests were performed in the 2nd campaign, using infrared thermometers for taking the measurements. In order to register the data, different electrode disposals were used. Disposal A consisted in steel deployé sheets, whereas, disposal B consisted of conductive electrodes of stainless steel threaded shanks of 6mm diameter and 30mm length, both presented in the sketches below (see Figure from 3.13. to 3.16.).

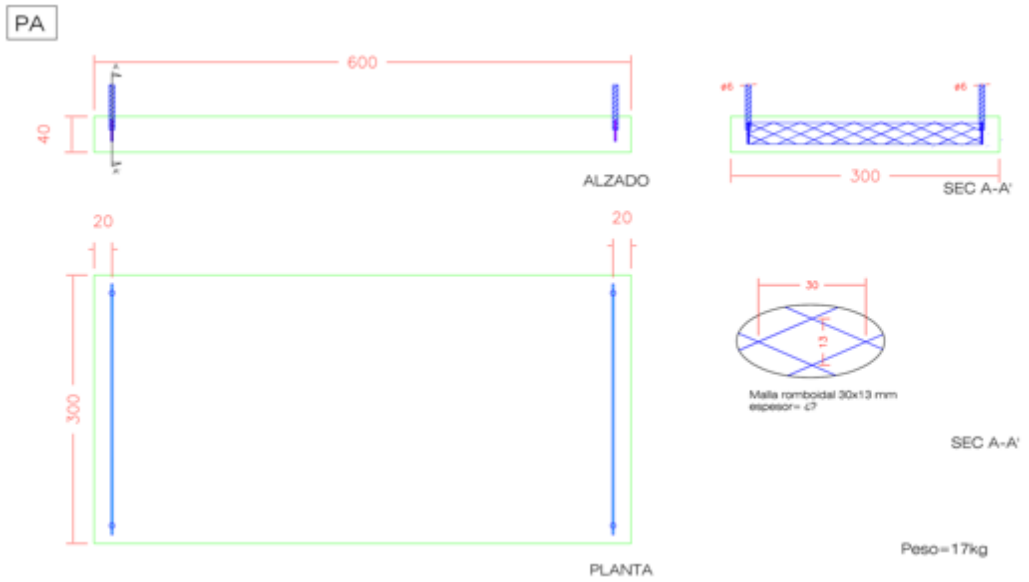


*Figure 3.13 Design of the conductive concrete slab sample 300x600x40mm with steel deployé sheets*

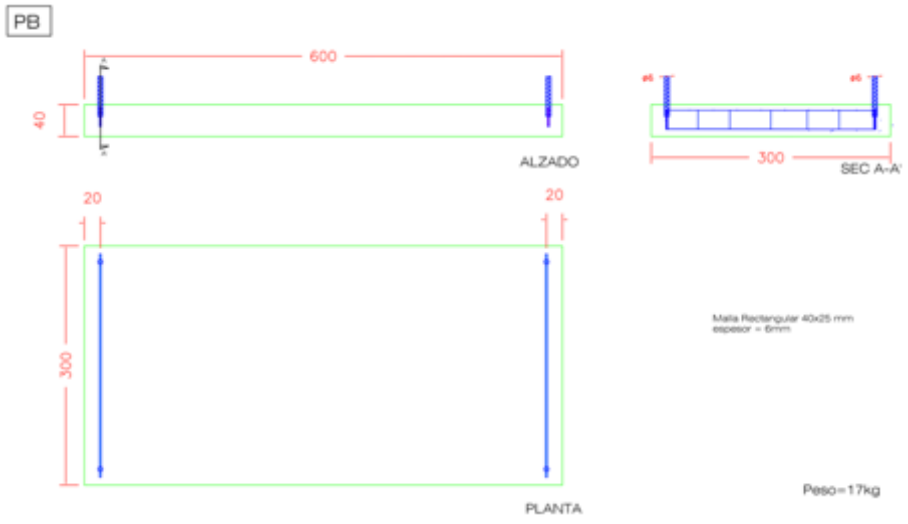


*Figure 3.14 Design of the conductive concrete slab sample 300x600x40mm with conductive electrodes of stainless steel threaded shanks of 6mm*

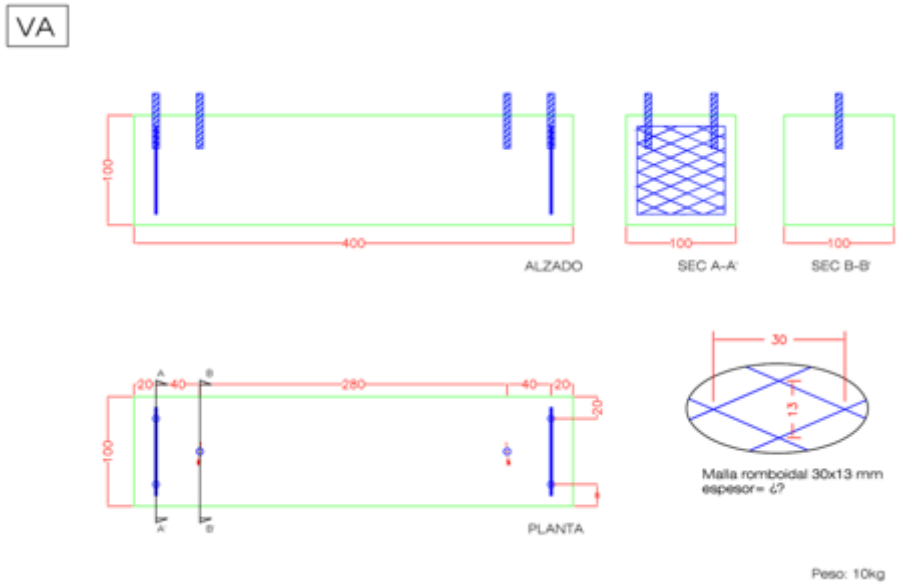


*Figure 3.15 Design of the conductive concrete beam sample 10x10x400mm with steel deployé sheets*

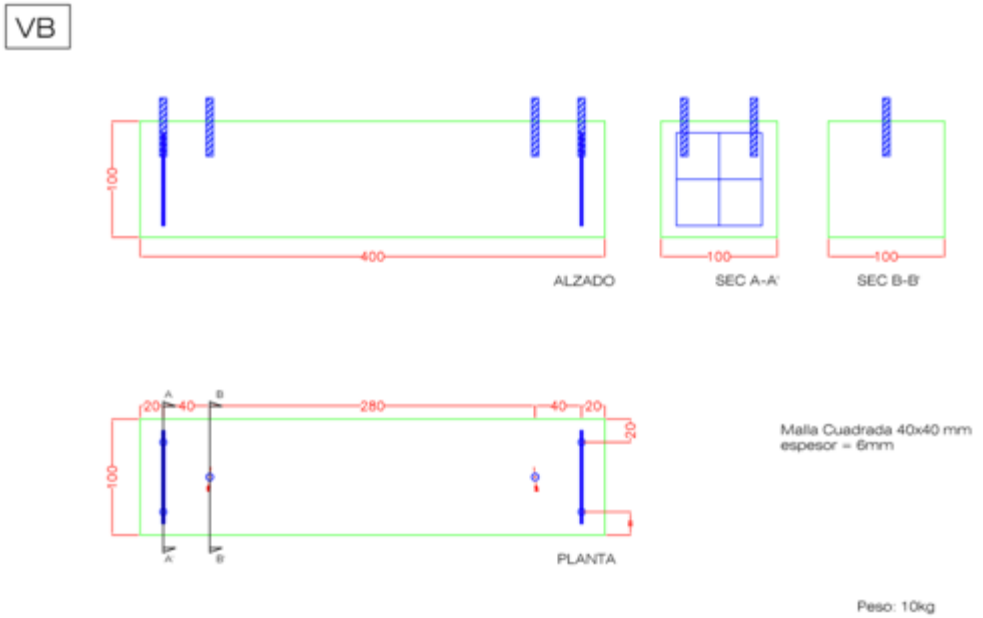


*Figure 3.16 Design of the conductive concrete beam sample 10x10x400mm with conductive electrodes of stainless steel threaded shanks of 6mm*

The thermal characterisations test campaign was carried out at the company Escofet 1886 headquarters.

In order to have a thermal characterization as wide as possible, the samples where submitted to 5 different tests changing the duration of the heating cycles and the moisture content. The heating cycles, were the time intervals during which the electrical current passed through the sample, generation heat. They ranged from 1,3,4,8 and even

48 hours, although, in the case of 48 hours, the total time interval was divided into sub-cycles of connection of 8 hours and disconnection of 16 hours.

Moreover, one of the test series was performed with the samples saturated of water in order to determine the influence of water in the electrical resistivity, and so, thermal conductivity. While each of the test cycles was performed applying various voltage differences 0.3V, 0.5V, 0.7V and 0.9V.

In the figure bellow, the measurement equipment, as well as the experimental assembly performed are presented (see Figure 3.17.).

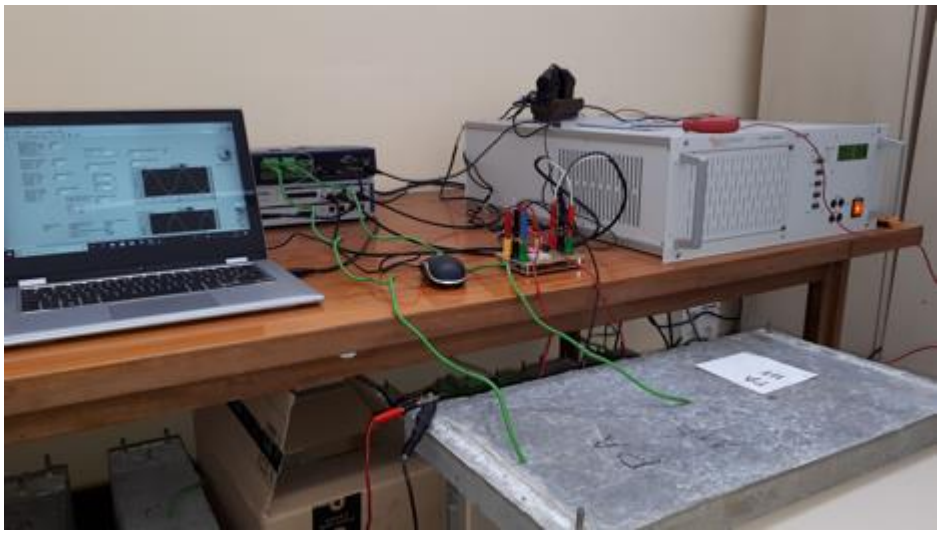

*Figure 3.17 Experimental assembly and equipment for the heat production and temperature increase measurement*

For the analysis and modelling of the heating process of the conductive concrete, a simplified approach of the system is taken, considering that in constitutes a very simple alternating current circuit formed by a generator, an impedance and a voltmeter, as the one presented in the illustration bellow (see Figure 3.18.).

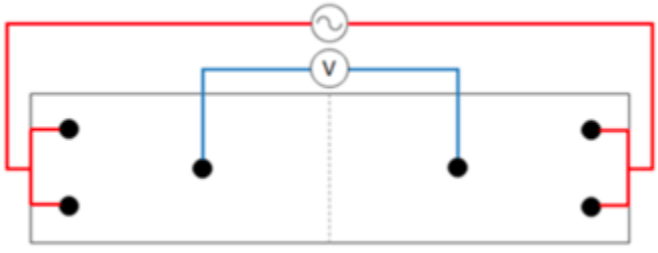


*Figure 3.18 Analysed circuit*

In this particular case, the impedance is only constituted by resistance as voltage and electrical current are in phase. Thus, $\alpha=0°$ and $Z=R\ [\Omega]$. Therefore, the Ohm's law

applies in this case, and the electrical resistance can be computed using the following equation (see Equation 3.6.).

$$R = \frac{V_{eff}}{I_{eff}} \tag{3.6}$$

The heating behaviour is produced due to the Joule effect, which states that a resistance transforms the electrical energy into heat. Therefore, if the electrical resistance is known, the electrical potential is also known and, the total electrical energy can be computed (see Equations 3.7. and 3.8.).

$$P = V_{eff} \cdot I_{eff} = V_{eff}^2 \cdot R = I_{eff}^2 \cdot R \tag{3.7}$$

$$E = P \cdot t \tag{3.8}$$

# 4. ANALYSIS OF THE RESULTS OF THE EXPERIMENTAL CAMPAIGN

## 4.1. ANALYSIS OF THE ELECTRICAL BEHAVIOUR

In this part of the experimental campaign, both conductive additions were studied apart, aiming at describing the properties of each carbonaceous material and their contribution to the conductivity of concrete. Each of the resulting conductive composite materials – FC-CT-05 and FCM-20 – was tested 7 times fixing a different value of voltage for every experiment from low to high.

The main results extracted from these tests were the phase, $\alpha[°]$, and the impedance, $Z[\Omega]$. So as to be able to compute values for resistivity and conductivity of the material which directly influence the development of thermal characteristic.

### 4.1.1. Correlation between the phase angle frequency dependence and the percolation threshold

In this section the analysis of the phase angle obtained in the conductivity tests is presented as a pre-requisite to understand the concrete impedance values and its electrical conductivity capacity.

Along these lines, it is important to consider the heterogeneity of this material, as a material containing conductive and dielectric phases.

The phase difference determined during the tests correspond to the existing difference between voltage and electrical current in AC. This phase difference can be higher or lower depending on the homogeneity level of the material and the percolation threshold.

Moreover, comparing the results of the material containing FC-CT-05 addition with the material containing a 1.65% vol. micronized carbon fibre addition which is above percolation threshold, the results and the patterns presented in the plots are quite different.

On the one hand, the material below percolation presents a much more random behaviour for low frequencies and it is very difficult to adapted to a representative function for all measurements. However, for higher frequencies it shows a more defined behaviour, increasing the phase value.

Whereas, on the other hand, the material containing FCM-20 in an amount above the percolation threshold have a very uniform and defined behaviour, following, even for low frequencies, a very similar shape for all 7 tests.

This effect is exhibited in the Frequency vs Phase semilogarithmic plot presented below (see Figures 4.1. and 4.2.).

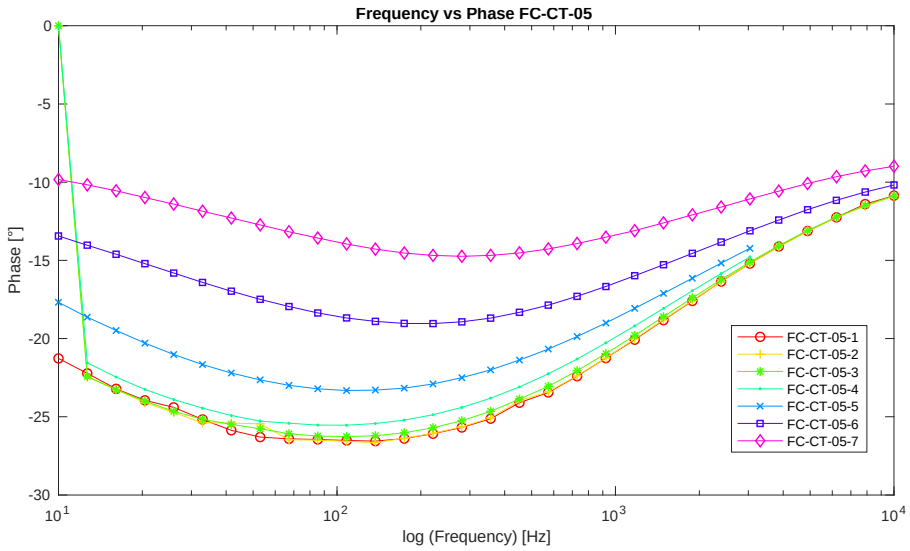


*Figure 4.1 Frequency vs Phase FC-CT-05 semilogarithmic diagram*

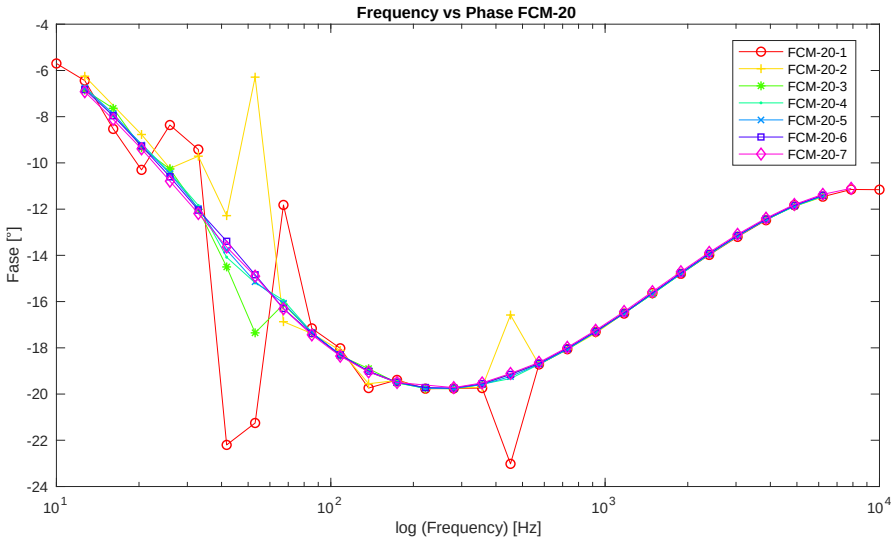


*Figure 4.2 Frequency vs Phase FCM-20 semilogarithmic diagram*

Aiming at analysing the phase behaviour with respect to the frequency, the data obtained from the tests has been processed and modelled, using a “polifit” coding of Matlab, in order to evaluate its tendency with a polynomial function (see Figure 4.3.).

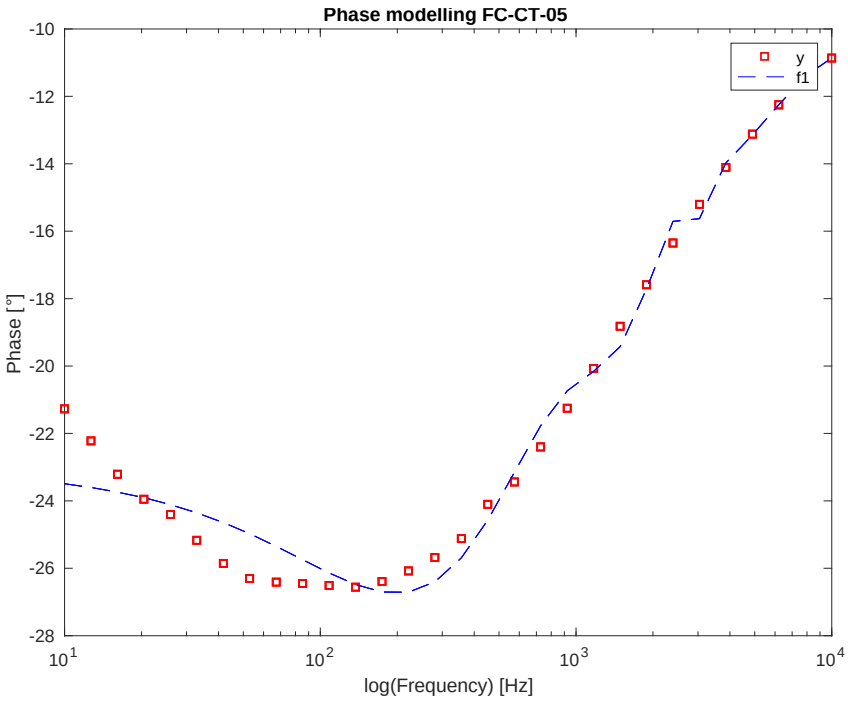


*Figure 4.3 Phase behaviour modelling for FC-CT-05*

The resulting approximation consisted in a polynomial function of degree 10, with the parameters and the $R^2$ accuracy coefficient presented below (see Table 4.1.).

| Material | Parameters | | | | | |
|---|---|---|---|---|---|---|
| | P1 | P2 | P3 | P4 | P5 | P6 |
| **FC-CT-05** | 1.049e-33 | -4.137e-29 | 6.83e-25 | -6.175e-21 | 3.346e-17 | -1.120e-13 |
| **FCM-20** | 2.377e-33 | -9.382e-29 | 1.55e-24 | -1.404e-20 | 7.620e-17 | -2.558e-13 |

| Parameters | | | | | |
|---|---|---|---|---|---|
| P7 | P8 | P9 | P10 | P11 | $R^2$ |
| 2.303e-10 | -2.787e-07 | 1.8e-04 | -0.045 | -23.062 | 0.979 |
| 5.280e-10 | -6.436e-07 | 4.234e-04 | -0.121 | -9.049 | 0.932 |

*Table 4.1 Parameters obtained from the adjustment of the phase values*

### 4.1.2. Impedance measurements

The analysis of the impedance measurements of the different dosages is presented using bode diagrams, which have proven to be the most representative and valuable manner to present the results in previous researches conducted by the department.

The plain UHPC concrete, has been proved to behave as an insulator in previous researches, exhibiting a small reduction of impedance at very high frequencies around $10^5$Hz, as a result of polarization effects that introduce a capacitance in parallel with the electrical resistance.

However, the incorporation of recycled carbon fibres to the cementitious mixtures drastically modifies the electrical behaviour of the material. It can be seen in the diagrams below that the impedance is reduced as the frequency of the applied current is increased. Large reductions in the impedance values are observed as the frequency is increased up to 10-$10^2$Hz. The decrease gradient is especially noticeable for the tests conducted with low voltages and rather softened for high voltages.

Comparing both addition types, there is a very clear difference in the impedance values presented in the diagrams below (see Figures 4.4. and 4.5.). In such a way, the impedance values for the FCM-20 addition are 45 time higher than the ones corresponding to the FC-CT-05, due to the nature of the material, the geometry and the dispersion. Furthermore, as described in the correlation of the phase and the frequency, the higher amount of micronized carbon fibre addition generates a much more uniform behaviour for all the different voltages tested as the frequency of the applied current is increased. Whereas, the lower percentage in volume of chopped recycled carbon fibre, produces a much more random and dispersed behaviour for low frequencies.

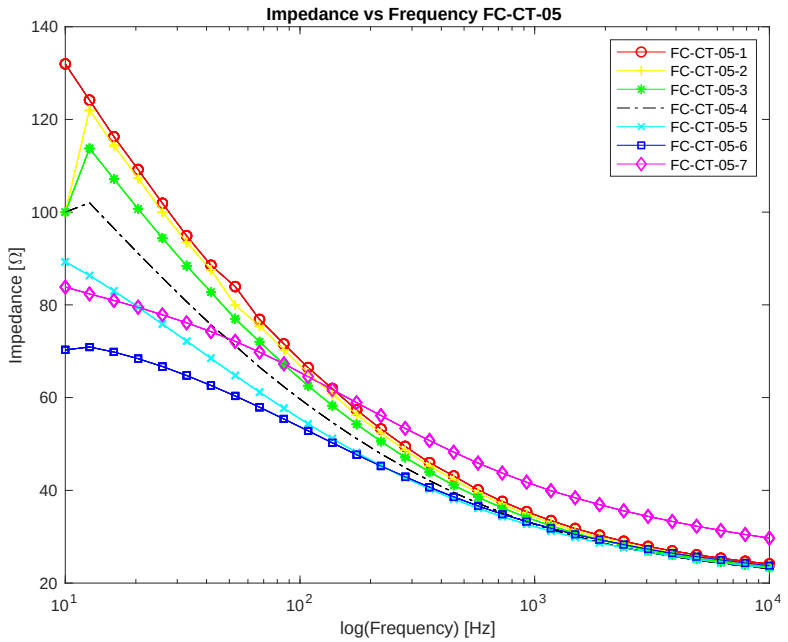


*Figure 4.4 Frequency vs Impedance FC-CT-05 semilogarithmic diagram*

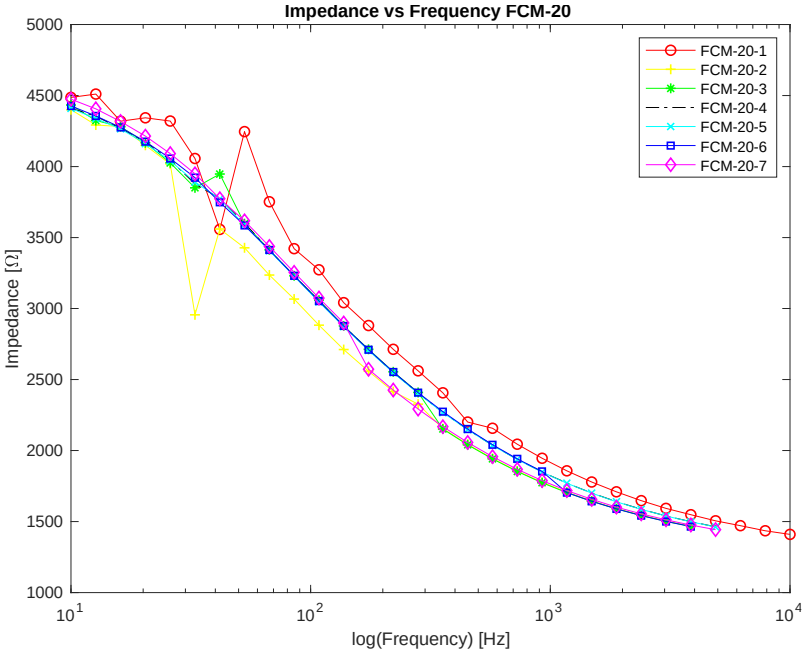


*Figure 4.5 Frequency vs Impedance FCM-20 semilogarithmic diagram*

Aiming at analysing the impedance behaviour with respect to the frequency, the data obtained from the tests has been processed and modelled with Matlab coding in order to evaluate its tendency. For this particular case, the correlation between both magnitudes was defined as a power law following the equation below (see Equation 4.1. and Figure 4.6.).

$$Z = a \cdot f^{b \cdot f^c} \tag{4.1}$$

Where Z is the impedance [Ω], $f$ is the frequency [Hz] and, a, b and c are the parameters of the approximation function.

In the following table, the results of the parameters and the $R^2$ coefficient for the accuracy of the approximation are presented for each material and each of the different voltages (see Table 4.2.).

| Material | Parameters | | | |
|---|---|---|---|---|
| | a | b | c | $R^2$ |
| **FC-CT-05-1** | 18.7294 | 2.5211 | -0.4805 | 0.9979 |
| **FC-CT-05-2** | 14.5102 | 2.3747 | -0.4261 | 0.9889 |
| **FC-CT-05-3** | 15.3286 | 2.3078 | -0.4351 | 0.9947 |
| **FC-CT-05-4** | 17.1063 | 2.2064 | -0.4563 | 0.9991 |
| **FC-CT-05-5** | 17.6449 | 1.9589 | -0.4502 | 0.9992 |
| **FC-CT-05-6** | 15.4776 | 1.5922 | -0.3868 | 0.9995 |
| **FC-CT-05-7** | 19.4715 | 1.4692 | -0.3758 | 0.9976 |
| **FCM-20-1** | 850.4594 | 1.7489 | -0.3875 | 0.9877 |
| **FCM-20-2** | 911.8860 | 1.7044 | -0.3975 | 0.9744 |
| **FCM-20-3** | 810.3526 | 1.7397 | -0.3793 | 0.9975 |
| **FCM-20-4** | 822.7771 | 1.7372 | -0.3822 | 0.9992 |
| **FCM-20-5** | 821.9786 | 1.7359 | -0.3820 | 0.9992 |
| **FCM-20-6** | 832.3567 | 1.7342 | -0.3836 | 0.9994 |
| **FCM-20-7** | 855.8517 | 1.7309 | -0.3865 | 0.9993 |

*Table 4.2 Parameters obtained from the adjustment of the impedance values*

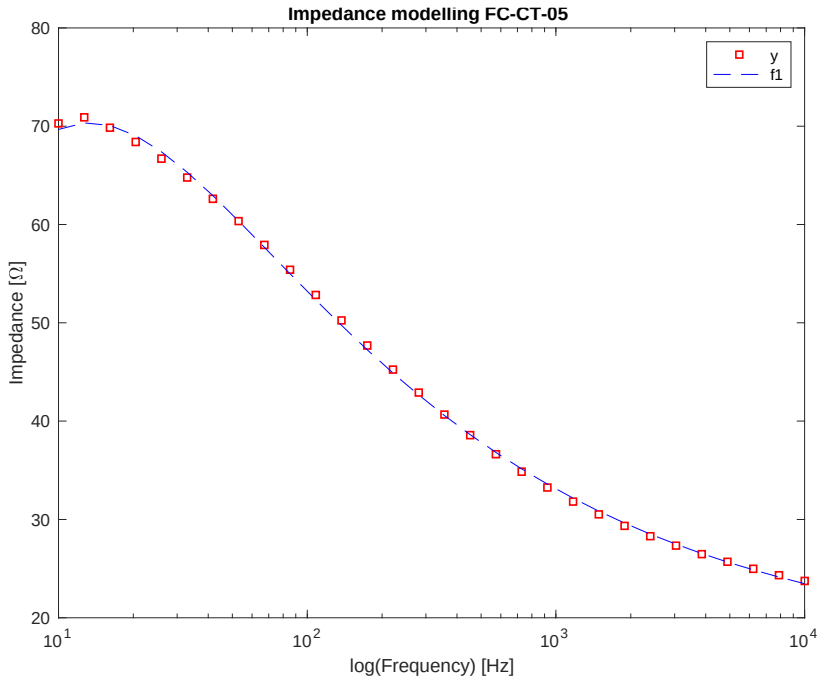


*Figure 4.6 Impedance behaviour modelling for FC-CT-05*

The electric behaviour exhibited by the conductive cementitious materials is based on the presence of two phenomena related with the existence of percolation paths. Along these lines, the carbon fibre reinforced carbonaceous materials frequently present a double percolation [58]. The first percolation is caused by the presence of carbon fibres in the matrix, which depending on the length of the fibre and the

percentage in volume provided, allow the generation of electrical conductivity in the system. The second percolation is associated with the presence of aggregates, which affect the existence of electrical conductivity in the cement paste.

This last phenomenon justifies the lower impedance observed in UHPC samples in which the aggregate size is significantly lower in this samples than in other standard concrete samples. Thereby, it allows a better development of electrical conductivity in the cementitious matrix.

### 4.1.3. Computation of the conductivity

Based on the impedance measurements it is possible to calculate the electrical conductivity of the material, by means of the following equations (see Equations 4.2. and 4.3.).

$$\rho = R \cdot \frac{S}{L} \tag{4.2}$$

$$\sigma = \frac{1}{\rho} \tag{4.3}$$

Conductivity increases with respect to frequency in a quite linear pattern. For higher frequencies, the conductivity is higher, because, even though the fibres are not perfectly dispersed along the sample or in the case of FC-CT-05 are a little bit below the percolation threshold, the electrical flux is increased creating a much more defined conductive path.

Comparing both addition types, there is a very clear difference in the conductivity values presented in the diagrams below (see Figures 4.7. and 4.8.). In such a way, the conductivity values for the FCM-20 addition are more than 10 times smaller than the ones corresponding to the FC-CT-05, due to high impedance and resistivity of the micronized carbon fibre addition.

Nevertheless, in this case, both materials present nearly identical behaviours with uniform patterns for both materials.

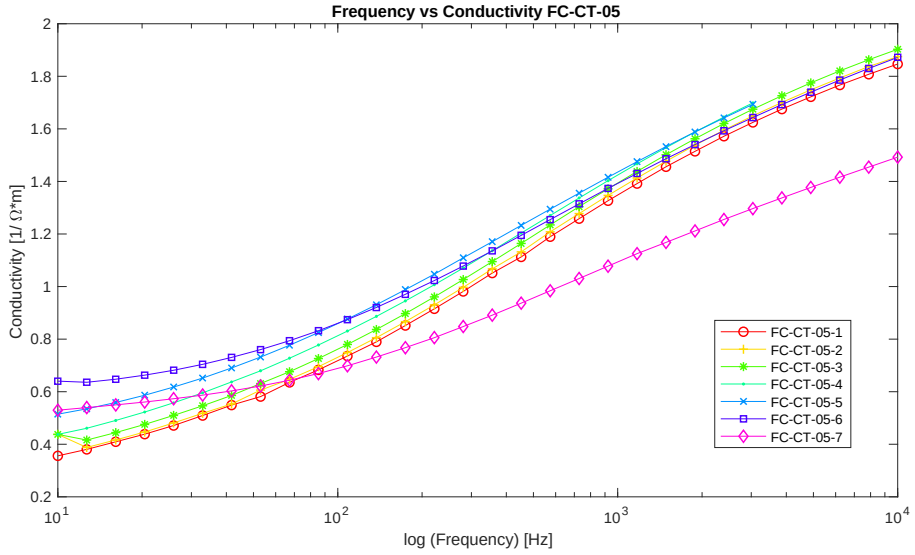


*Figure 4.7 Frequency vs conductivity FC-CT-05 semilogarithmic diagram*

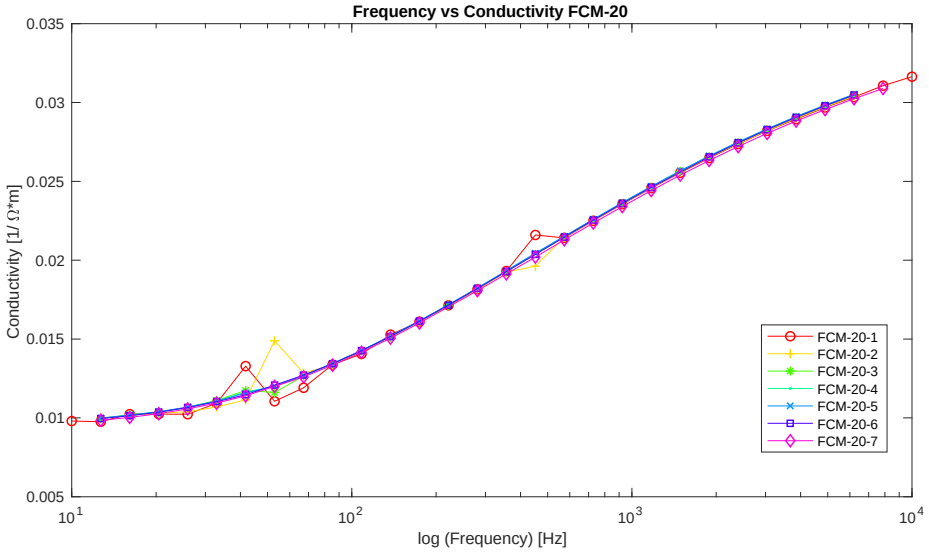


*Figure 4.8 Frequency vs conductivity FCM-20 semilogarithmic diagram*

Aiming at analysing the conductivity behaviour with respect to the frequency, the data obtained from the tests has been processed and modelled with Matlab coding in order to evaluate its tendency. For this particular case, the correlation between both magnitudes was defined as a logarithmic law following the equation below (see Equation 4.4. and Figure 4.9.).

$$C = a \cdot \ln(f) + b \tag{4.4}$$

Where C is the conductivity [S/m], $f$ is the frequency [Hz] and, a and b are the parameters of the approximation function.

In the following table, the results of the parameters and the $R^2$ coefficient for the accuracy of the approximation are presented for each material and each of the different voltages (see Table 4.3.).

| Material | Parameters | | |
|---|---|---|---|
| | a | b | $R^2$ |
| **FC-CT-05-1** | 0.1975 | 0.0245 | 0.9810 |
| **FC-CT-05-2** | 0.2370 | -0.2910 | 0.9882 |
| **FC-CT-05-3** | 0.2372 | -0.2651 | 0.9901 |
| **FC-CT-05-4** | 0.2337 | -0,2084 | 0.9931 |
| **FC-CT-05-5** | 0.2203 | -0.1014 | 0.9929 |
| **FC-CT-05-6** | 0.1975 | 0.0245 | 0.9810 |
| **FC-CT-05-7** | 0.1507 | 0.0584 | 0.9740 |
| **FCM-20-1** | 0.0036 | -0.0011 | 0.9789 |
| **FCM-20-2** | 0.0037 | -0.0018 | 0.9804 |
| **FCM-20-3** | 0.0037 | -0.0017 | 0.9830 |
| **FCM-20-4** | 0.0037 | -0.0017 | 0.9840 |
| **FCM-20-5** | 0.0037 | -0.0017 | 0.9840 |
| **FCM-20-6** | 0.0037 | -0.0017 | 0.9840 |
| **FCM-20-7** | 0.0037 | -0.0017 | 0.9840 |

*Table 4.3 Parameters obtained from the adjustment of the conductivity values*

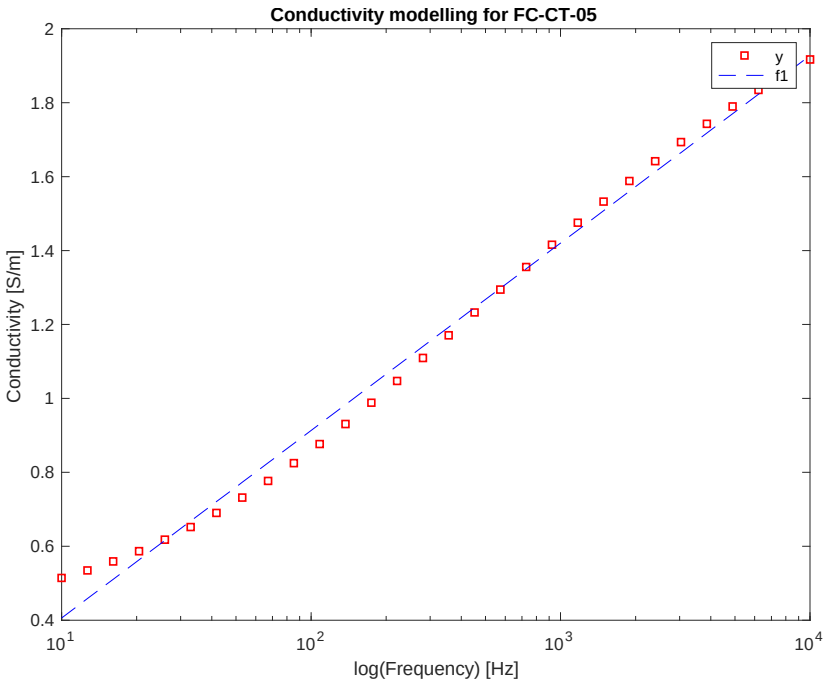


*Figure 4.9 Conductivity behaviour modelling for FC-CT-05*

Besides, taking the frequency value of 50Hz, which is the usual value for domestic alternate current in Europe, the conductivity values have been evaluated for each material with respect to the voltage as presented in the two diagrams below (see Figures 4.10. and 4.11.).

It can be seen that for the FC-CT-05 there is a quite linear increase of the conductivity with an increase of the voltage applied up to a pick value corresponding to 0.76 S/m and 60,7 V and then a noticeable decrease occurs.

However, the behaviour is completely different for the FCM-20 material, which present the conductivity pick up to 0.01223S/m at a very low voltage of 1.4V and then exhibits a very steep drop up to very low values of conductivity and remains barely unchanged with the increase of the voltage applied.

The physical characteristics of the fibres themselves can have an important influence in these results, presenting possible difficulties of distribution in the matrix or limiting characteristic properties of the materials, like the Young's modulus in order to adapt and fit in the cementitious material skeleton.

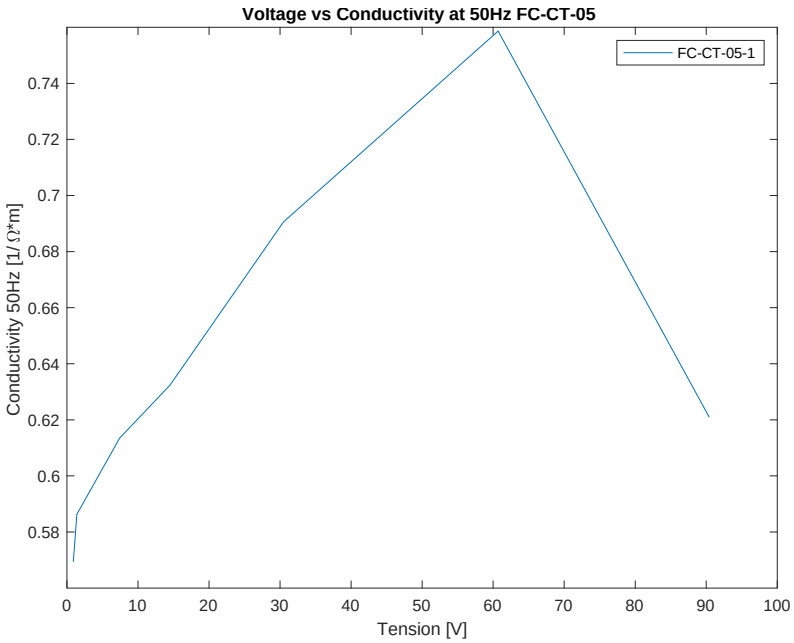


*Figure 4.10 Voltage vs conductivity diagram at 50Hz for FC-CT-05*

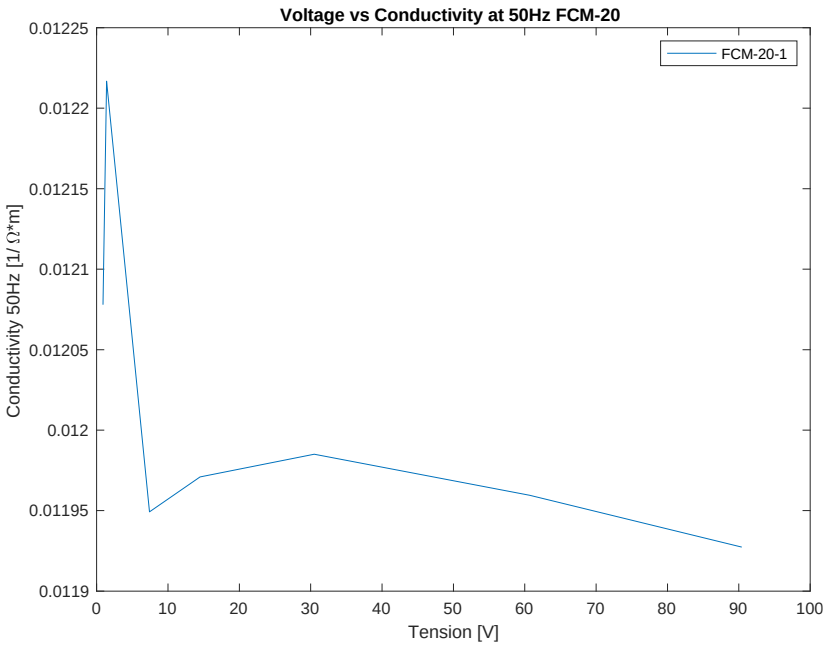


*Figure 4.11 Voltage vs conductivity diagram at 50Hz for FCM-20*

## 4.2. ANALYSISI OF THE THERMAL BEHAVIOUR

In this part of the experimental campaign, the resulting conductive composite cementitious material is studied with two different dosages, firstly, with only chopped recycled carbon fibre and, secondly, with both recycled carbon fibre and micronized carbon fibre addition. Aiming at describing the contribution of each carbonaceous material to the thermal properties of concrete. The material was tested in different ways. For some tests rectangular concrete slabs (PA and PB) were used and for other prismatic concrete beams (VA and VB) were used, so as to identify the influence of the geometric parameters and the fibres distribution inside the cementitious matrix to the final thermal characterization.

In this section, the results of the tests are presented and analysed for each type of sample, electrodes disposal, connection cycle and voltage, in order to compare the properties developed for the different material set at the same conditions.

The main results extracted from these tests were the temperature difference achieved for each sample with respect to time, so as to be able to analyse if it is possible to develop a self-heating material.

### 4.2.1. Temperature recording for 1 hour cycles in slabs

The first tests performed with no previous references were conducted in cycles of one hour duration. For this first test series, the research was focused on the

rectangular concrete slab with conductive electrodes of stainless steel threaded shanks of 6mm diameter and 30mm length and only recycled carbon fibre addition - PB-MF.

For this test series, the samples were submitted to three different effective voltage values – 7.43V, 11.03V and 14.73V – as stated in the diagrams below (see Figures from 4.12. to 4.17.). In these diagrams, every set of boundary conditions is indicated at the right top and the temperature evolution at the left electrode of the sample, at the centre of the specimen and room temperature are indicated in the plots.

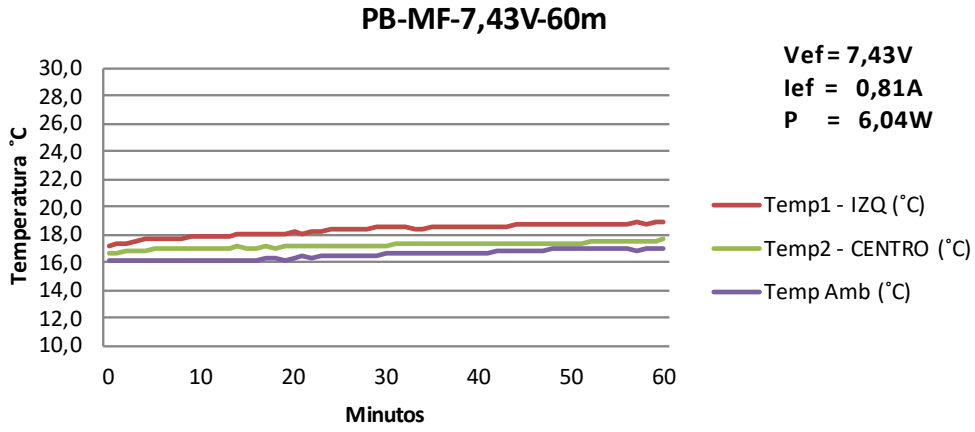


*Figure 4.12 Temperature vs time diagram for PB-MF at 7.43V for 1-hour cycle*

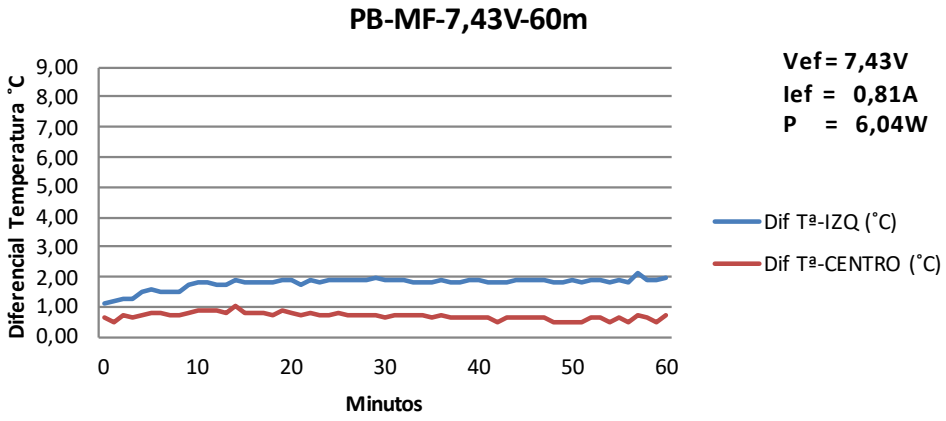


*Figure 4.13 Temperature differential developed vs time diagram for PB-MF at 7.43V and 1-hour cycle*

In this first case, the test was performed at the lowest voltage and therefore the electric power and the electric energy applied to the sample is relatively low (see Figures 4.12 and 4.13.). As aforementioned, the generation of heat is induced by the Joule effect, in which the electrical energy passing through a resistance is transformed into heat. However, in this case being the power relatively low, the heat generation is rather small, with a differential temperature development between 0 and 2 °C, increasing the temperature along the sample from the room temperature, reaching values around 19°C at the left end.

Furthermore, another phenomenon is exhibit in these diagrams. It can be seen that the temperature differential at the left end of the sample, where the power inlet to the sample is located, is higher than the differential developed at the centre of the slab.

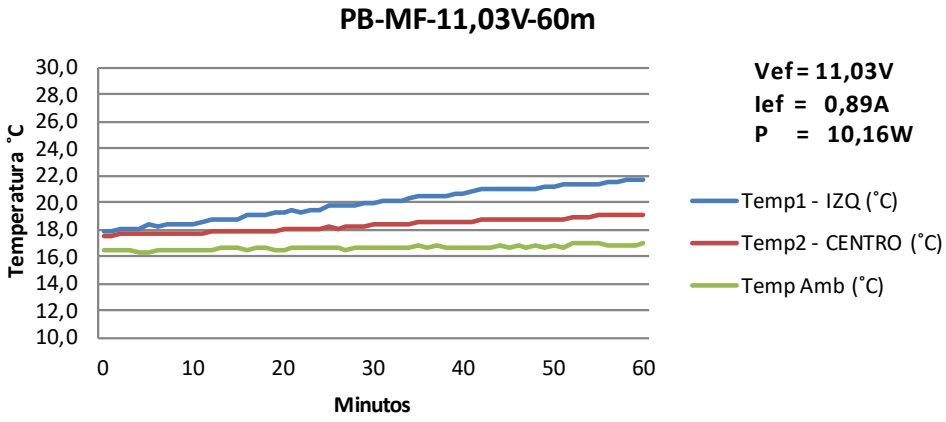


*Figure 4.14 Temperature vs time diagram for PB-MF at 11.03V for 1-hour cycle*

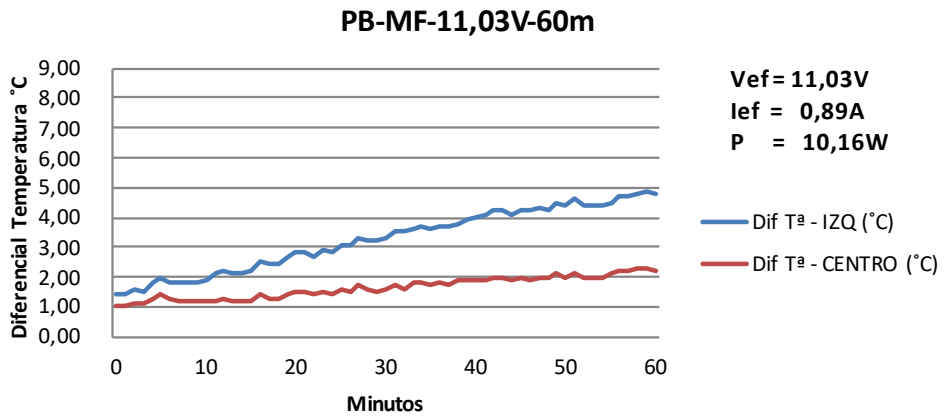


*Figure 4.15 Temperature differential developed vs time diagram for PB-MF at 11.03V for 1 hour cycle*

For the second boundary conditions, the increase in voltage, and so, in electric power is translated in a more noticeable increase of the temperature (see Figures 4.14. and 4.15.). The overall differential temperature developed in this case climbs up to 5°C. Moreover, in the temperature diagram the sample temperature at both studied locations rose, distancing from the room temperature for a couple of degrees Celsius, unlike the first case. In this case, the temperature recordings rise up to 22°C.

Nevertheless, the aforementioned effect of overheating at of the inlet electrode is increased. This problem in the electric voltage inlet to the material might be caused by a deficiency in the connection between the electrode and the carbon fibre throughout the cementitious matrix.

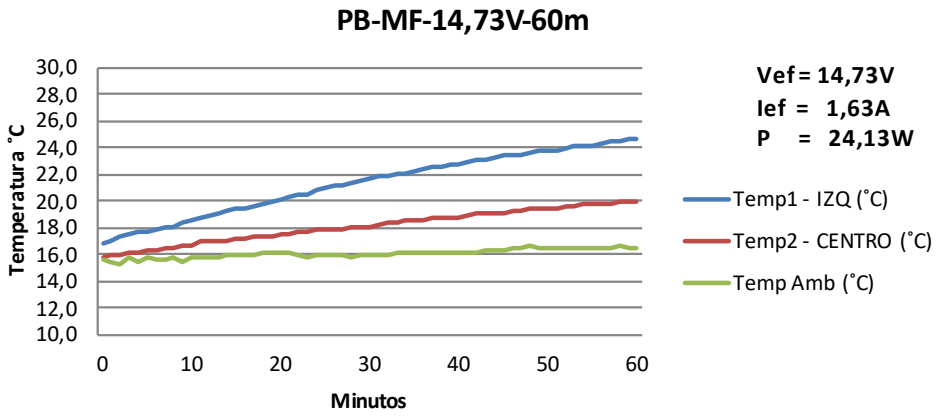


*Figure 4.16 Temperature vs time diagram for PB-MF at 14.73V for 1-hour cycle*

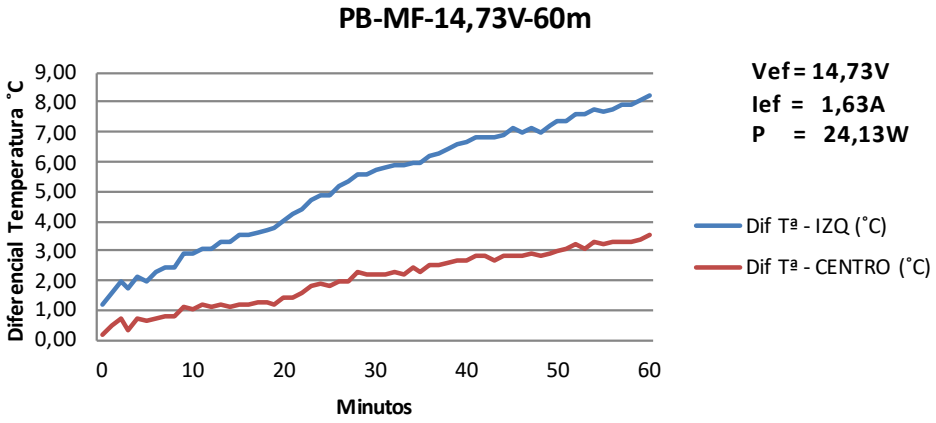


*Figure 4.17 Temperature differential developed vs time diagram for PB-MF at 14.73V for 1-hour cycle*

Finally, for the last case, the tendency extracted from the previous tests is confirmed. The voltage applied in this test doubled the initial one, and so, did the electric power. Thereby, the heat developed was outstanding compared to the first one, with the generation of a temperature differential by the end of an hour up to 8°C. Furthermore, as the electric energy is directly dependent on the time, the generation of heat is strictly increasing with respect to time. The temperature recordings reach their maximum at the end of the 1-hour cycle with a value of 25°C.

Besides, as evinced in the other tests, the temperature difference between the electrode and the centre of the slab is very pronounced with high temperatures.

### 4.2.2. Temperature recording for 3 hours cycles in slabs

For this test series, the research was performed in rectangular concrete slabs with both types of electrodes disposal and both types of carbonaceous materials addition – PA-MF, PA-MAF, PB-MF and PB-MAF.

In this case, the voltage applied was increase, considering the previous results, and 4 different voltages were applied at a fixed frequency pf 50Hz, as shown in the table below (see Table 4.4.) and the time cycles were stretched on up to 3 hours.

Indeed, the increase of the excitement voltage was performed gradually in steps of 0.2V until obtaining maximum temperature recordings of 50°C.

| | Vexcit (V) | | | | Vpp (V) | | | | Ipp (A) | | | |
|---|---|---|---|---|---|---|---|---|---|---|---|---|
| **PA-MF** | 0.3 | 0.5 | 0.7 | - | 30.1 | 50.5 | 70.8 | - | 3.9 | 6.8 | 9.7 | - |
| **PA-MAF** | 0.3 | 0.5 | 0.7 | 0.9 | 30.5 | 50.9 | 71.4 | 92.2 | 2.8 | 4.8 | 6.7 | 8.3 |
| **PB-MF** | 0.3 | 0.5 | 0.7 | - | 30.3 | 50.4 | 70.1 | - | 4.8 | 8.2 | 12 | - |
| **PB-MAF** | 0.3 | 0.5 | 0.7 | 0.3 | 31.1 | 52 | 72.1 | 93.8 | 2 | 3.4 | 4.3 | 5 |

| Vef (V) | | | | Ief (A) | | | | P(W) | | | | |
|---|---|---|---|---|---|---|---|---|---|---|---|---|
| 10.6 | 17.8 | 25.0 | - | 1.4 | 3.4 | 3.4 | - | 14.8 | 43 | 86.1 | - | **PA-MF** |
| 10.8 | 18.0 | 25.2 | 32.6 | 1 | 1.7 | 2.4 | 2.9 | 10.7 | 30.4 | 59.8 | 95.7 | **PA-MAF** |
| 10.7 | 17.8 | 24.8 | - | 1.7 | 2.9 | 4.1 | - | 18.1 | 51.4 | 101 | - | **PB-MF** |
| 11.0 | 18.4 | 25.5 | 33.2 | 0.7 | 1.2 | 1.5 | 1.8 | 7.81 | 21.8 | 38.5 | 59.1 | **PB-MAF** |

*Table 4.4 Boundary conditions for each test*

The results of each test are presented below (see Figure form 4.18. to 4.38.) using different types of diagrams:

- Temperature variation with respect to time for dosage and electrode disposal typologies at different voltages and, temperature-time recording diagrams (Figures from 4.18. to 4.30.). Both diagrams were produced for each test, resulting in a total of 28 figures. Therefore, in this section only the most relevant once are featured.

- Comparative of the temperature behaviour for the same matrix and different electrode disposal (Figures from 4.31. to 4.34.)

- Comparative of the temperature behaviour for the same electrode disposal and different matrix (Figures from 4.35 to 4.38.)

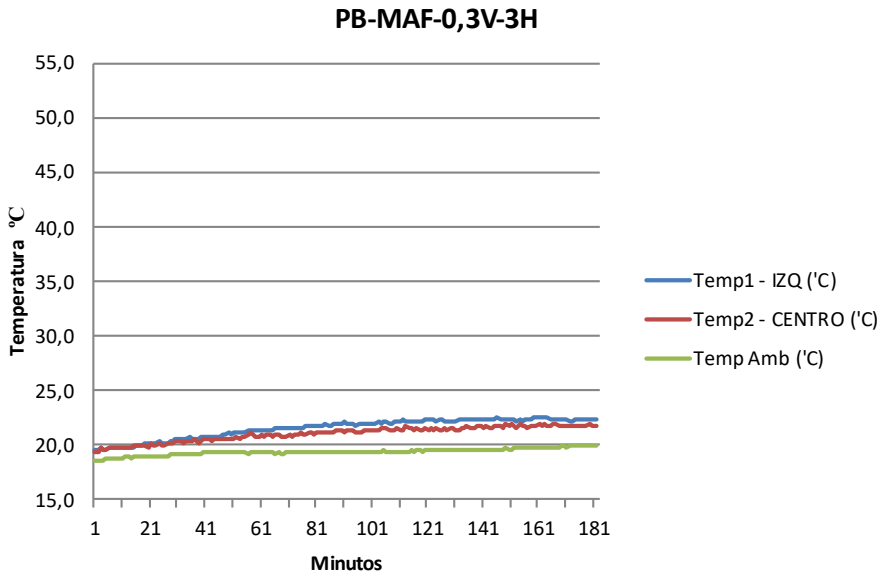


*Figure 4.18 Temperature vs time diagram for PB-MAF at Vexcit 0.3V for 3 hours cycle*

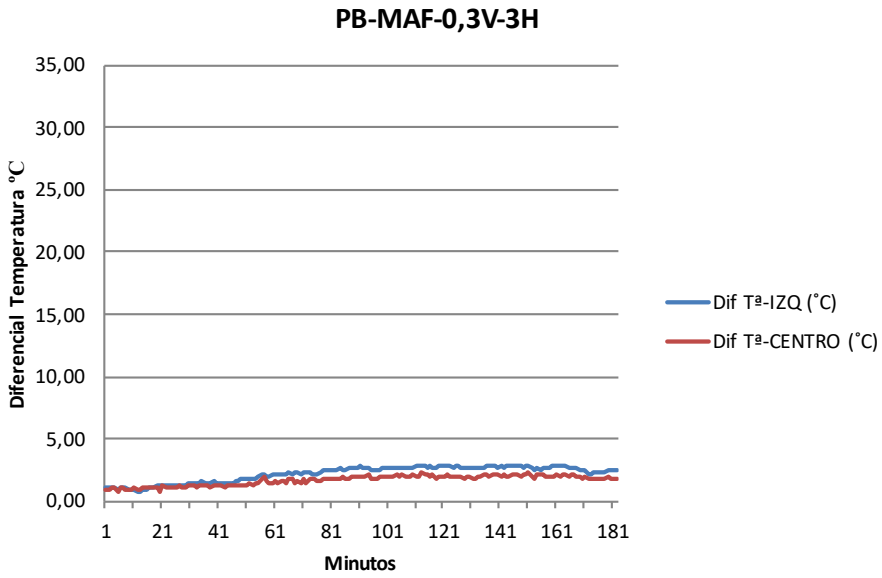


*Figure 4.19 Temperature variation vs time diagram for PB-MAF at a Vexcit of 0.3V for 3 hours cycle*

The two diagrams above for the test with PB-MAF-0.3V-3H (see Figures 4.18. and 4.19.) present the minimum heat production of all the 3 hours cycle test series. In this case, the temperature differential generated during 3 hours was very low, barely producing heat emission. Thereby, the temperature recorded in both measurement locations of the sample rose a total amount of 2°C and the room temperature increased around 1°C in 3 hours.

These results can be explained by the fact that the voltage applied for this test was the lowest one and, consequently, the electric energy passing through the sample and dissipating into heat was very small.

Furthermore, the PB-MAF were the samples with the poorest performance of all the material specimens tested. One of the reasons might be the low contribution in terms of conductivity of the FCM-20 carbonaceous additive, a deficiency in the dispersion of this addition inside the cementitious matrix or a shortfall connection between the electrodes and the carbonaceous materials and between the fibres inside the matrix, failing to provide a proper percolation path for electrical current.

Nevertheless, as the temperature variations and heat production were such small, the differences in temperature recording between the centre and the left end of the sample were barely noticeable, leading to a much homogeneous temperature distribution along the sample, unlike the majority of the tests.

Indeed, very similar results were obtained for the test of PA-MAF-0.3V-3H presented in the diagrams below (see Figures 4.20. And 4.21.). In spite of this, the output temperatures and differential temperatures in this case are 1 or 2°C higher, even though the trends are practically the same.

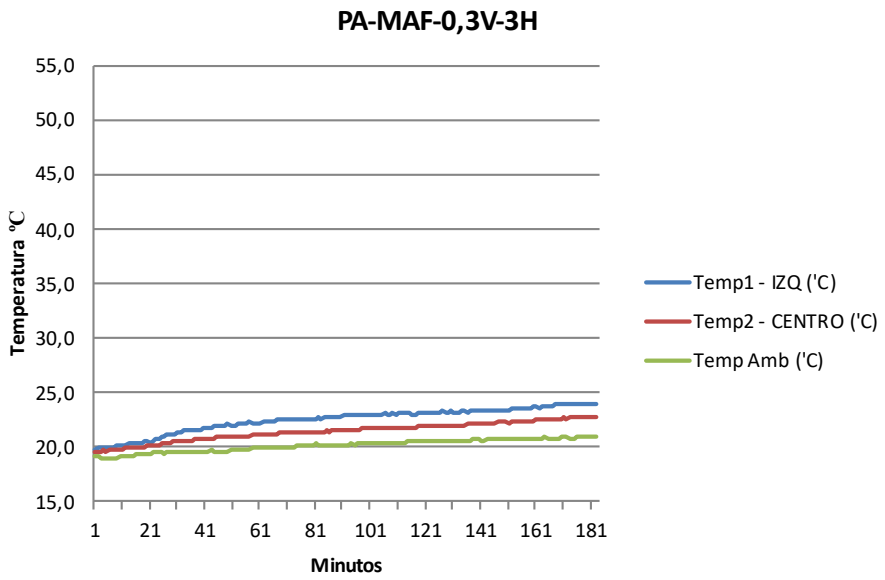


*Figure 4.20 Temperature vs time diagram for PA-MAF at Vexcit 0.3 V for 3 hours cycle*

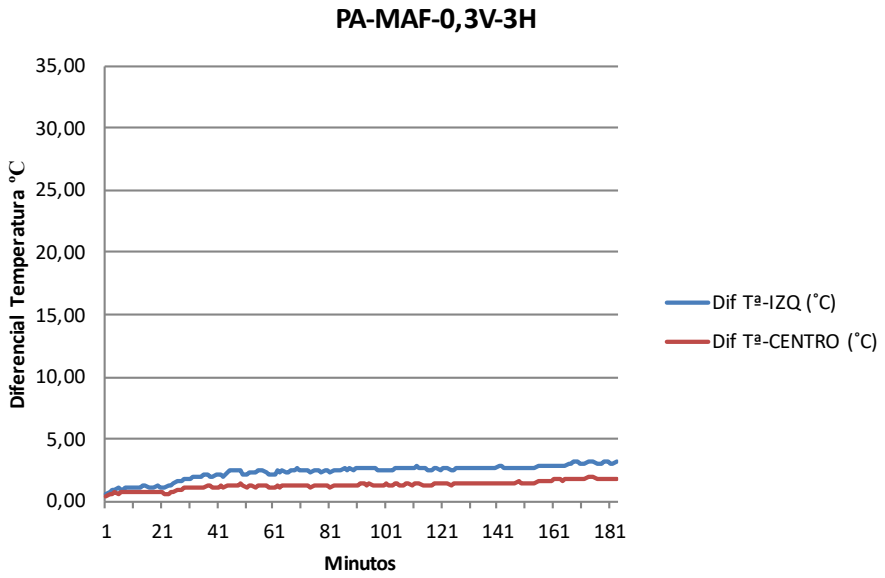


*Figure 4.21 Temperature variation vs time diagram for PA-MAF at a Vexcit of 0.3V for 3 hours cycle*

However, when it comes to the samples containing MF dosage, the results for the lower and intermediate low voltages are improved, providing the possibility of developing relatively temperature differentials with low electrical power as presented in the PA-MF-[0.3V/0.5V]-3H diagrams below (see Figures 4.22., 4.23., 4.24. and 4.25.).

Although, a clear difference is illustrated in these results between using $V_{ef}$ = 10.6V and $V_{ef}$ = 17.8V, for the lowest voltage the PA-MF specimens are developing up to 5°C temperature differentials and reaching temperatures above 25°C, increasing in 2°C the room temperature. The results for the same specimens at a $V_{excit}$ = 0.5V are improved reaching temperature variations up to 12°C and rising the recorded temperatures up to 32°C.

However, in these tests, were the heat production is increased, the thermal difference between the left end and the centre of the samples are enhanced, unlike in the results for low voltages using MAF dosage. This induces to a heterogeneous temperature distribution in the concrete element, which should be avoided for future applications in reality.

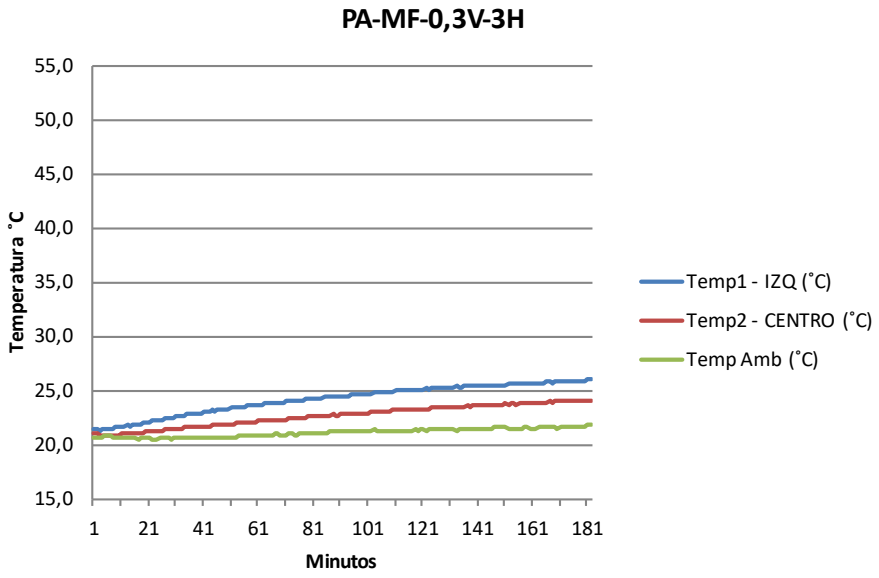


*Figure 4.22 Temperature vs time diagram for PA-MF at Vexcit 0.3 V for 3 hours cycle*

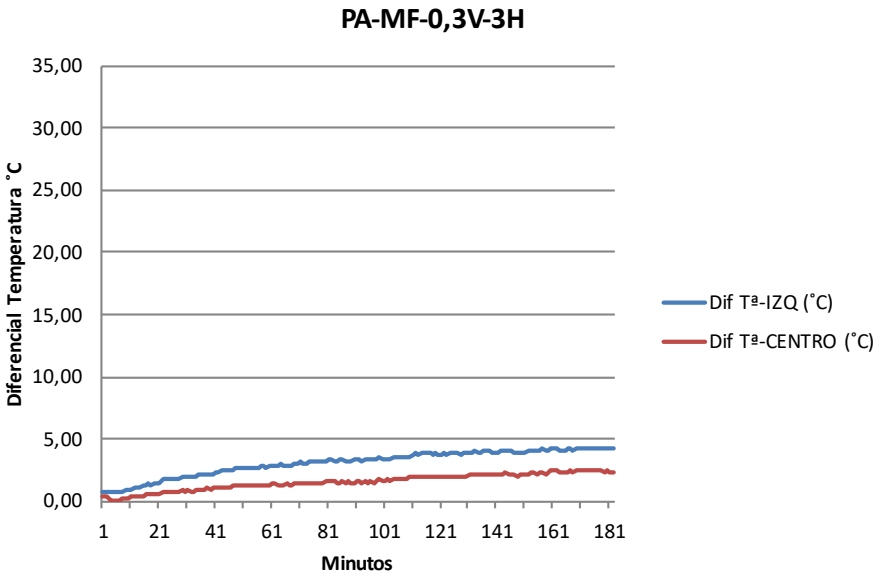


*Figure 4.23 Temperature variation vs time diagram for PA-MF at a Vexcit of 0.3V for 3 hours cycle*

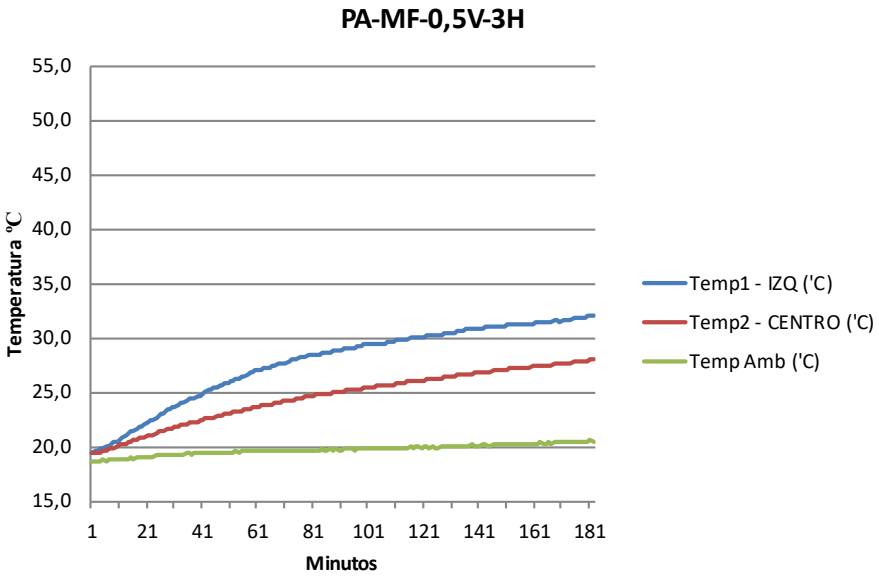


*Figure 4.24 Temperature vs time diagram for PA-MF at Vexcit 0.5 V for 3 hours cycle*

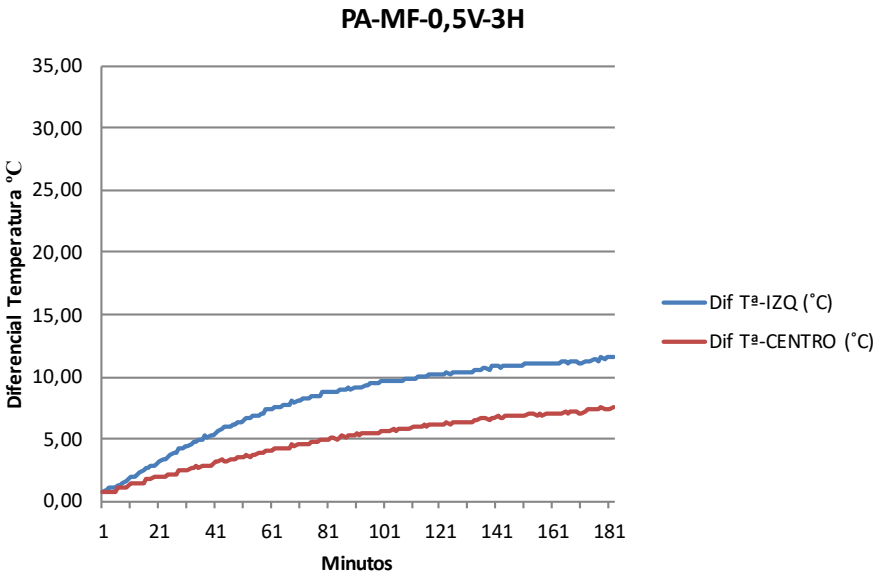


*Figure 4.25 Temperature variation vs time diagram for PA-MF at a Vexcit of 0.5V for 3 hours cycle*

Very similar results were obtained for the PB-MF samples' testing. The tendencies, the proportions and the behaviour of the material resulted to be nearly equal than the PA-MF samples, however, the output temperature differentials and the temperature reached after 3 hours where slightly higher, due to a steeper slope. This phenomenon is illustrated in the diagram below, where the temperatures reached for medium-low voltage in PB-MF are drown (see Figure 4.26.).

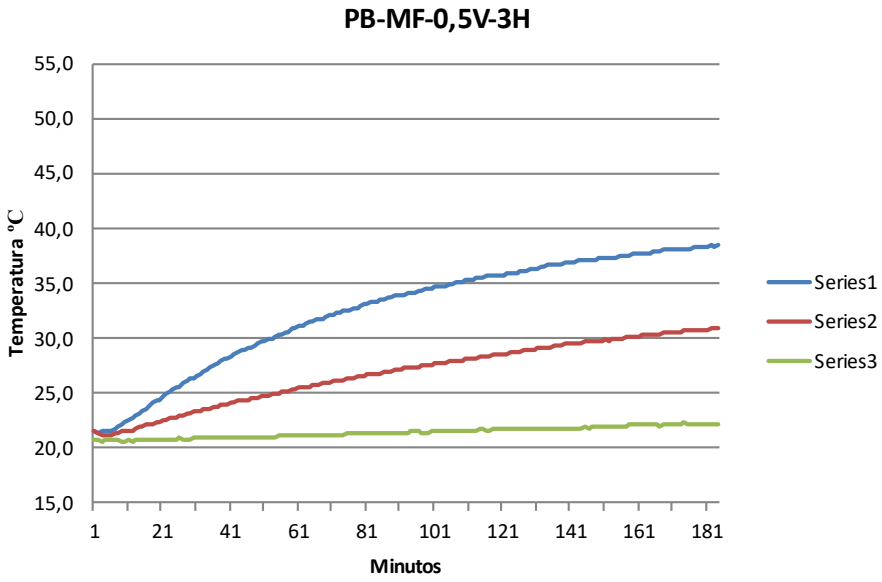


*Figure 4.26 Temperature vs time diagram for PB-MF at Vexcit 0.5V for 3 hours cycle*

Actually, the specimens of PB-MF had the best performance in terms of heat production from all test performed, together with the PA-MAF for high voltages. The higher temperature recordings were achieved applying a $V_{ef}$ = 24.8V to concrete slab with chopped recycled fibre addition and steel deployé sheet electrodes disposal, as presented in the diagrams below (see Figures 4.27. and 4.28.).

This temperature-time recording diagram shows that the maximum temperature was reached at the left end of the sample, where the electric power inlet is located, with a value of 52°C. Nevertheless, it exhibits the highest recorded temperature difference between the centre and the left end of the sample, generating the most heterogeneous concrete element from this test series, with a maximum difference at the end of the 3 hours cycle of 14°C.

Regarding the temperature differential developed, the PB-MF samples were able to produce remarkable increases in temperature both for the left end and the centre. The left end recorded a total temperature variation at the end of the 3 hours cycle of 31°C, with an average heating rate of 0.172°C/min increasing 1°C every 5.8 min. While at the centre of the sample less temperature differential was produced, around 17°C in 3hours, with an average heating rate of 0.094°C/min, increasing 1°C every 10.59 min.

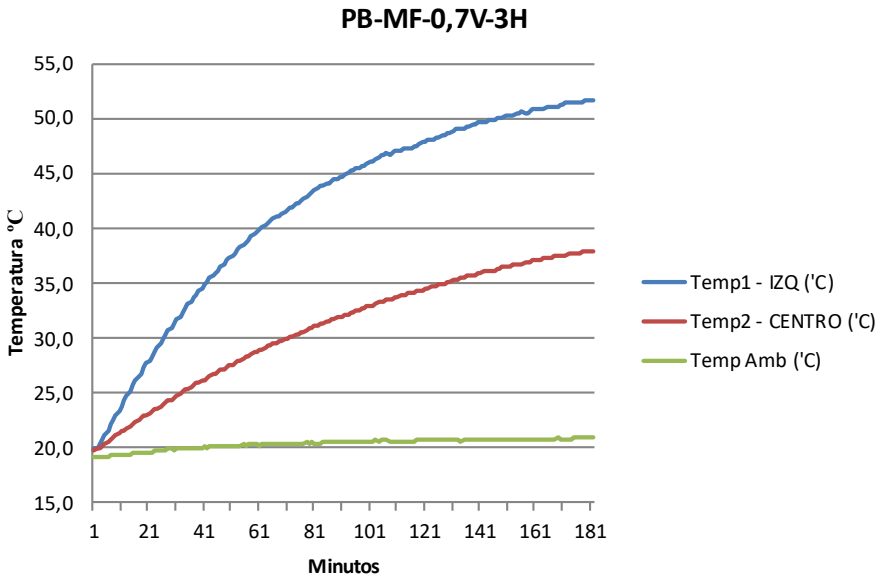


*Figure 4.27 Temperature vs time diagram for PB-MF at Vexcit 0.7V for 3 hours cycle*

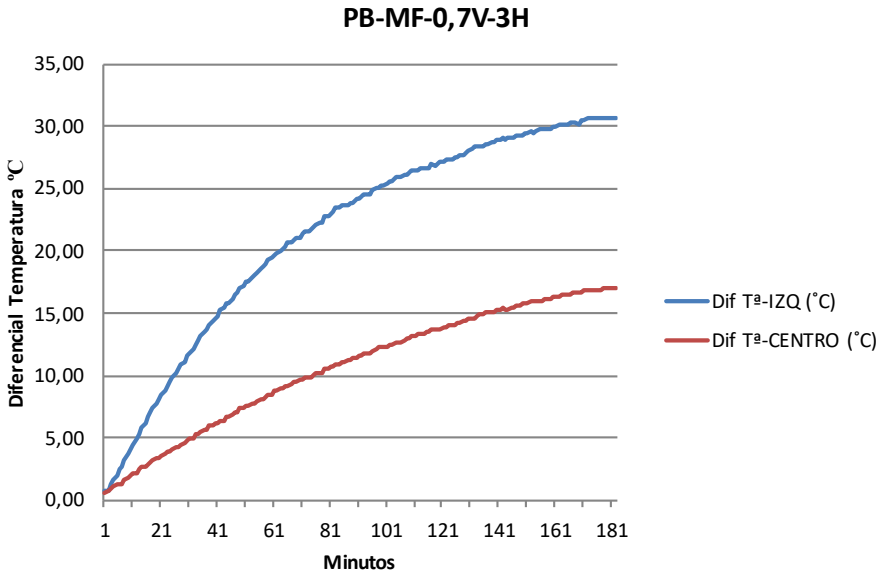


*Figure 4.28 Temperature variation vs time diagram for PB-MF at a Vexcit of 0.7V for 3 hours cycle*

Alternately, the samples PA-MAF submitted to a $V_{ef}$ = 32.6V presented a very similar behavior with nearly the same results, as shown in the diagrams below (see Figures 4.29. and 4.30.). However, the performance cannot be catalogued as optimal as the one for PB-MF samples, since the required voltage and, consequently, the electric power needed for developing such remarkable results is higher than for the previous case.

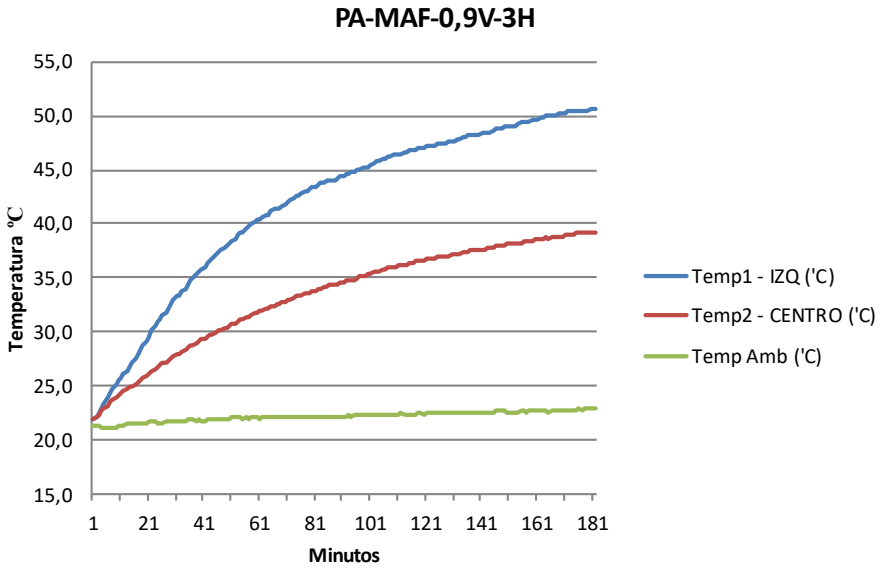


*Figure 4.29 Temperature vs time diagram for PA-MAF at Vexcit 0.9V for 3 hours cycle*

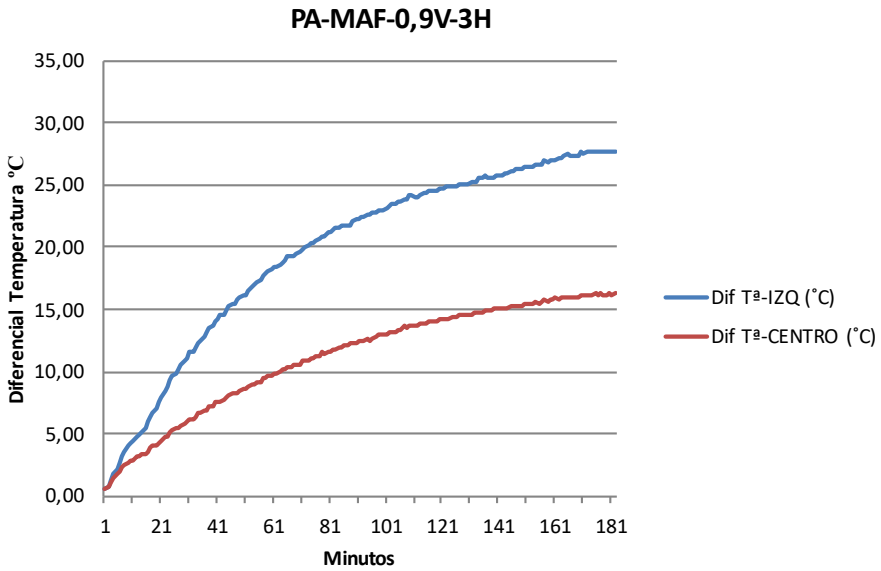


*Figure 4.30 Temperature variation vs time diagram for PA-MAF at a Vexcit of 0.9V for 3 hours cycle*

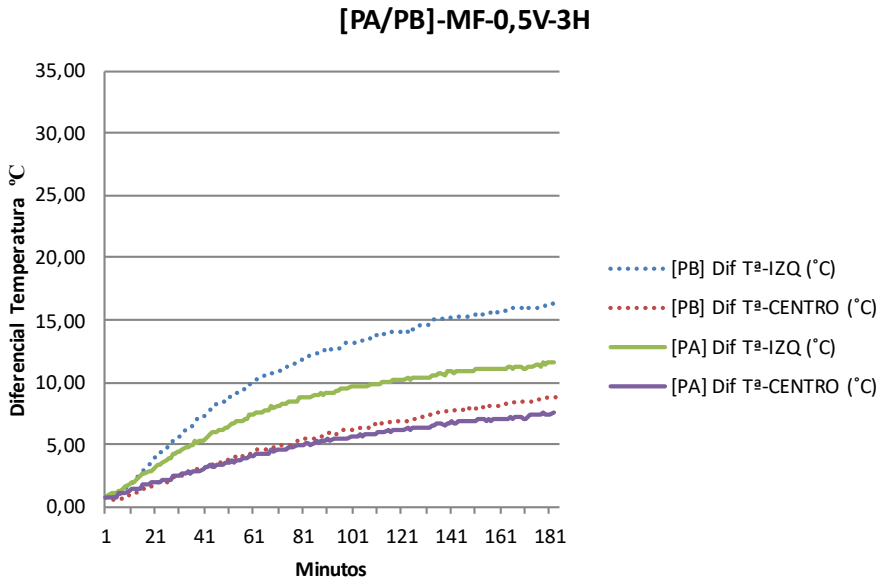


*Figure 4.31 Temperature behaviour comparative diagram for the same matrix MF but different electrodes disposal PA and PB for a Vexcit of 0.5V*

This comparative diagram (see Figure 4.31.) makes clear the different temperature results for different electrode disposal. Whereas the temperature at the centre of the sample does barely change between disposal A – rea electrodes of 6mm – and disposal B – steel deployé sheets –, the difference is lionised for the left end of the sample, where the power inlet electrode is located. However, these results show that a homogeneous temperature distribution on the sample has not yet been achieved.

On the other hand, it is remarkable that with an applied $V_{ef}$ = 17.8V in both cases the temperature differential developed in 3 hours is higher 10°C for the left end of the sample. Besides, the diagram illustrates the difference between the temperature variation generation capacity between both samples. The electrodes configuration B is able to generate a larger temperature variation up to 16°C, with an average heating rate of 0.089°C/min increasing 1°C every 11.25 min. While the electrodes configuration A is able to generate less temperature differential around 12°C in 3hours, with an average heating rate of 0.067°C/min, increasing 1°C every 15 min.

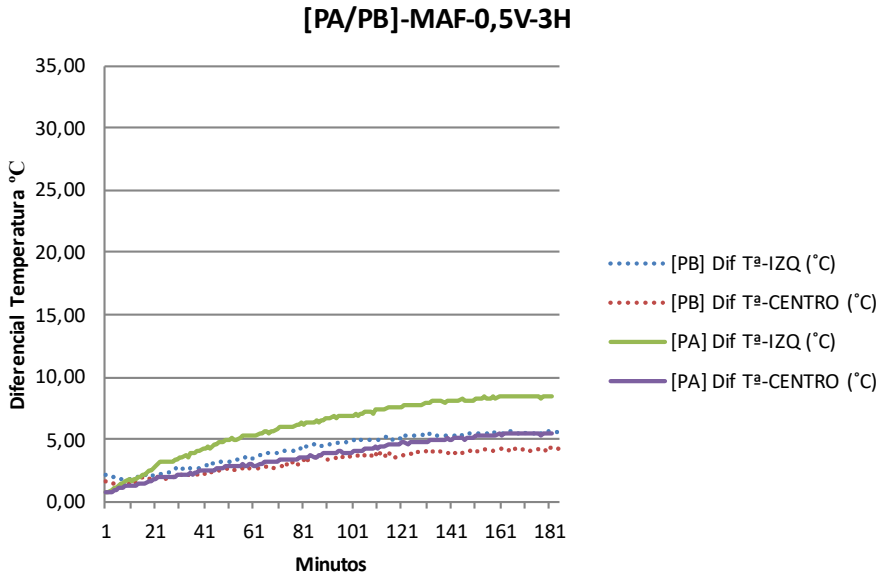


*Figure 4.32 Temperature behaviour comparative diagram for the same matrix MAF but different electrodes disposal PA and PB for a Vexcit of 0.5V*

This comparative diagram (see Figure 4.32.) a much different behaviour from the previous one in which it only changes the matrix of the conductive concrete. In this case, contrary to what has been seen before, the electrodes disposal A generates a larger temperature differential than disposal B. In spite of this, in both cases the temperature variation experienced by the samples in 3 hours is much smaller than previously. Whereas the PA samples were able to generate a temperature difference of 8°C, increasing 1°C every 22.5 min, the PB samples were able to increase only up to 5°C in 3 hours, increasing 1°C every 36 min.

Moreover, in this particular case, since the temperature differentials generated are much smaller, the phenomena for which the temperature differential at the left end of the sample is normally higher than the differential developed at the centre of the slab. Is not as pronounced as in previous tests, especially, for PB samples, which follow nearly the same tendency.

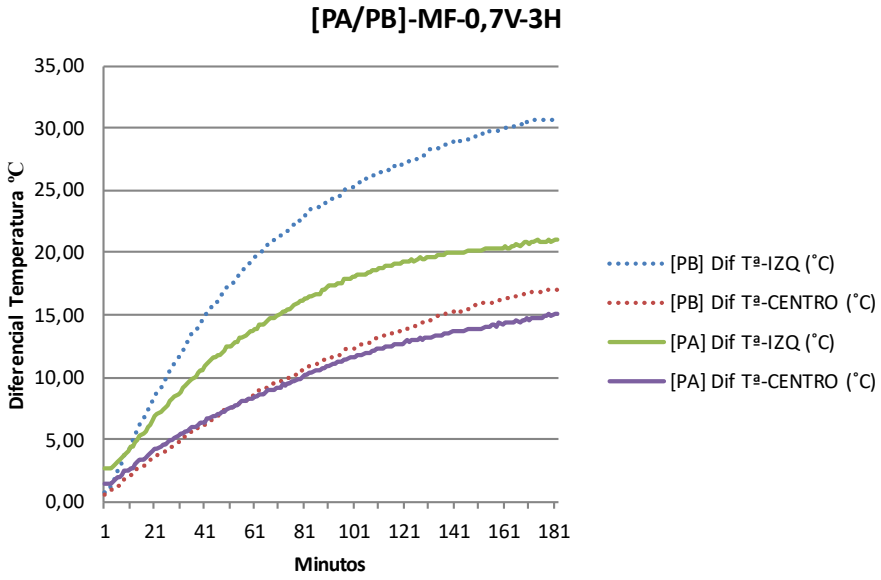


*Figure 4.33 Temperature behaviour comparative diagram for the same matrix MF but different electrodes disposal PA and PB for a Vexcit of 0.7V*

This comparative diagram (see Figure 4.33.) clearly exhibits again the different temperature results for different electrode disposal and locations from the sample. Whereas the temperature at the centre of the sample does barely change between disposal A – rea electrodes of 6mm – and disposal B – steel deployé sheets –, the difference is lionized for the left end of the sample, where the power inlet electrode is located. However, these results ratify the non-homogeneous temperature distribution on the sample.

On the other hand, it is remarkable that with an applied $V_{ef}$ = 25V in both cases the temperature differential developed in 3 hours is higher 20°C for the left end of the sample. Besides, the diagram illustrates the difference between the temperature variation generation capacity between both samples. The electrodes configuration B is able to generate a larger temperature variation up to 31°C, with an average heating rate of 0.172°C/min increasing 1°C every 5.8 min. While the electrodes configuration A is able to generate less temperature differential around 21°C in 3hours, with an average heating rate of 0.117°C/min, increasing 1°C every 8.57 min.

Comparing these results with the ones corresponding to the tests with [PA/PB]-MF-0.5V-3H (see Figure 4.31.) shows that the increase of the applied voltage to the samples, and so, of the electric power is directly translated in a higher increase of the temperature variation generated. Along these lines, the by increasing the $V_{ef}$ applied from 17.8V to 25V, the temperature differential produced was doubled, from a maximum in the left end of the PB specimen of 16°C to a maximum at the same location and sample of 31°C.

Besides, the change of electrical power has not been translated in a change in the tendency of the data, meaning that the order and the relation between data is maintained.

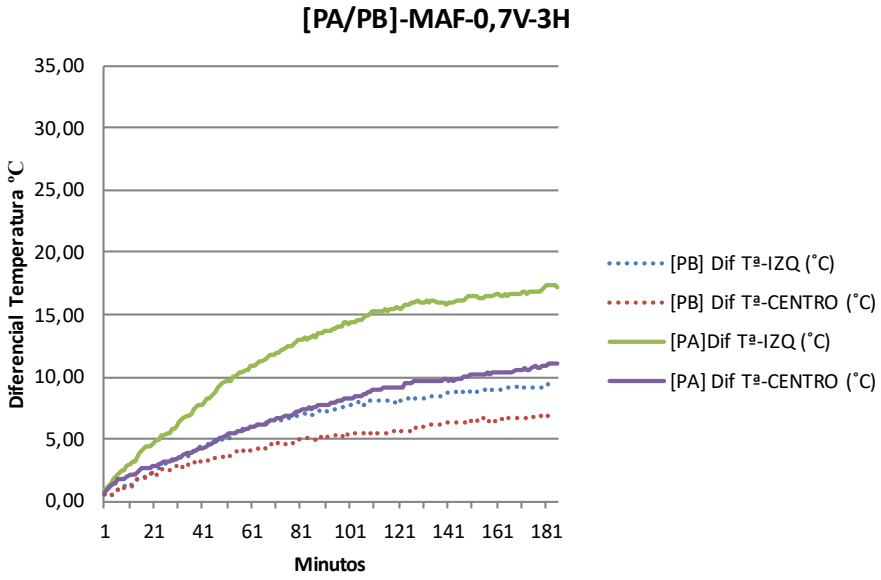


*Figure 4.34 Temperature behaviour comparative diagram for the same matrix MAF but different electrodes disposal PA and PB for a Vexcit of 0.7V*

This comparative diagram (see Figure 4.34.) exhibits again the different temperature results for different electrode disposal and locations from the sample, but in the opposite way from MF matrix. In this case, the electrodes disposal A generated a larger temperature differential than disposal B. The temperature at the centre of the sample change in smaller proportion than the one at the left end of the sample, where the power inlet electrode is located. Furthermore, the temperature different locations is more pronounced for PA than for PB, enhancing the heterogeneous temperature distribution along the sample.

On the other hand, with an applied $V_{ef}$ = 25V in both cases the temperature differential developed in 3 hours is higher 10°C for the left end of the sample. Besides, the diagram illustrates the difference between the temperature variation generation capacity between both samples. The electrodes configuration A is able to generate a larger temperature variation up to 17°C, with an average heating rate of 0.094°C/min increasing 1°C every 10.59 min. While the electrodes configuration B is able to generate less temperature differential around 11°C in 3hours, with an average heating rate of 0.061°C/min, increasing 1°C every 16.36 min.

Comparing these results with the ones corresponding to the tests with [PA/PB]-MAF-0.5V-3H (see Figure 4.32.) shows that the increase of the applied voltage to the

samples, and so, of the electric power is directly translated in a higher increase of the temperature variation generated, also for this case. Along these lines, the by increasing the $V_{ef}$ applied from 17.8V to 25V, the temperature differential produced was doubled, from a maximum in the left end of the PA specimen of 8°C to a maximum at the same location and sample of 17°C.

Nevertheless, the change of electrical power, in this case, has been translated in a change in the tendency of the data, such that in the case of PB the temperature differential generated at the centre and the left end of the sample separated one each other and, for both materials, the temperature variation at the centre of the sample was no longer in the same trend and values.

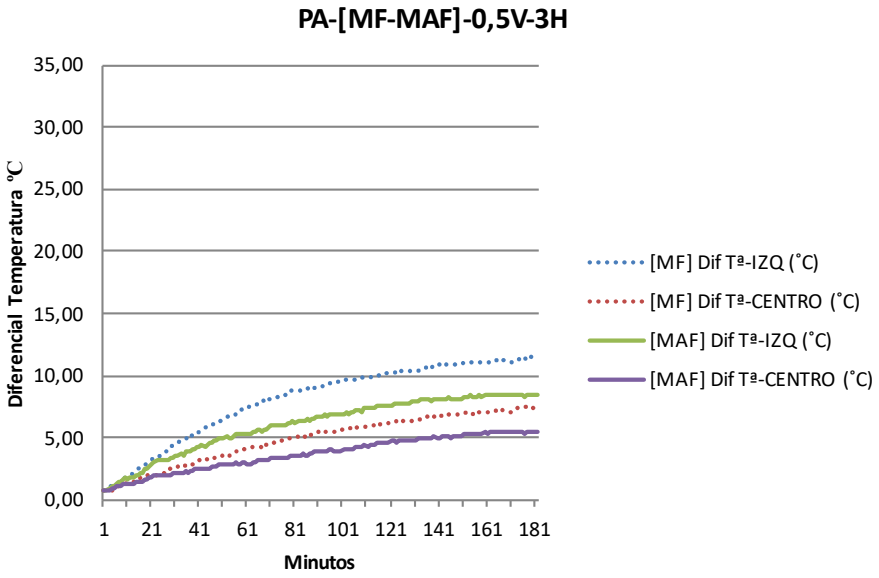


*Figure 4.35 Temperature behaviour comparative diagram for the same sample and electrodes disposal PA but different matrices MF and MAF for a Vexcit of 0.5V*

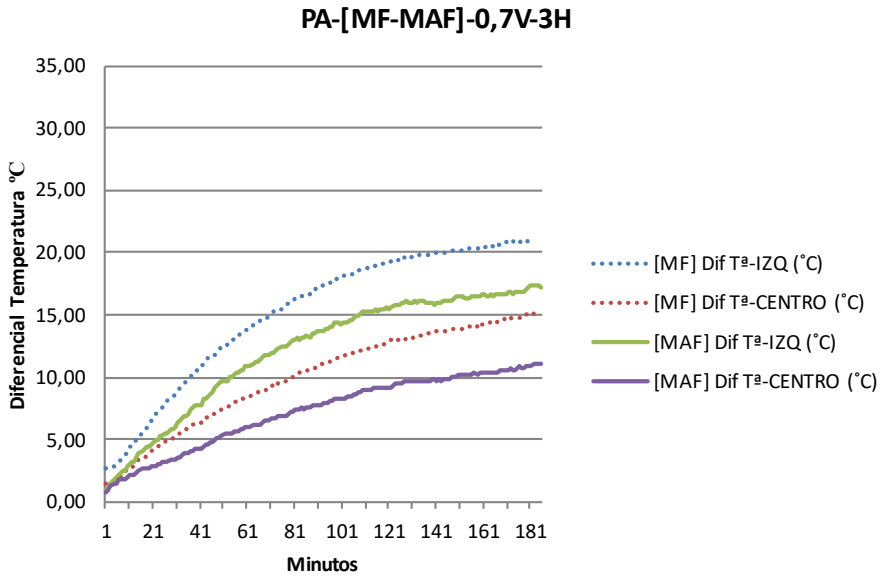


*Figure 4.36 Temperature behaviour comparative diagram for the same sample and electrodes disposal PA but different matrices MF and MAF for a Vexcit of 0.7V*

The comparative diagrams above (see Figures 4.35. and 4.36.) evinces that the data obtained from testing the rea 6mm electrodes disposal for MF matrix and MAF matrix has the same shape, follows the same trends and maintain the very same proportions only changing the output values for the differential temperature developed along 3 hours, due to a difference of slope.

The first diagram presents the temperature differential developed for a concrete slab with electrode disposal A and both types of dosage at a $V_{excit}$ = 0.5V. Whereas, the second presents the temperature differential for the same materials at a $V_{excit}$ = 0.7V. In both cases the proportionality of the overall difference between the left end and the centre end is maintained along the whole cycle, so that MF and MAF present the same behaviour and characteristics for each test.

These plots also show that the MF matrix reaches higher temperature variations than the MAF matrix with the same electric power, effective voltage and time interval values. This might be caused due to a different dispersion of the dosages in the composite cementitious material and the effect of the low conductivity of FCM-20, measured in the electrical behaviour characterisation section, in the contribution to the overall electrical properties of the material.

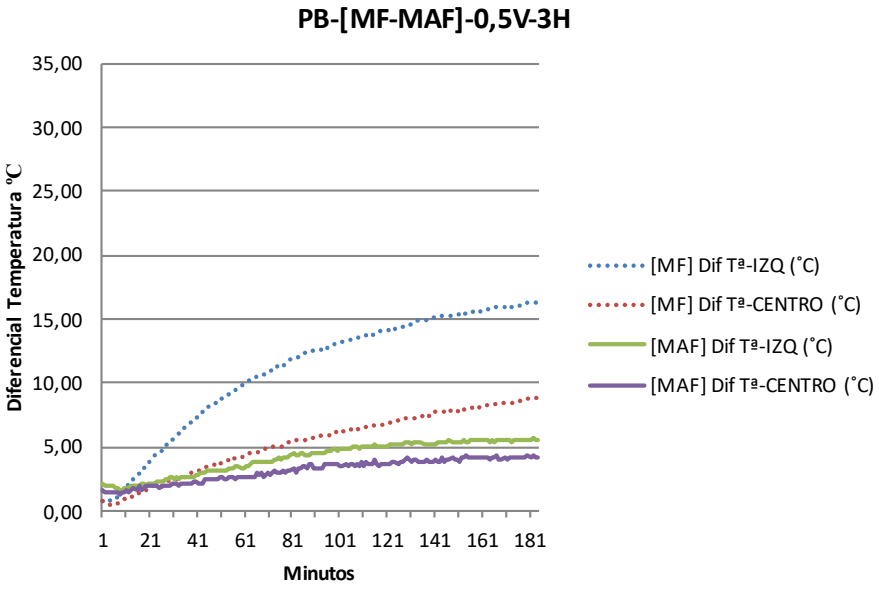


*Figure 4.37 Temperature behaviour comparative diagram for the same sample and electrodes disposal PB but different matrices MF and MAF for a Vexcit of 0.5V*

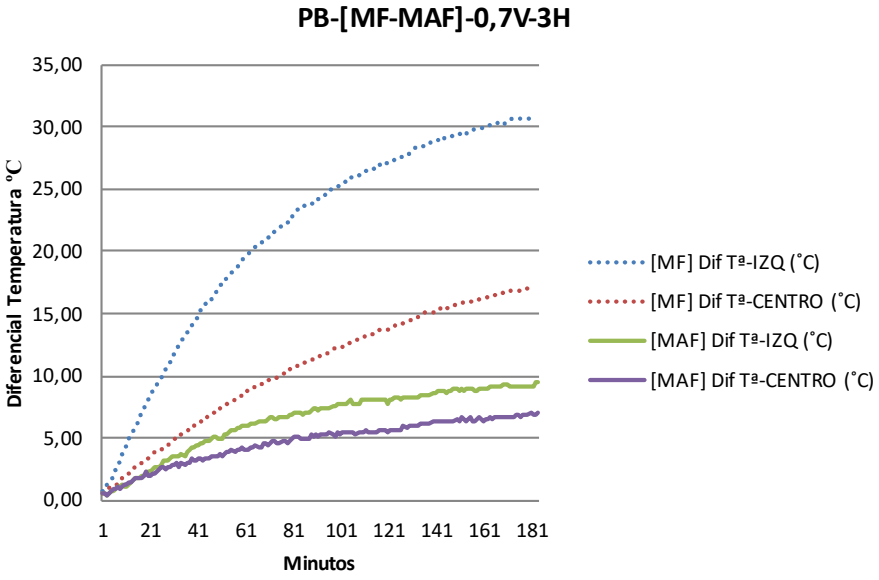


*Figure 4.38 Temperature behaviour comparative diagram for the same sample and electrodes disposal PB but different matrices MF and MAF for a Vexcit of 0.7V*

The comparative diagrams above (see Figures 4.37. and 4.38.) evinces that the data obtained from testing the steel deployé sheet electrodes disposal for MF matrix and MAF matrix has very different shape, proportions, slopes and output temperature differential for both cases.

The first diagram presents the temperature differential developed for a concrete slab with electrode disposal B and both types of dosage at a $V_{excit}$ = 0.5V. Whereas, the second presents the temperature differential for the same materials at a $V_{excit}$ = 0.7V. In

both tests, the MF material develops much higher temperature differentials with steep lines and a very pronounced difference on heat production between left end and centre of the sample. Whereas, the MAF material describes the opposite behaviour, developing much smaller temperature differentials, with much softer slopes and producing very little difference between the left end and the centre of the sample in terms of heat production.

These plots also show that the MF matrix reaches higher temperature variations than the MAF matrix with the same electric power, effective voltage and time interval values. This might be caused due to a different dispersion of the dosages in the composite cementitious material and the effect of the low conductivity of FCM-20, measured in the electrical behaviour characterisation section, in the contribution to the overall electrical properties of the material.

### 4.2.3. Temperature recording for 48 hours cycles in slabs

For this test series, the research was performed in rectangular concrete slabs with both types of electrodes disposal and both types of carbonaceous materials addition – PA-MF, PA-MAF, PB-MF and PB-MAF.

The temperature recording cycles consisted in 48 hours cycles at the maximum voltages reached for the 3 hours cycles series, by means of sequences of connection/disconnection of 8 h/16 h until completing the 48 hours cycle.

The maximum voltages to which the samples were submitted in the 3 hours cycles were 25V for the MF dosages and 33V for the MAF dosages.

From the 4 tests performed, the results were quite unalike and could be grouped in 3 different behaviours.

- 1st case: corresponds to the results for the PB-MAF sample. In this case, the slab behaved differently from the previous tests with 3 hours cycles from the beginning. Neither they reach the previous current intensity nor they reach the same temperatures recorded before.

- 2nd case: corresponds to the tests performed to the PA-MAF and PB-MF samples. In this particular case, the slabs achieved a similar behaviour than the one recorder previously. However, during the tests, the current intensity decreased affecting the temperature recordings.

- 3rd case: corresponds to the testing of PA-MF samples, which behaved in a similar way than for the 3 hours cycles during the whole cycle of 48 hours.

When the loss of conductivity took place at the beginning or in the first cycle, which is the case for the PA-MAF and the PB-MAF, the sequence for the total 48 hours could not be completed as the terminals overheated.

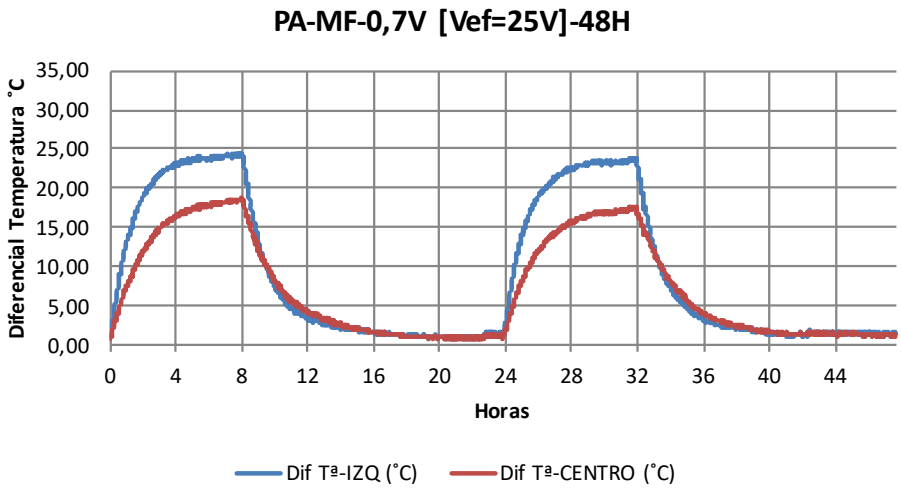


*Figure 4.39 Temperature differential developed with respect to time diagram for the full sequence of 48 hours for PA-MF ata a Vexcit = 0.7V*

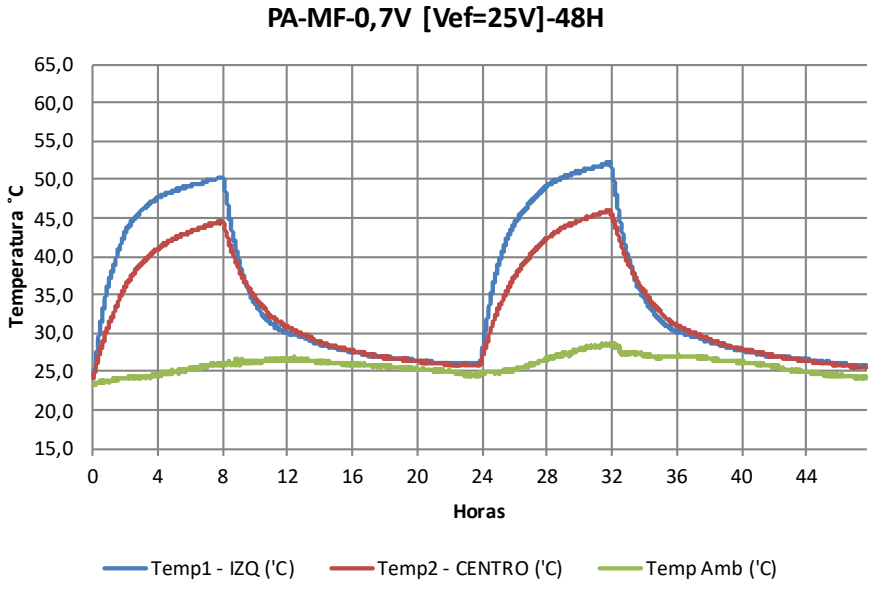


*Figure 4.40 Temperature-time recordings diagram for the full sequence of 48 hours of PA-MF at a Vexcit = 0.7*

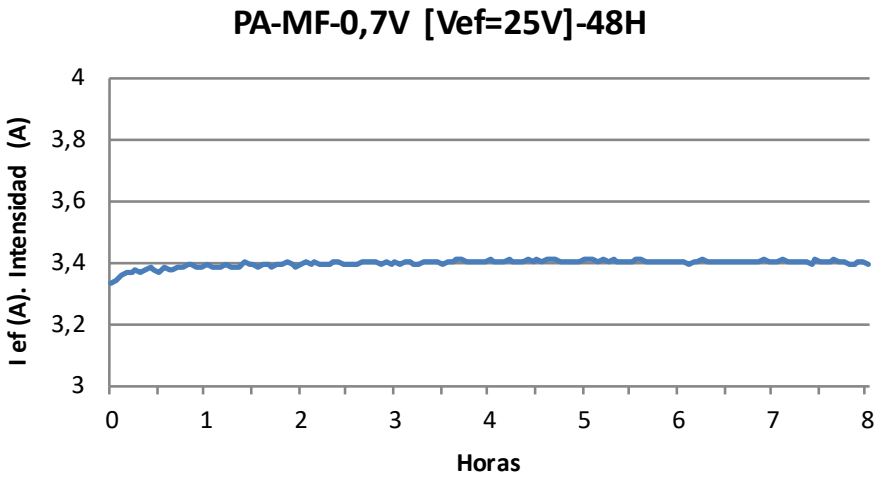


*Figure 4.41 Measurements of the intensity for the test of PA-MF at Vexcit = 0.7V for the first 8 hours connection sequence*

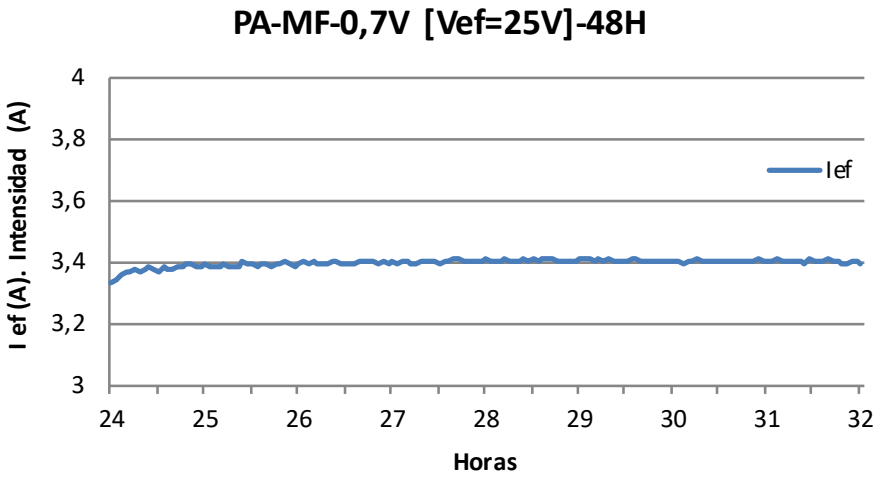


*Figure 4.42 Measurements of the intensity for the test of PA-MF at Vexcit = 0.7V for the second 8 hours connection sequence*

The four diagrams above (see Figures from 4.39. to 4.42.) show the results for the test performed on PA-MF which had the most promising results. The slab reached a temperature 5°C higher than the one recorded in the 3 hours cycles and it is sensed that the temperature could continue to increase. Another pattern that the temperature-time diagram exhibits is the regularity of the behaviour and the shape for the connected and disconnected sequence. Both connected sequences describe exactly the same patterns, during the heating cycle it is strictly increasing until it reaches a plateau, whereas the disconnected sequences behave in the opposite way, strictly decreasing until reaching a plateau where it stabilises, so that, after 16 hours with the system turned off, the temperature at both locations of the sample gets equal to the room temperature and the following 8 hours sequence starts.

Regarding the first of the four figures for this test, it can be seen that quite large temperature differentials are developed, reaching a maximum for the left end of 25°C variation but slowly along time, with a first stage steeper up to the 3rd hour and a second stage gradually softening the slope until the 8th hour. This leads to an average heating rate for the left end of 0.052°C/min increasing 1°C every 19.2 min. Besides, it can be seen that significant different between the recordings for the left end and the centre of the sample, only occur during the heating sequence, after the 1st hour of the process is completely and gradually increasing until reaching a maximum of a 5°C difference between both locations.

Regarding the intensity measurement diagrams, it can be seen that for both connected 8 hours heating sequences, the current intensity remains constant at every time, which is optimal for a proper thermal and electrical performance, which is distinctive from all the other tests performed in this section.

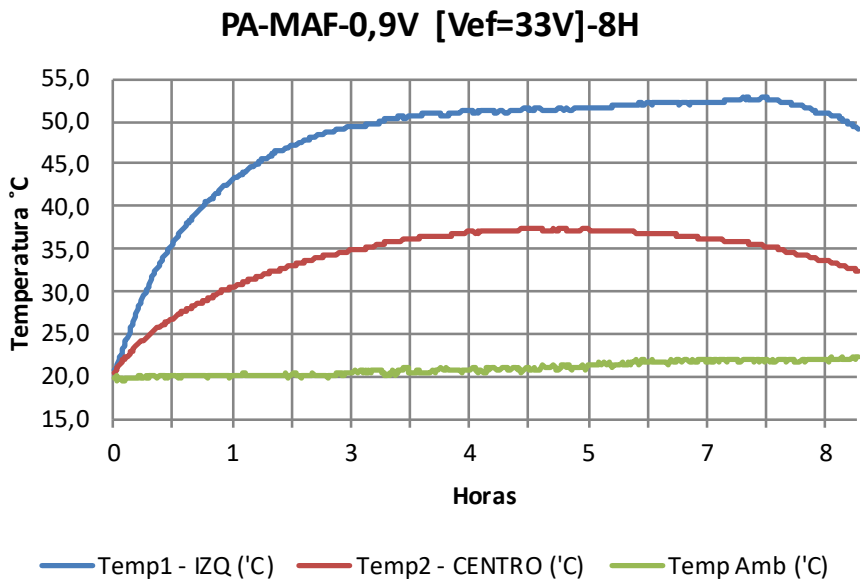


*Figure 4.43 Temperature-time recordings diagram for the first 8 hours heating sequence of PA-MAF at a Vexcit=0.9V*

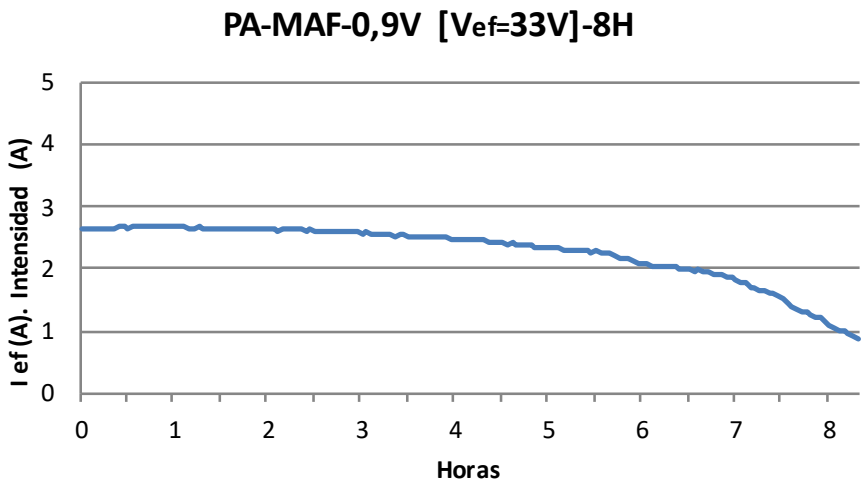


*Figure 4.44 Measurements of the intensity for the test of PA-MAF at Vexcit = 0.9V for the first 8 hours connection sequence*

The two diagrams above (see Figures 4.43. and 4.44.) present the behavior of the PA-MAF sample, which corresponds to the second case of the aforementioned catalogue of the tests. The initial behavior of the slab at the heating sequence is the one expected from the previous experiences with 3 hours cycles. However, at a certain point around the 4$^{th}$ hour of the cycle, the intensity starts decreasing and so does the temperature record. Moreover, there is a significant temperature difference between both terminals that is not reversible, even changing the terminals from the power inlet.

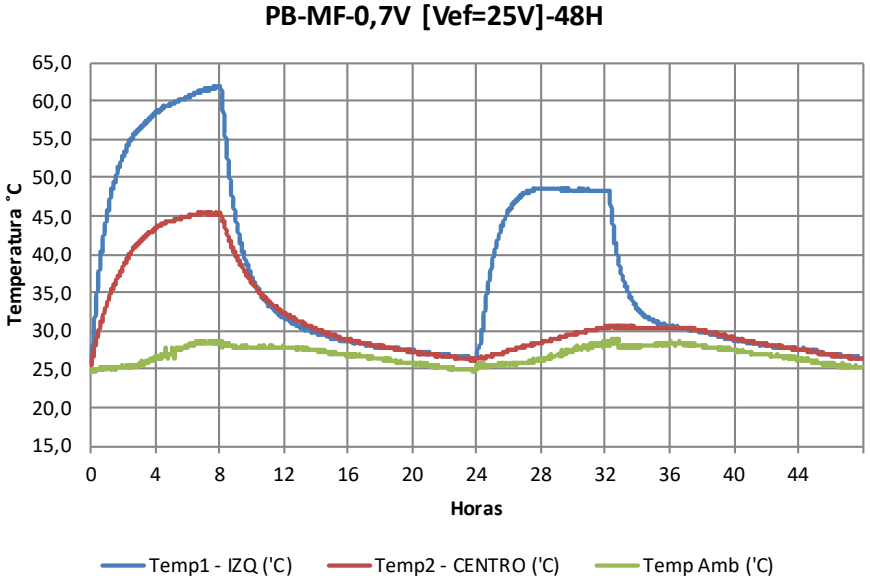


*Figure 4.45 Temperature-time recordings diagram for the full sequence of 48 hours of PB-MF at a Vexcit = 0.7V*

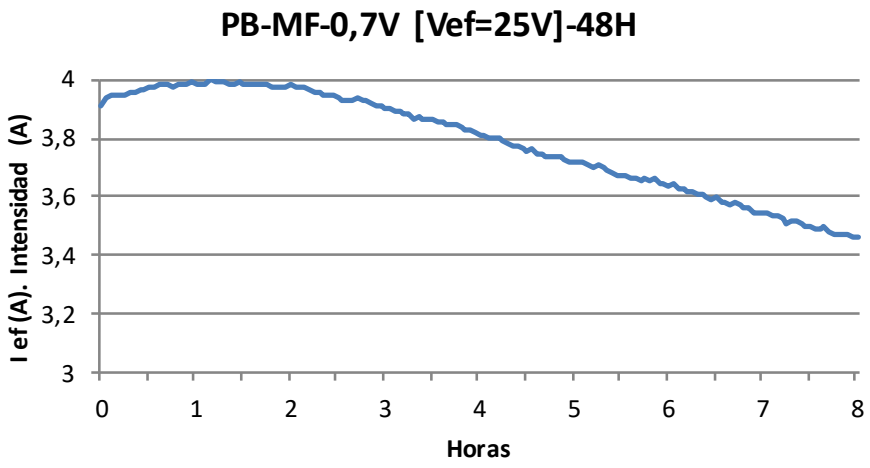


*Figure 4.46 Measurements of the intensity for the test of PB-MF at Vexcit = 0.7V for the first 8 hours connection sequence*

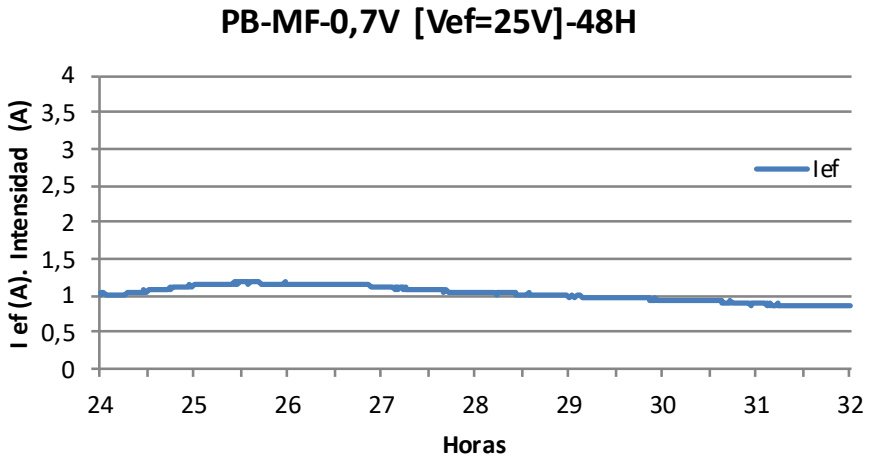


*Figure 4.47 Measurements of the intensity for the test of PB-MF at Vexcit = 0.7V for the second 8 hours connection sequence*

The three diagrams above (see Figures 4.44., 4.45. and 4.46.) represent the results for the PB-MF test. In this case the sample behaves in the same way as the previous test. Nevertheless, in this case the drop of temperature is not detected and the sequence is continued completing the full 48 hours cycle.

In general terms, the shape of the results is quite similar to the optimal one drawn for the PA-MF test, although in this case, there is a lack of regularity in the

sequences having a first heating sequence that reaches much higher temperatures than the second one.

However, during the second heating sequence, an unusual effect is exhibited, since the left end terminal located at the power inlet continues to warm up, whereas central electrode registers an insignificant increase of temperature for the second cycle, enhancing in a very pronounced way the difference in heat production between both locations of the same sample.

The analysis of the current intensity shows that the drop of intensity in this case started at the beginning of the first heating sequence, after approximately 2 hours, whereas for the second heating cycle, even though the values of the intensity are quite low due to the previous drop, it remains nearly constant for the whole sequence.

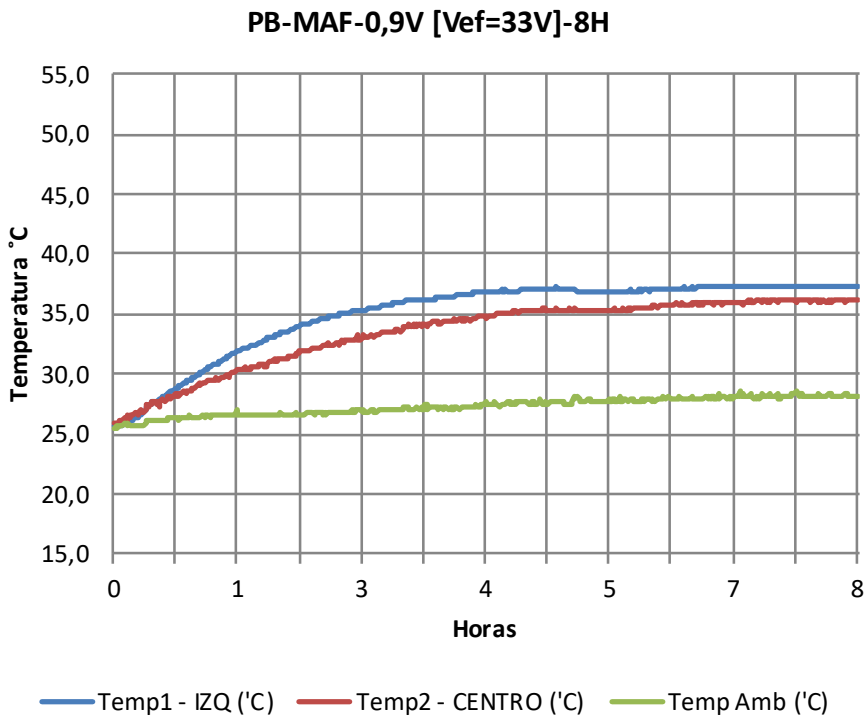


*Figure 4.48 Temperature-time recordings diagram for the first 8 hours heating sequence of PB-MAF at a Vexcit=0.9V*

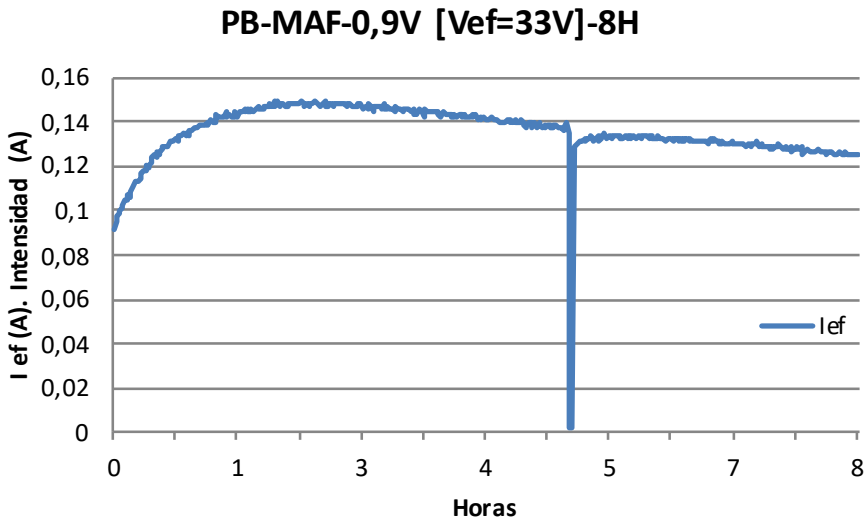


*Figure 4.49 Measurements of the intensity for the test of PB-MAF at Vexcit = 0.9V for the first 8 hours connection sequence*

The two diagrams above (see Figures 4.48. and 4.49.) present the test results for the PB-MAF sample. These results are embraced on the first case from the three cases aforementioned. Although, comparatively, a very significant difference in temperature recording is not observed between this test and the 3 hours cycle one, when the temperature at the opposite terminal is verified a clear difference shows up, together with a difference in electrical current. In such a manner, that in the 3 hours cycles test the tendency of the temperature was a sustained increase, whereas for the 8 hours cycles it stabilizes and then reduces.

After analysing all the results from the 48 hours cycles test series, it can be concluded that there is a reduction of the conductive properties of the material due to the effect of temperature and the time at which the sample is submitted to a certain sustained temperature. Indeed, the higher the conductivity, the later this phenomenon appears. Similarly, for alike conductivities, the higher the temperature reached the more likely this phenomenon appears.

This short circuit point is gradual but cannot be recovered once it has begun, being irreparable. In such a manner, that even cutting the passing of current through the sample the conductivity continues to decrease.

Besides, asymmetric behaviours for the different electrodes can be observed, so that one of the terminals has always much higher temperature than the other, even if the polarities are changed.

### 4.2.4. Temperature recording for 8 hours cycles in beams

For this test series, the research was performed in prismatic concrete beams with both types of electrodes disposal and both types of carbonaceous materials addition – VA-MF, VA-MAF, VB-MF and VB-MAF.

The temperature recording cycles consisted in 8 hours cycles with excitement voltages of 0.4V, 0.55V and 0.7V. Furthermore, for beams the measurement system uses 4P, unlike the slabs.

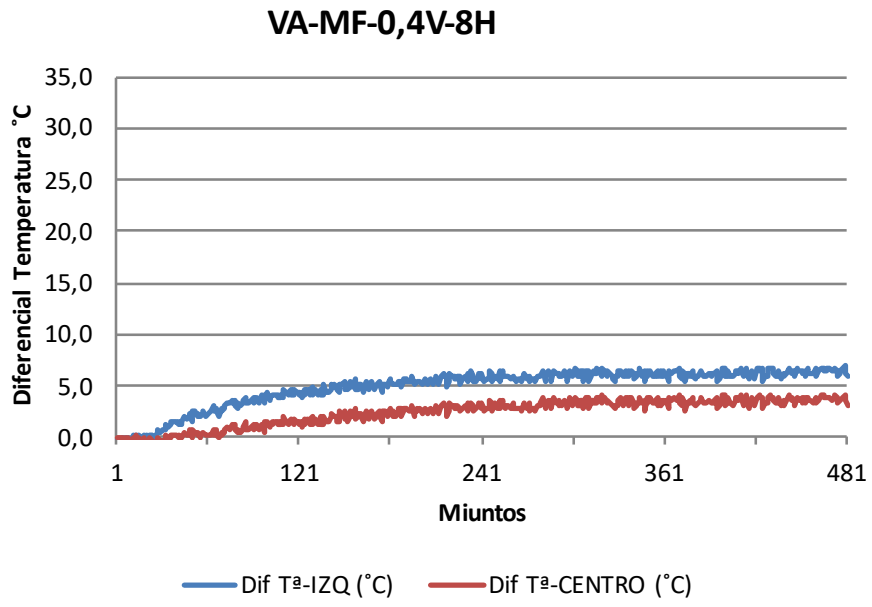


*Figure 4.50 Temperature variation vs time diagram for VA-MF at a Vexcit of 0.4V for 8 hours cycles*

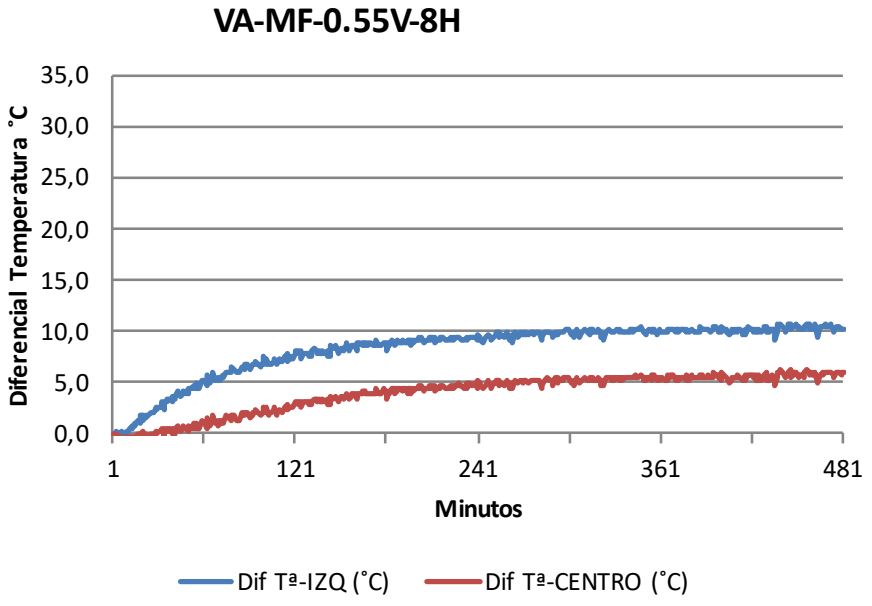


*Figure 4.51 Temperature variation vs time diagram for VA-MF at a Vexcit of 0.55V for 8 hours cycles*

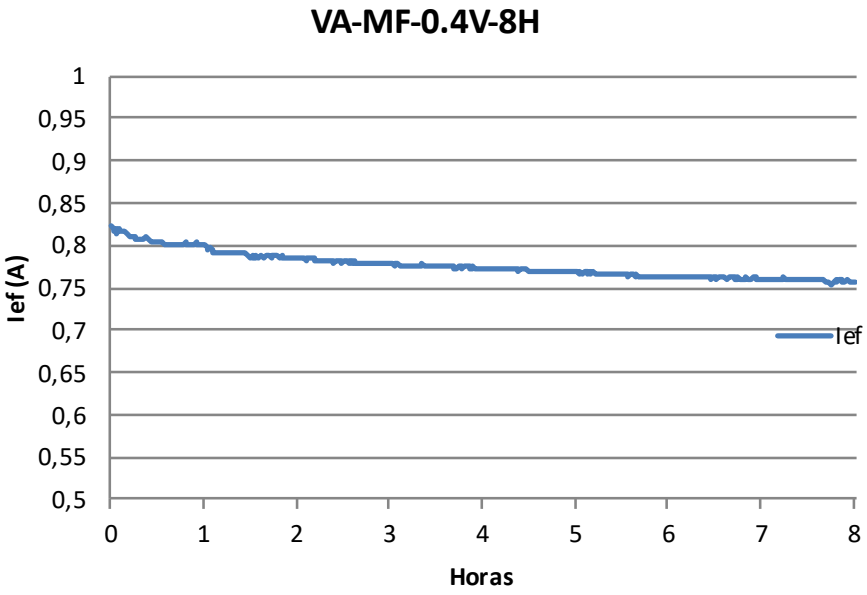


*Figure 4.52 Measurements of the intensity for the test of VA-MF at Vexcit = 0.4V for 8 hours cycles*

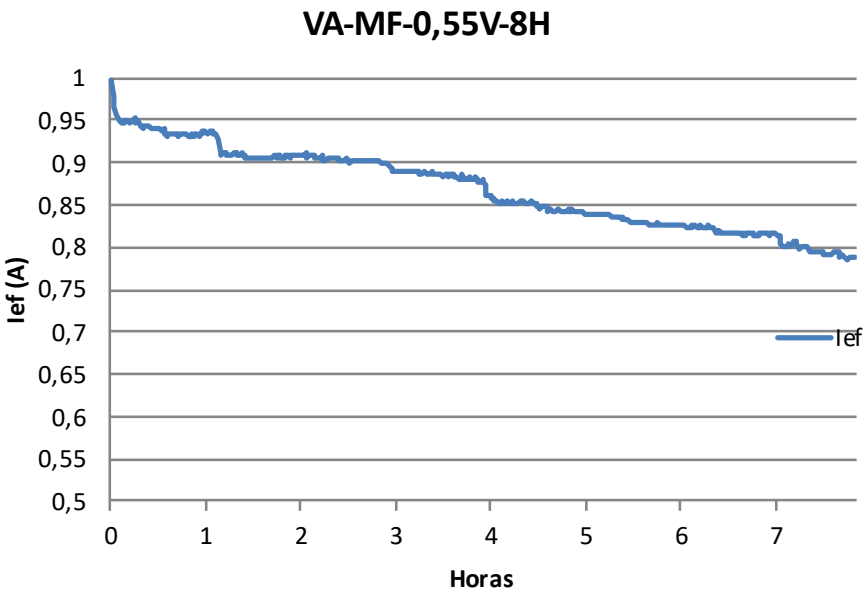


*Figure 4.53 Measurements of the intensity for the test of VA-MF at Vexcit = 0.55V for 8 hours cycles*

The 4 diagrams above (see Figures from 4.50. to 4.53.) present the results from the 8 hours cycles tests for VA-MF at excitement voltages of 0.4V and 0.55V, and their correspondent electrical current intensity evolution, for each test.

In both cases, the temperature differential is strictly positive, smooth and with gentle slope and in both cases a little difference between the centre and the left end of the sample in terms of heat production is exhibited.

Comparing the results obtained with different values of excitement voltage, the sample tested at $V_{excit}$ = 0.55V develops a higher temperature differential, due to the higher electric energy passing through the sample, reaching its highest value at the end of the 8 hours interval equal to 11°C, with an average heating rate of 0.0229°C/min increasing 1°C every 43.64 min, which is much smaller than the results obtained for the same time interval for concrete slabs, which indicates the influence of the geometric parameters for the samples' heat production.

This contrasts with the results obtained for a $V_{excit}$ = 0.4V which are even smaller, with a maximum temperature differential of 7°C after 8 hours of connection. With an average heating rate of 0.015°C/min increasing 1°C every 68.57 min. Therefore, in this case the results were practically insignificant compared with other set ups.

Regarding the current intensity measurements, in both cases they exhibit a gradual decrease along time, more pronounced for the $V_{excit}$ = 0.55V case. This might be one of the reasons for which the results are as low.

The same pattern and same behaviour are exhibit in the results for the PB-MF sample, presented in the 4 diagrams below (see Figures from 4.54. to 4.57.).

In this case, the characterization would practically the same, only changing the final differential temperature output, due to a slightly steeper slope. The maximum variation of temperature developed after 8 hours of connection is reached at $V_{excit}$ = 0.55V with value 16°C, with an average heating rate of 0.033°C/min increasing 1°C every 30 min.

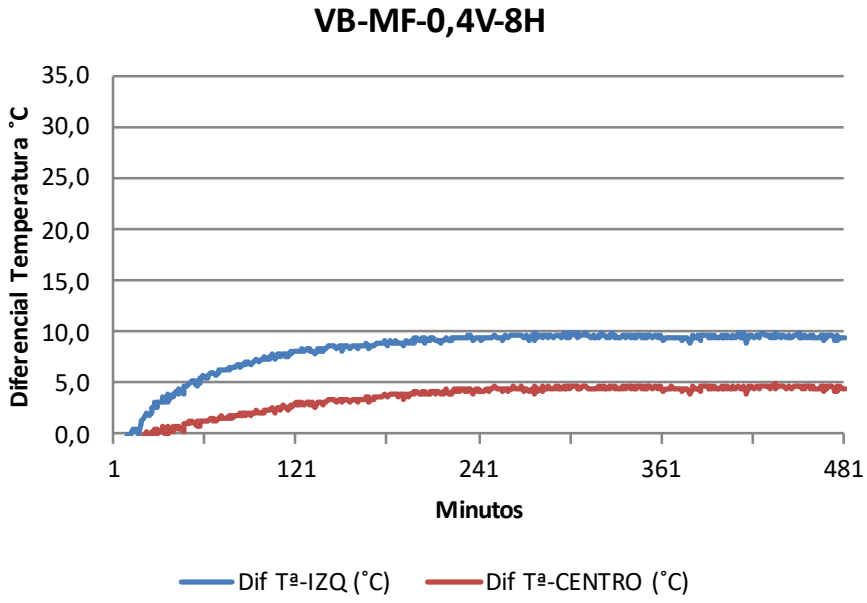


*Figure 4.54 Temperature variation vs time diagram for VB-MF at a Vexcit of 0.4V for 8 hours cycles*

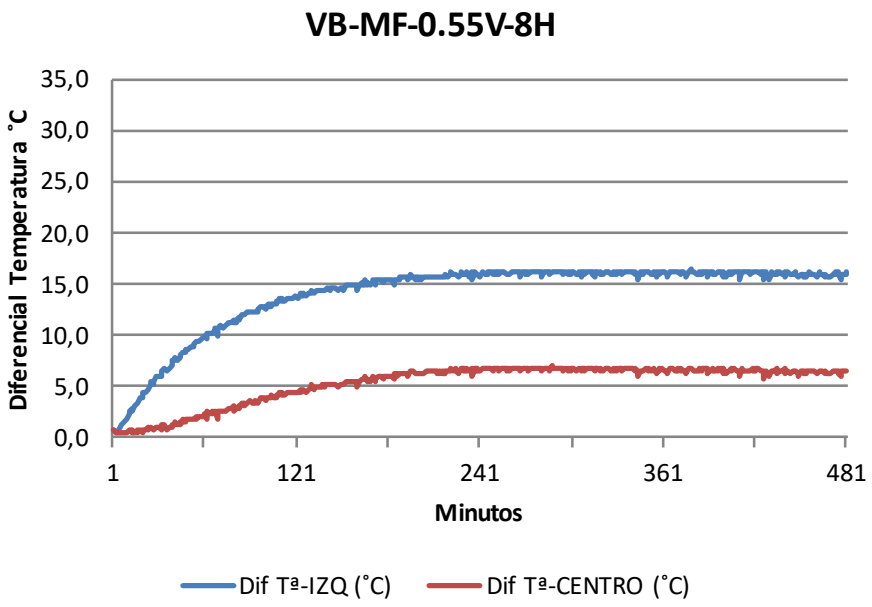


*Figure 4.55 Temperature variation vs time diagram for VB-MF at a Vexcit of 0.55V for 8 hours cycle*

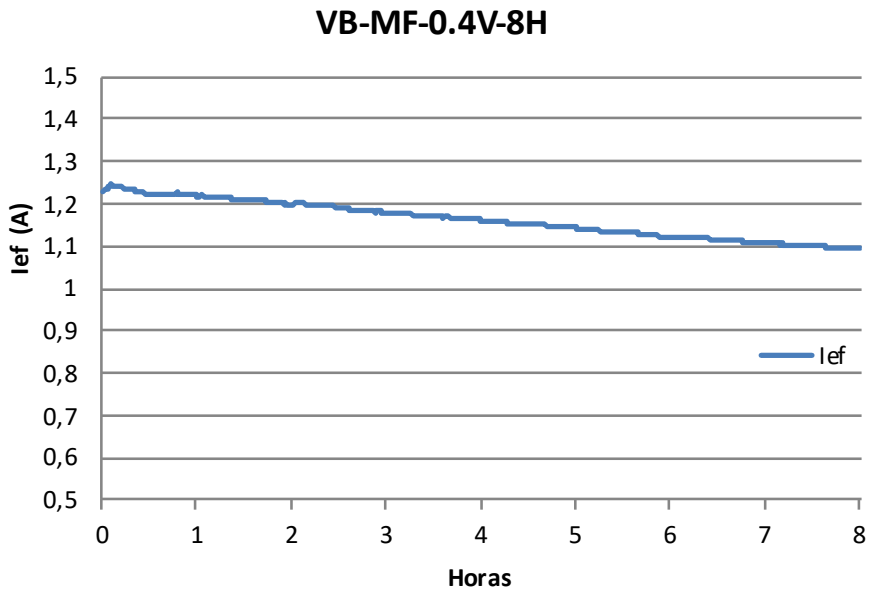


*Figure 4.56 Measurements of the intensity for the test of VB-MF at Vexcit = 0.4V for 8 hours cycles*

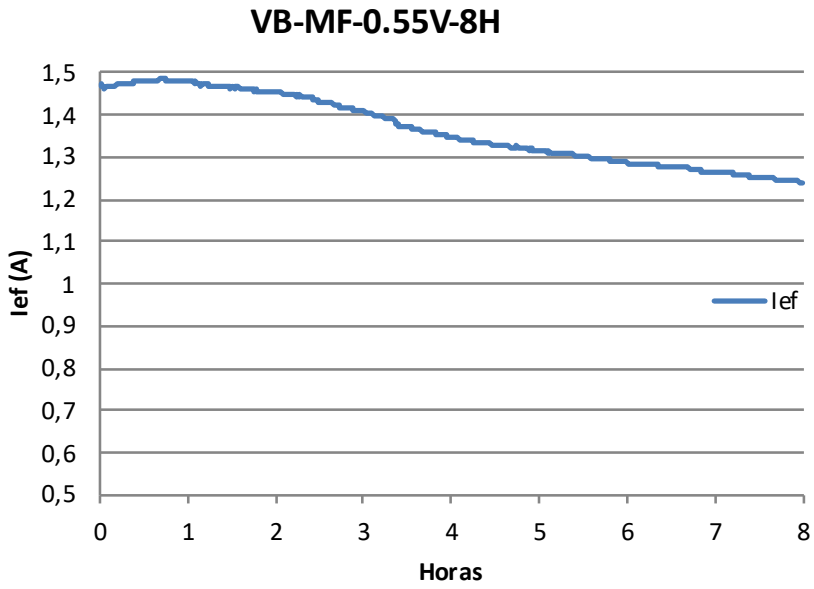


*Figure 4.57 Measurements of the intensity for the test of VB-MF at Vexcit = 0.55V for 8 hours cycles*

In this particular case, the results of the tests were exactly the same for MF and MAF, therefore the behaviour and the output values presented for the VA-MF are valid for VA-MAF and, idem, for VB-MF and VB-MAF.

Furthermore, one of the conclusions extracted from the tests is that, unlike the heat production tests performed with slabs, with beams a decrease in current intensity occurs from the first moment and its values is smaller than it would be expected.

Besides, the temperature difference between electrodes along the sample is very pronounced and, due to the fact that for beams a 4P system is used, the voltage at each of the terminals also decreases along time.

### 4.2.5. Temperature recording for 4 hours cycles in saturated slabs

For this test series, the research was performed in rectangular concrete slabs with both types of electrodes disposal and both types of carbonaceous materials addition – PA-MF, PA-MAF, PB-MF and PB-MAF – and fully saturated. The slabs used for these tests, where previously submitted to the heat production tests of 48 hours cycles, where some of their properties were deteriorated and afterwards they were saturated. The heating and the saturation process induce changes in weight and density of the slabs as presents in the tables below (see Tables 4.5. and 4.6.).

The temperature recording cycles consisted in 4 hours cycles with a unique excitement voltage of 0.5V.

| | PA-MF | PB-MF | PA-MAF | PB-MAF |
|---|---|---|---|---|
| **Initial weight after manufacturing** | 17 | 17 | 17 | 17 |
| **Wight slabs after the heating process** | 14.30 | 15.15 | 14.90 | 14.90 |
| **Weight slabs after 4 days submerged in water** | 15.55 | 15.40 | 15.10 | 15.15 |
| **Weight slabs after 4 days of drying** | 14.45 | 15.30 | 15.00 | 15.00 |

*Table 4.5 Weight recording for the slabs' saturation process in Kg*

| | PA-MF | PB-MF | PA-MAF | PB-MAF |
|---|---|---|---|---|
| **Density slabs after the heating process** | 1986.11 | 2104.17 | 2069.44 | 2069.44 |
| **Density slabs after 4 days submerged in water** | 2159.74 | 2138.89 | 2097.22 | 2104.17 |
| **Density slabs after 4 days of drying** | 2006.94 | 2125.00 | 2083.33 | 2083.33 |

*Table 4.6 Density recording for the slabs' saturation process in (Kg/m³)*

The results are presented in the diagrams below (see Figures from 4.58. to 4.65.) for each of the different samples.

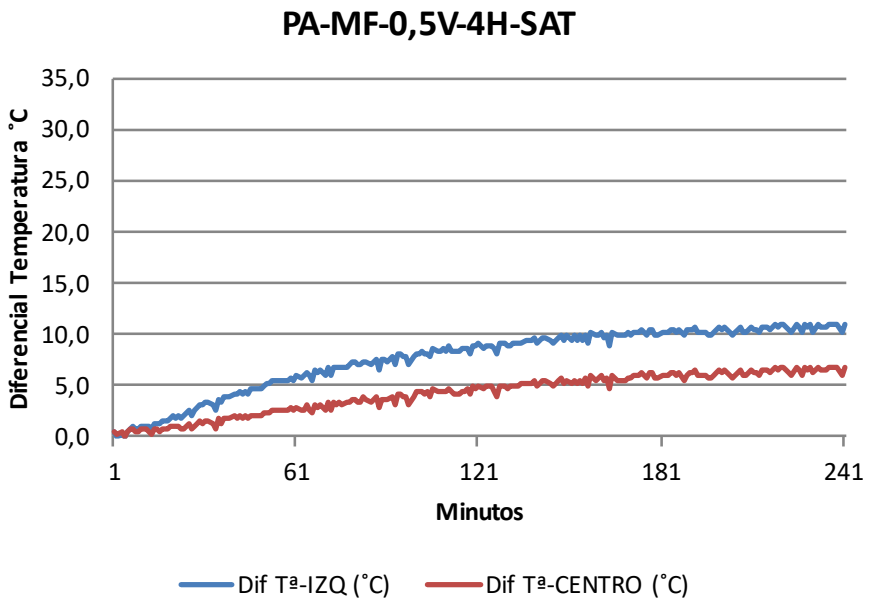


*Figure 4.58 Temperature variation vs time diagram for PA-MF-SAT at a Vexcit of 0.5V for 4 hours cycles*

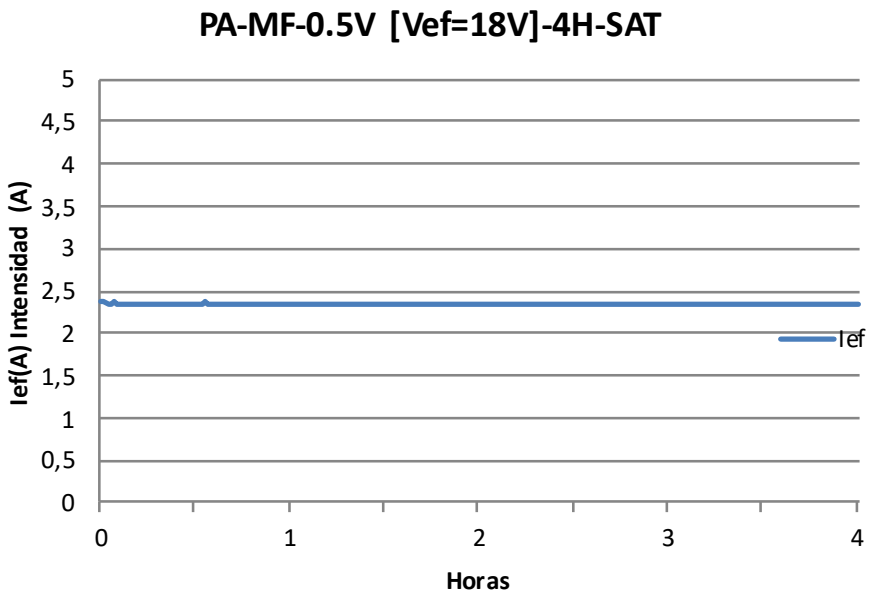


*Figure 4.59 Measurements of the intensity for the test of PA-MF-SAT at Vexcit = 0.5V for 4 hours cycles*

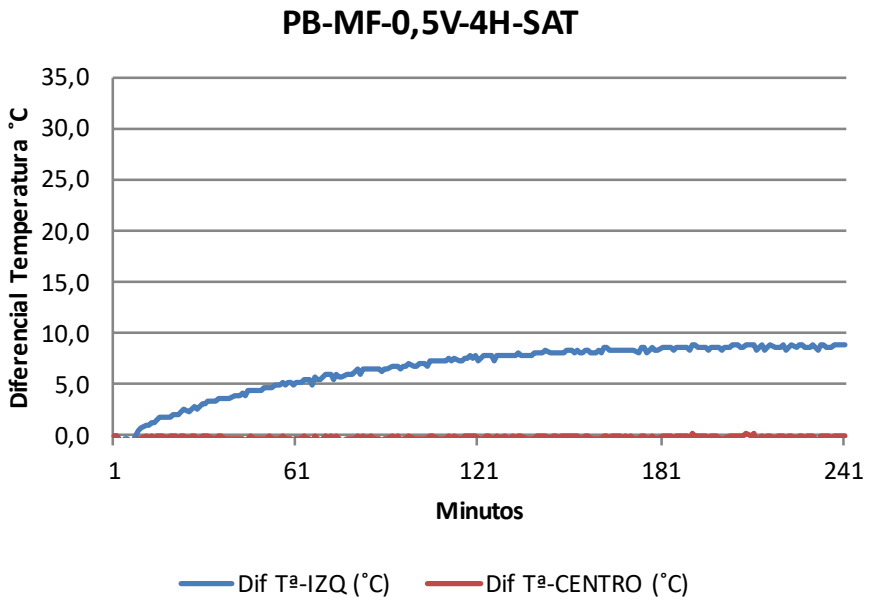


*Figure 4.60 Temperature variation vs time diagram for PB-MF-SAT at a Vexcit of 0.5V for 4 hours cycles*

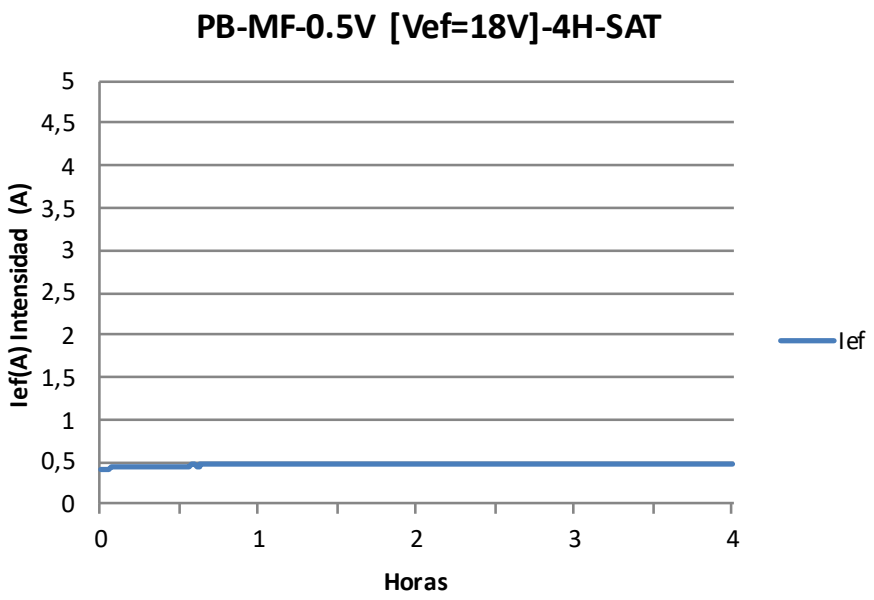


*Figure 4.61 Measurements of the intensity for the test of PB-MF-SAT at Vexcit = 0.5V for 4 hours cycles*

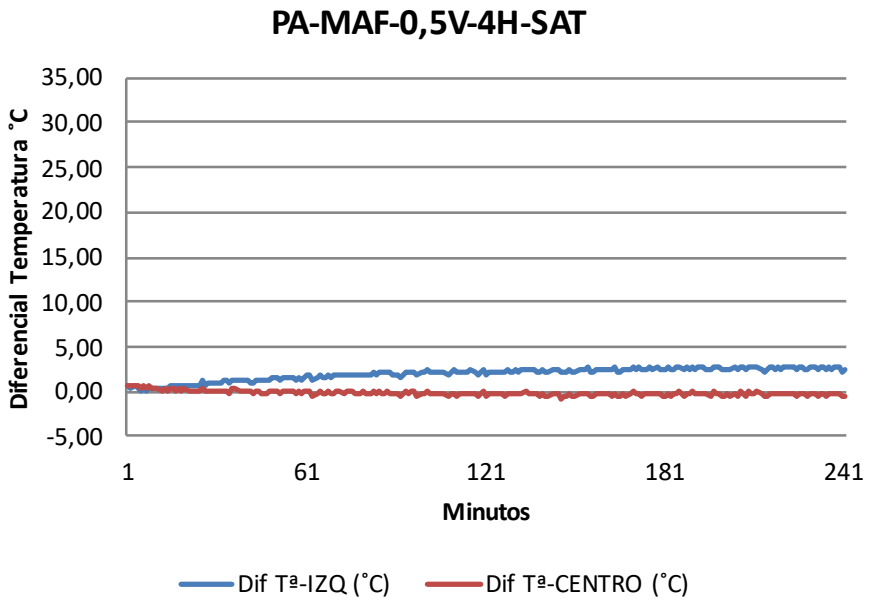


*Figure 4.62 Temperature variation vs time diagram for PA-MAF-SAT at a Vexcit of 0.5V for 4 hours cycles*

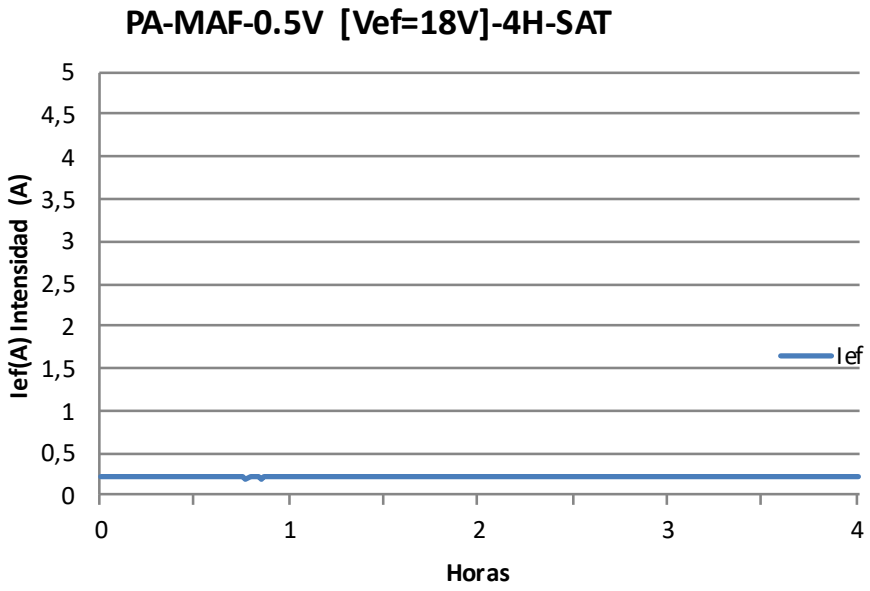


*Figure 4.63 Measurements of the intensity for the test of PA-MF-SAT at Vexcit = 0.5V for 4 hours cycles*

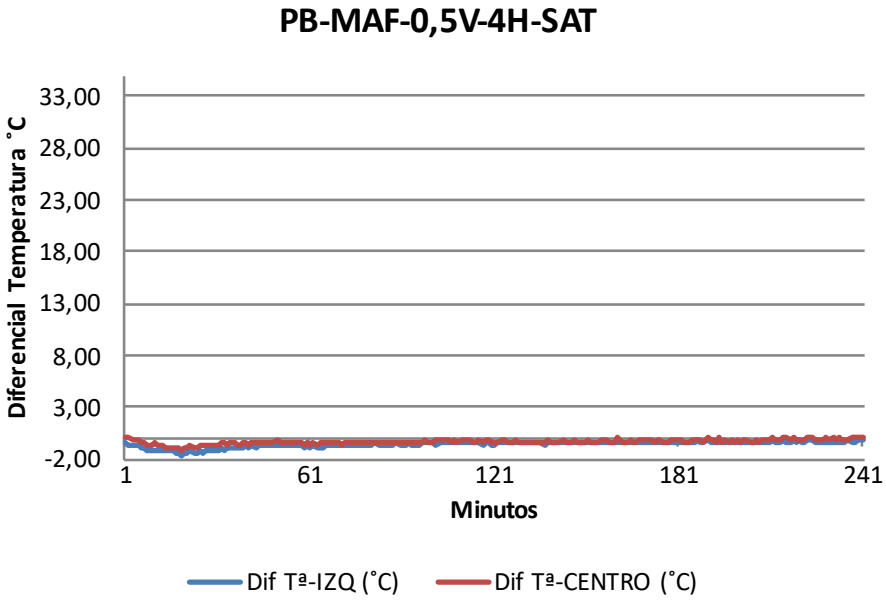


*Figure 4.64 Temperature variation vs time diagram for PB-MAF-SAT at a Vexcit of 0.5V for 4 hours cycles*

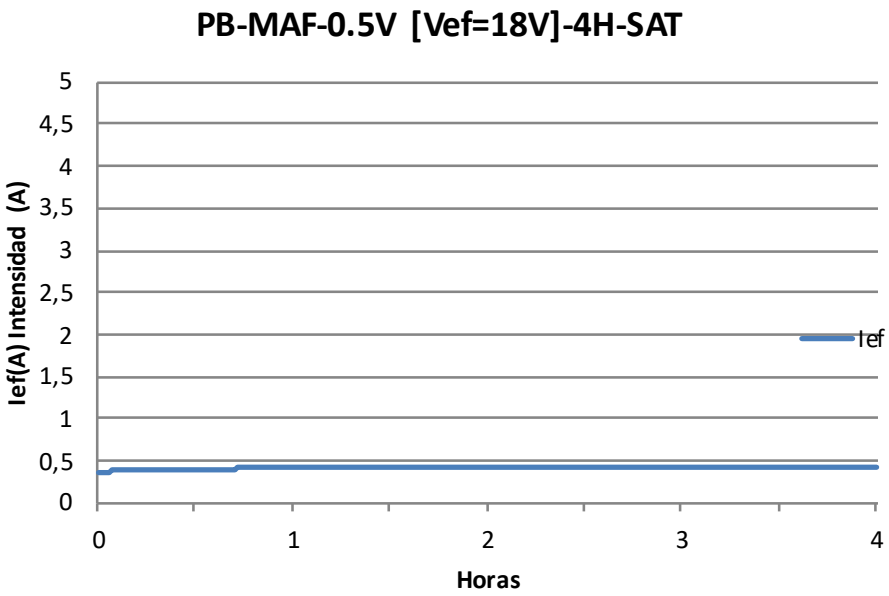


*Figure 4.65 Measurements of the intensity for the test of PB-MAF-SAT at Vexcit = 0.5V for 4 hours cycles*

An important diversity of results was obtained, with a common factor. In all the tests, the current intensity was kept constant in all cases with no drops. However, in general, but specially for the MAF materials the values of the current intensity were very low. This might have influenced the very poor results in terms of heat production and temperature differential development from the MAF materials.

In general, the temperature variations achieved at the end of 4 hours were quite low. Nevertheless, the final temperature differential developed for [PA/PB]-MF at a $V_{excit}$ = 0.5V at the end of the 4 hours cycle was very similar to the one developed for the initial 3 hours cycles testing. This was considered a very good result, considering that the slabs were already degraded from the 48 hours cycle and, also showed, that in this case the effect of the pore water in the concrete element helped the conductive properties and the heat production.

The best results recorded correspond to the PA-MF sample reaching a maximum temperature differential of 11°C, with an average heating rate of 0.046°C/min increasing 1°C every 21.82 min. Whereas, with the electrodes disposal B the results were affected by a very low current intensity value that was traduced in a large difference of temperature variation between the left end and the centre of the, being the second one nearly 0°C for the whole time interval.

Contrary to the MF materials results, the temperature differential for the MAF materials was completely insignificant up to the point that for the PB-MAF sample the result was 0°C for the whole test.

Consequently, it can be concluded that, even though, the moisture content is a parameter that has been proven to have a direct impact on the thermal properties of conductive concrete, in this case it has not been translated in very different results. Although, a decrease of the resistivity was detected due to the effect of a high moisture content in the sample.

### 4.2.6. Modelling of the thermal behaviour

After the analysis of the results conducted in the previous sections for each tests series, the attention was directed in seeking if it was possible to describe a regular behaviour for the heat production of our conductive composite cement-based material for all the scenarios produced.

Aiming at analysing the behaviour of the temperature differential development and the temperature recordings with respect to time, the data obtained from the tests was processed and modelled using Matlab coding, R studio and Excel in order to evaluate its tendency. In this manner, a better understanding of the self-heating process could be developed.

As a starting point, the correlation between the temperature differential and the time for each cycle was analysed, considering that the Joule effect, which describes the transformation of the electric energy into heat, states a direct relation between both magnitudes. After processing the data, it was found that this correlation could be analysed by means of a polynomial approximation. Consequently, a “polifit” coding of Matlab was used, in order to evaluate its tendency with a polynomial function (see Figures 4.66. and 4.67.).

After trying polynomial approximations of different degree, a polynomial function of degree 6 was taken, since the accuracy of the results was considered good enough, with the parameters and the $R^2$ accuracy coefficient presented below (see Figures 4.66. and 4.67.).

The modelling of the results was performed for every type of test scenarios and materials. However, only a couple of examples are provided in this report, due to the impossibility of presenting so many diagrams and equations. Therefore, only the most representative diagrams which are thought to have a better contribution to the understanding of the reader are presented.

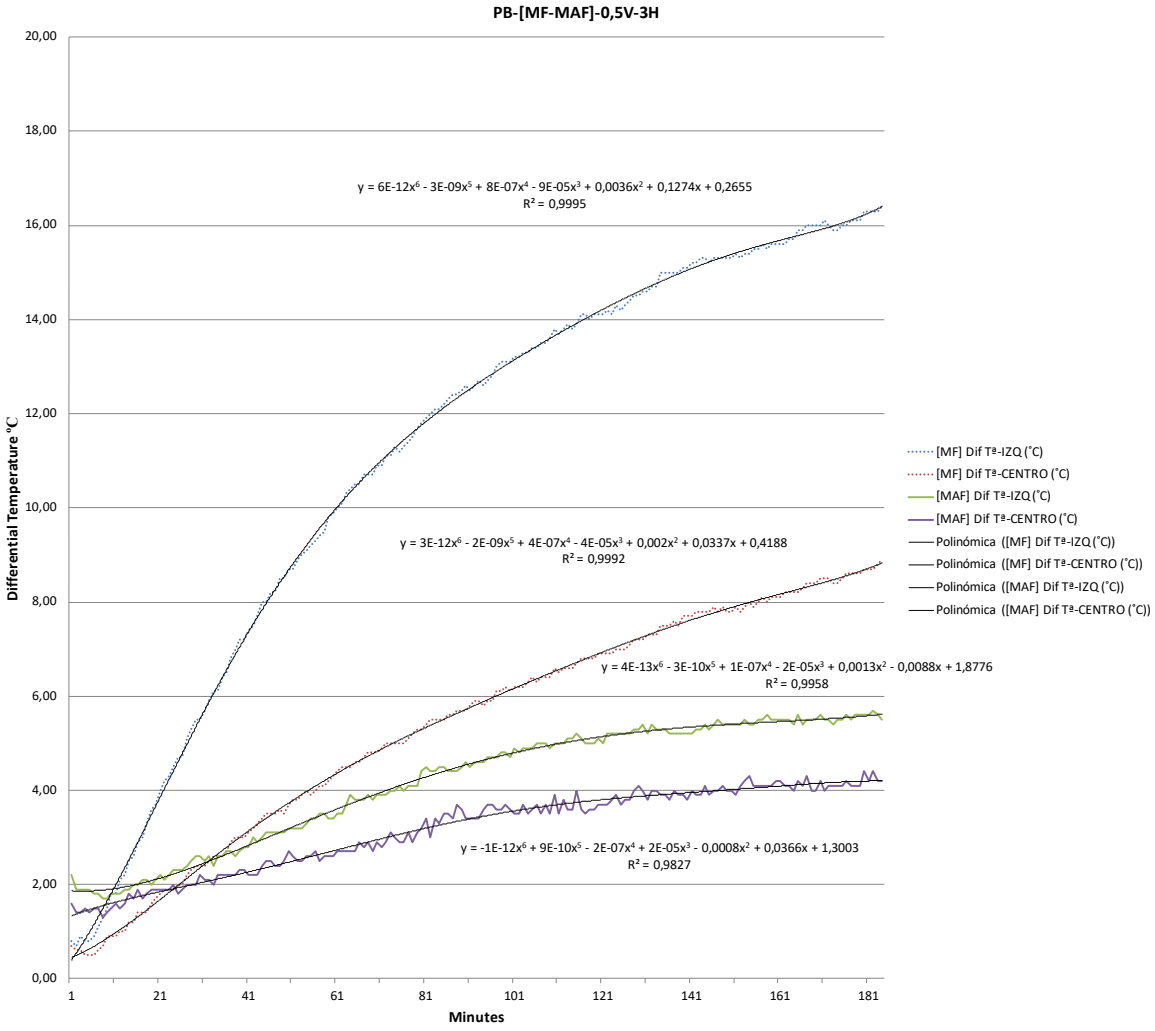


*Figure 4.66 Modelling of the correlation between Temperature Differential and Time for the case of PB-[MF/MAF] samples at Vexcit = 0.5V for 3 hours cycles*

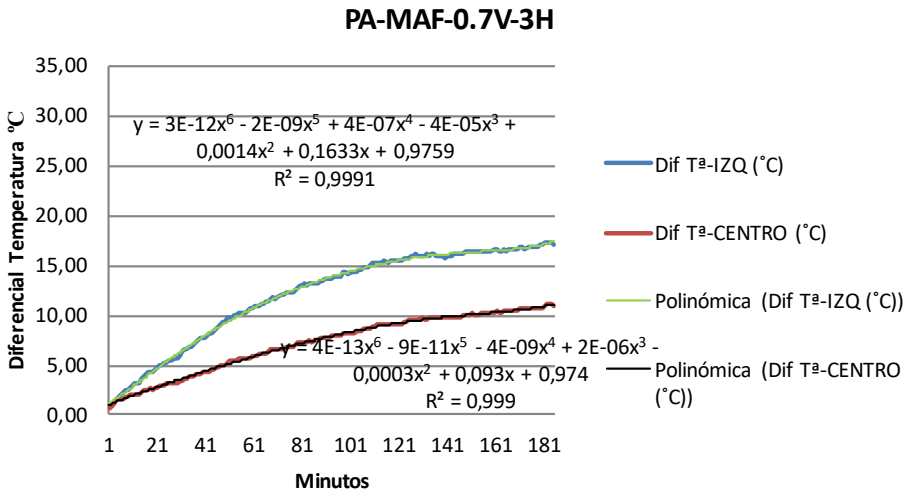


*Figure 4.67 Modelling of the correlation between Temperature Differential and Time for the case of PA-MAF sample at Vexcit = 0.7V for 3 hours cycles*

The results obtained showed that a polynomial approximation function of degree 6 fitted extremely good with the heating process results, representing the correlation between temperature differential and time. Besides, since in nearly all the experiences the temperature differential at the centre of the sample was lower than at the left end, generally, the polynomial function coefficients for the central electrode were smaller than for the left end, generating softer slopes and smaller gradients.

Afterwards, the correlation between the temperature recordings and the time for each cycle was analysed, with the hypothesis that it would follow a very similar behaviour from the correlation obtained for the temperature differential. After processing the data, it was found that this correlation could be analysed by means of a polynomial approximation, too.

Consequently, a "polifit" coding of Matlab was used, in order to evaluate its tendency with a polynomial function, also resulting in a polynomial function of degree 6, for which the accuracy of the results was considered good enough, with the parameters and the $R^2$ accuracy coefficient presented below (see Figures 4.68. and 4.69.).

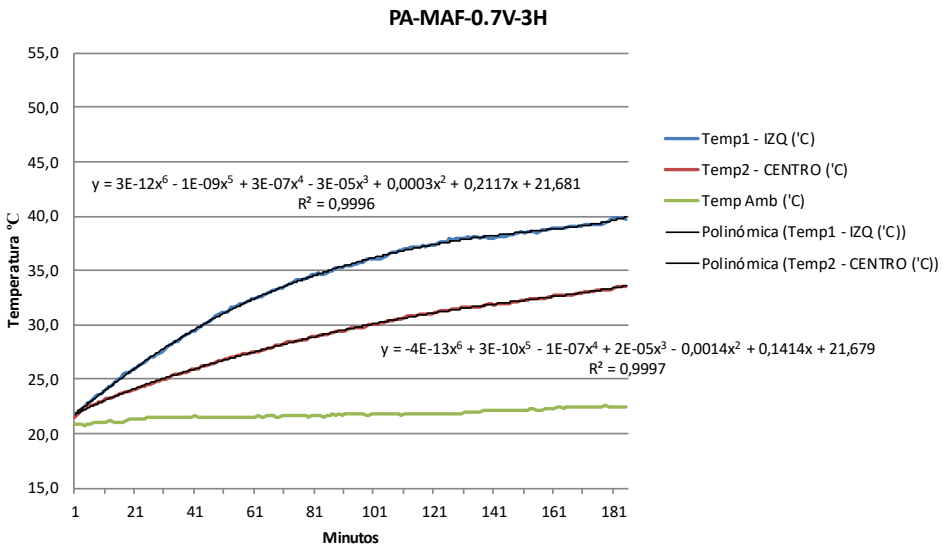


*Figure 4.68 Modelling of the correlation between Temperature recordings and Time for the case of PA-MAF sample at Vexcit = 0.7V for 3 hours cycles*

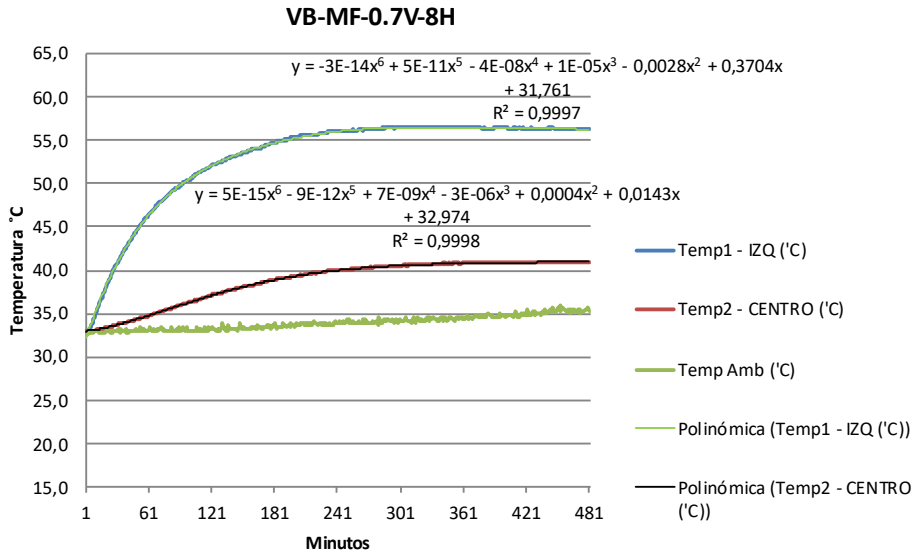


*Figure 4.69 Modelling of the correlation between Temperature recordings and Time for the case of VB-MF sample at Vexcit = 0.7V for 8 hours cycles*

However, a special analysis was conducted for the test scenario of 48 hours cycles, since, in this experience, not only the warm up trends were evaluated, but also the cooling behaviour. In order to analyse both behaviours, the data from the PA-MF sample at a $V_{excit}$ = 0.7V was taken, due to the fact that it was the test which exhibited the closest behaviour to the desired one.

Then, the data was modelled for temperature differential and temperature recordings with respect to time, first for the heating cycle of 8 hours and the for the cooling cycle of 16 hours. The results are presented in the following figures, were an extremely good fitting is exhibited (see Figures 4.70., 4.71., 4.72. and 4.73.), while the parameters from the polynomial approximative function and the $R^2$ accuracy coefficients are presented in the tables below (see Tables 4.7. and 4.8.).

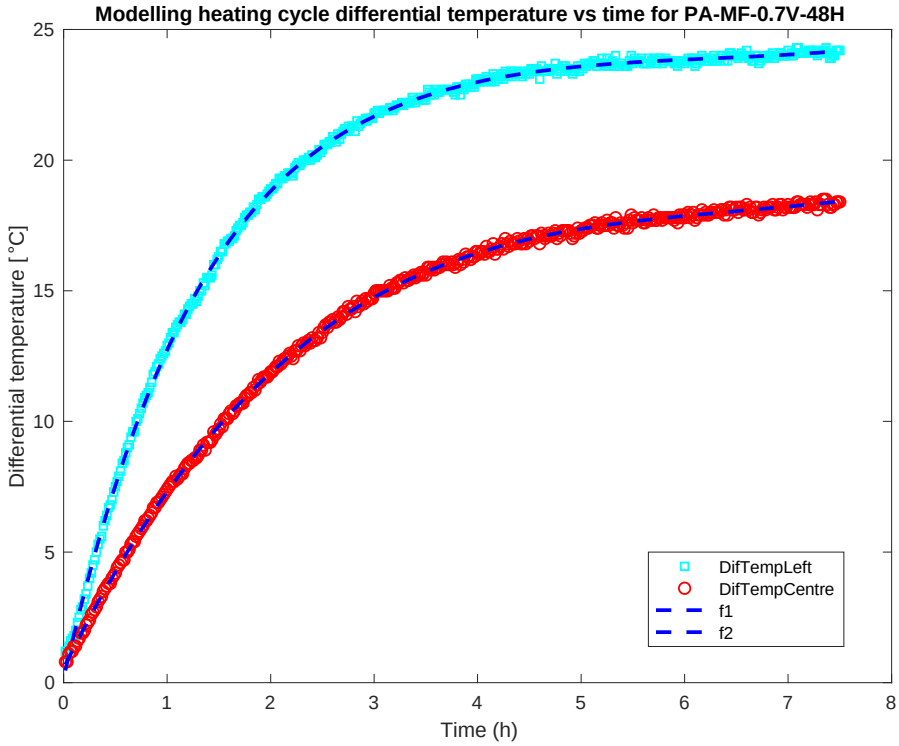


*Figure 4.70 Modelling of the correlation between Differential Temperature developed and Time for the case of PA-MF sample at Vexcit = 0.7V for the heating cycle of 8 hours within the 48 hours cycles*

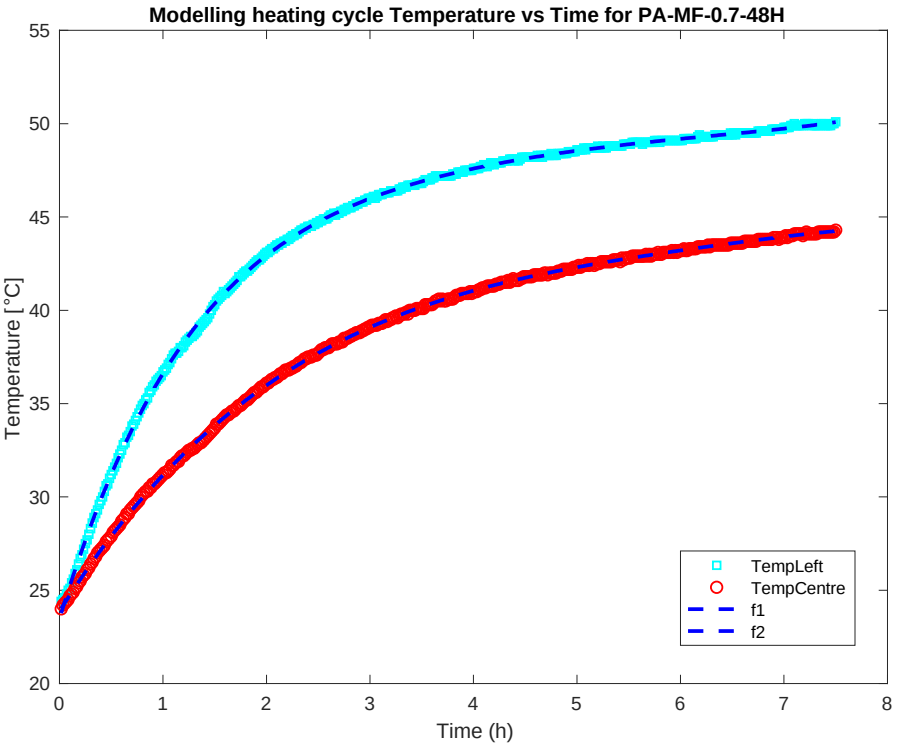


*Figure 4.71 Modelling of the correlation between Temperature recordings and Time for the case of PA-MF sample at Vexcit = 0.7V for the heating cycle of 8 hours within the 48 hours cycles*

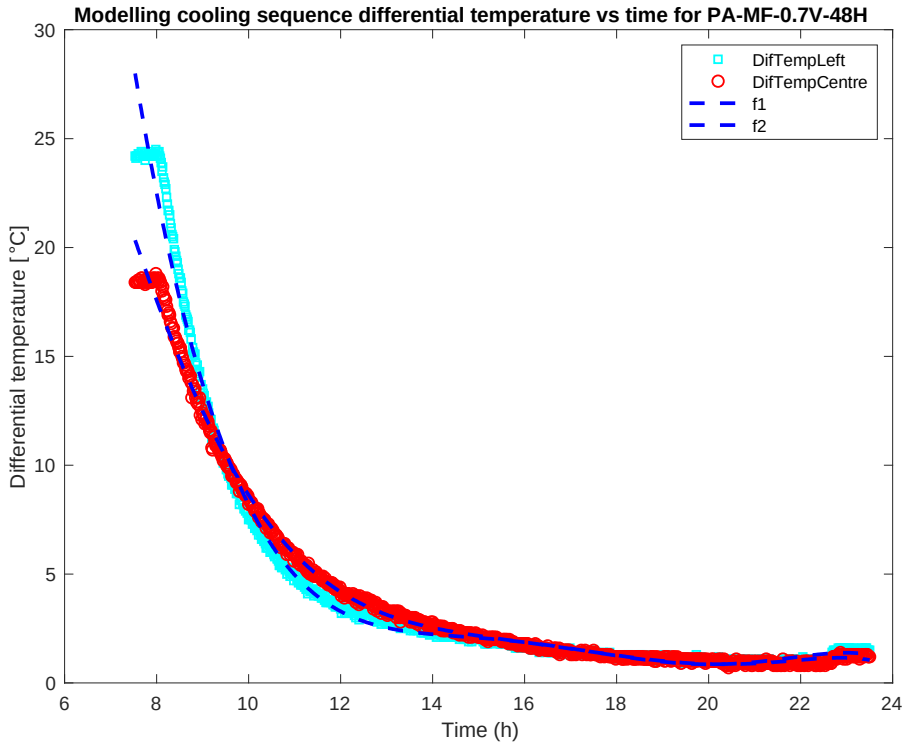


*Figure 4.72 Modelling of the correlation between Differential Temperature developed and Time for the case of PA-MF sample at Vexcit = 0.7V for the cooling cycle of 8 hours within the 48 hours cycles*

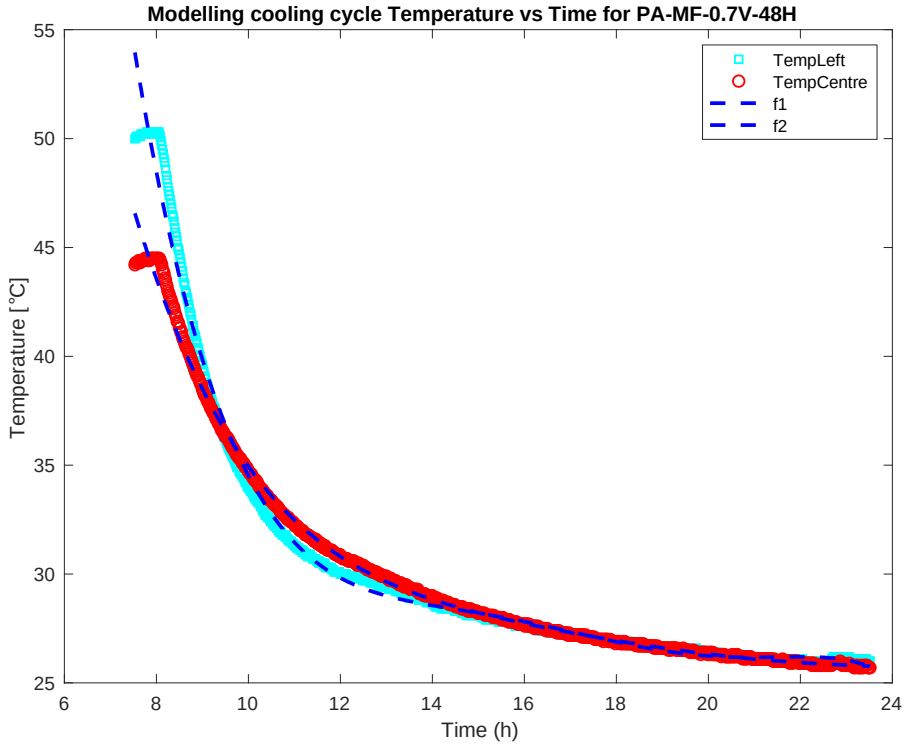


*Figure 4.73 Modelling of the correlation between Temperature recordings and Time for the case of PA-MF sample at Vexcit = 0.7V for the cooling cycle of 8 hours within the 48 hours cycles*

| Cycles | | Parameters | | |
|---|---|---|---|---|
| | | P1 | P2 | P3 |
| **Heating Cycle (8 hours)** | Left End | -2.642e-04 | 0.0095 | -0.1425 |
| | Centre | 0.0000 | 0.0000 | -0.0026 |
| **Cooling Cycle (16 hours)** | Left End | -1.230e-05 | 9.017e-04 | -0.0210 |
| | Centre | -1.996e-05 | 0.0018 | -0.0667 |

| Parameters | | | | |
|---|---|---|---|---|
| P4 | P5 | P6 | P7 | $R^2$ |
| 1.1831 | -5.9243 | 17.4336 | 0.1772 | 0,99953279 |
| 0.1053 | -1.3990 | 8.0499 | 0.5564 | 0,99957864 |
| 0.0412 | 5.3185 | -76.8721 | 335.4937 | 0,9915033 |
| 1.2113 | -11.0397 | 41.4732 | -9.3066 | 0,99638076 |

*Table 4.7 Parameters from the polynomial approximative function and R2 accuracy coefficients from the modelling the differential temperature of heating and cooling cycles for the case of PA-MF sample at Vexcit = 0.7V for 48 hours cycles*

| Cycles | | Parameters | | |
|---|---|---|---|---|
| | | P1 | P2 | P3 |
| **Heating Cycle (8 hours)** | Left End | -2.117e-04 | 0.0089 | -0.1470 |
| | Centre | -1.251e-04 | 0.0029 | -0.0309 |
| **Cooling Cycle (16 hours)** | Left End | -7.477e-06 | 4.089e-04 | 7.497e-04 |
| | Centre | 0.0000 | -7,147e-05 | 0.0069 |

| Parameters | | | | |
|---|---|---|---|---|
| P4 | P5 | P6 | P7 | $R^2$ |
| 1.2673 | -6.3077 | 18.3219 | 23.4664 | 0,99975332 |
| 0.2572 | -1.8447 | 8.9219 | 23.8637 | 0,99984857 |
| -0.3827 | 10.0829 | -103.8677 | 421.6709 | 0,99193225 |
| -0.2635 | 5.0336 | -48.5415 | 218.7922 | 0,99657632 |

*Table 4.8 Parameters from the polynomial approximative function and $R^2$ accuracy coefficients from the modelling the temperatures of heating and cooling cycles for the case of PA-MF sample at Vexcit = 0.7V for 48 hours cycles*

After the analysis, the post processing and the modelling of the 8- and 16-hours sequences from the 48 hours cycles test series, it has been concluded that for long heating and cooling cycles a thermal equilibrium is reached in which the electric power per unit of time applied to the system is the same as the power released as heat to the outside. Since the increase in temperature is not large, the electric resistance of the sample as well as the power applied to the system remains nearly constant. Therefore, the temperature increases up to a constant value, drawing a plateau and reaching a

steady state. This occurs when the energy losses to the environment are equal to the electrical energy applied.

Nevertheless, the same reasoning cannot be applied in other tests that recorded gradual decreases in the current intensity, producing a decrease of the electric power, and so, of the temperature recordings, such as in the case of the test for the PA-MAF sample at a $V_{excit}$ = 0.9V for 8 hours heating cycle.

Consequently, it was thought that it could be very useful to model the correlation between the electric power and the temperature differentials developed, as well as with the current intensity.

Aiming at understanding better the relation between these magnitudes, the modelling of this concept was based on the results obtained in a research focused, precisely, in modelling this phenomenon [10]. In this paper, they stated that the changes of thermal energy in the sample were due to the applied electrical power minus the rate of energy loss by cooling which could be calculated with the Newton's law of cooling, as shown in the equation below (see Equation 4.5.).

$$mC_p \cdot \frac{dT}{dt} = P - hA(T - T_r) \tag{4.5}$$

Where T [°C] is the average temperature of the sample, t [s] is the time, m [kg] is the mass of the sample. $C_p$ [J/kg°C] is the specific heat of the material of the sample, P [W] is the applied electrical power, h [W/m$^2$ °C] is a parameter that measures the rate of energy transport towards the outside, A [m$^2$] is the surface of sample exposed and $T_r$ [°C] is the room temperature.

Integrating this equation with the initial condition t = $t_1$ being the time at which the application of the electrical potential difference starts, the following expression is obtained (see Equation 4.6.):

$$T = T_r + \frac{P}{hA} \cdot [1 - e^{-\frac{hA}{mC_p}(t-t_1)}] \tag{4.6}$$

When the time interval is long enough the steady state is reached and the temperature stays constant, like in the PA-MF of 48 hours cycles. Therefore, for t -> ∞ the equation is transformed into the equation below (see Equation 4.7.).

$$T = T_r + \frac{P}{hA} \tag{4.7}$$

Consequently, in steady state, the electric power supplied turns out to be equal to the energy loss calculated using Newton's law of cooling, following the equation below (see Equation 4.8.).

$$P = hA \cdot (T - T_r) \tag{4.8}$$

Along these lines, if the geometry of all the samples is the same, the representation of the electric power against the maximum temperature rise for each experiment should be a straight line of slope hA.

In order to compare our results with the model proposed in this study, the test results were divided in two categories: PA-[MF/MAF] samples and PB-[MF/MAF] samples, considering that, even though the main geometry defined by the dimensions is the same in both cases, the electrodes disposal affects the development of the thermal properties and the recording of the results.

The data sets consisted in the values of maximum differential temperature registered for each test and the correspondent electrical power value. Few tests were not considered due to defective results, together with the tests performed with beams, which could not be considered in the same geometry categories as slab. Besides there were too few data to perform a model only for beam samples with representative results.

In both cases, the data has been post-processed with Rstudio, since it is a program that provides a large number of tools for an accurate study of linear and multilinear regressions and, the correlation between data sets, using different kinds of plots and residuals analysis.

Previously the correlation between the power values and the maximum differential temperature developed, in order to understand the relation between the data, the trend that presents and the possibility of exhibiting collinearity issues. For both sample categories the correlation was defined around 0.95, which indicated a strong positive relationship between data and a high possibility of collinearity. After performing a collinearity check no issues were found.

On the one hand, the obtained results from the linear regression for PA fit quite descent way with a straight line of slope hA = 2.7163 W/°C with $R^2$ = 0.896, as shown in the figure below (see Figure 4.74.). Nevertheless, the model plots indicate the existence of some outliers increasing the range of the data in the boxplot, that the linearity assumption is not met with the accuracy required, that there is a lack of normally distributed errors and the presence of an important leverage in some residuals.

Therefore, the data does not fit adequately with the straight line proposed in the aforementioned model, which can be illustrated by the fact that the hA slope value is a quite inaccurate estimation compared to the stated values for these parameters. This analysis is presented in the figure below (see Figure 4.75.).

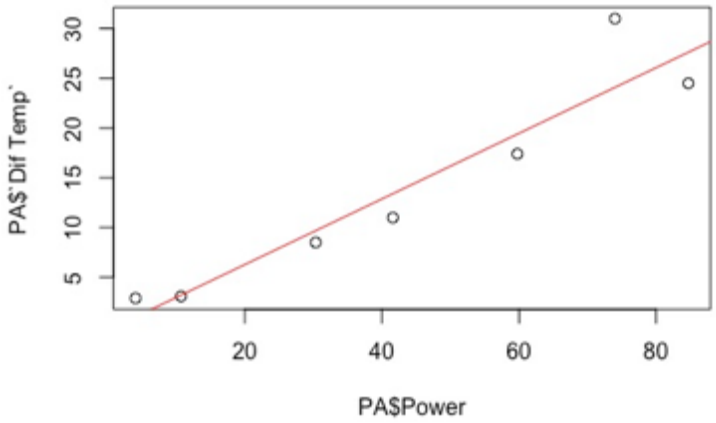


*Figure 4.74 Linear regression from experimental data of Max Differential Temperature vs Power according to Equation 4.8. for PA Geometry*

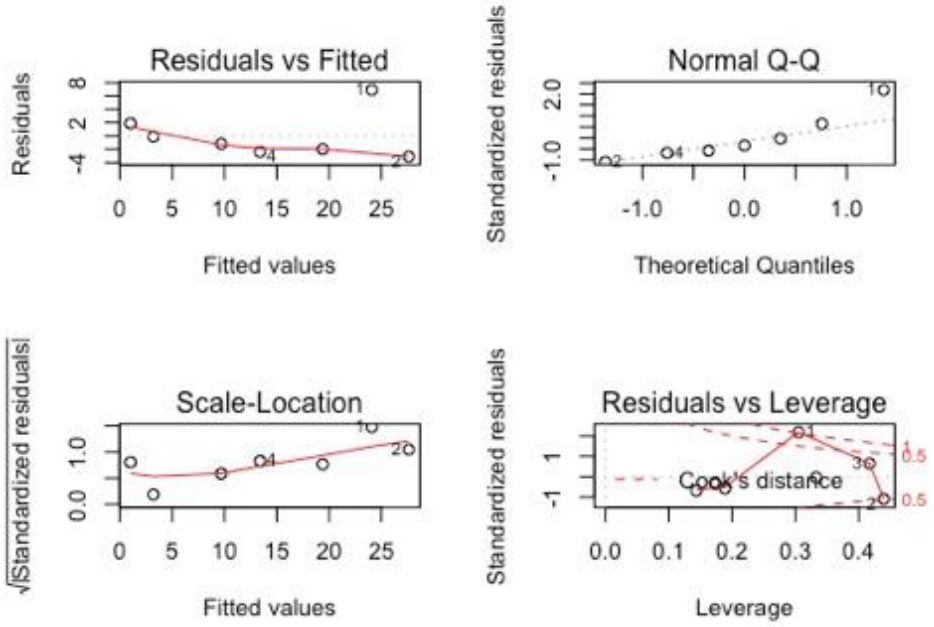


*Figure 4.75 Plots of the residuals and analysis of the Linear regression from experimental data of Max Differential Temperature vs Power according to Equation 4.8. for PA Geometry*

On the other hand, the obtained results from the linear regression for PB fit, in a very similar way to the PA results, in a descent way with a straight line of slope hA = 2.93 W/°C with $R^2$ = 0.893, as shown in the figure below (see Figure 4.76.).As in the previous case, the hA slope value cannot be considered as an accurate estimation, because it

does not correspond to the physical values of these parameter. Likewise, for PB, the model plots indicate the existence of some outliers increasing the range of the data in the boxplot, that the linearity assumption is not met with the accuracy required, that there is a lack of normally distributed errors and the presence of an important leverage in some residuals. This analysis is presented in the figure below (see Figure 4.77.).

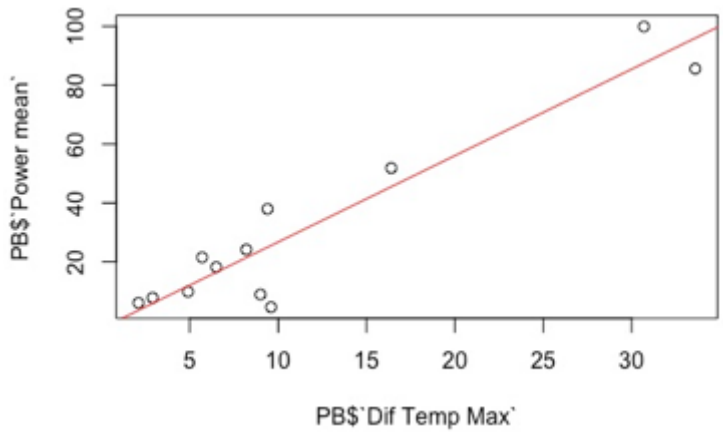


*Figure 4.76 Linear regression from experimental data of Max Differential Temperature vs Power according to Equation 4.8. for PB Geometry*

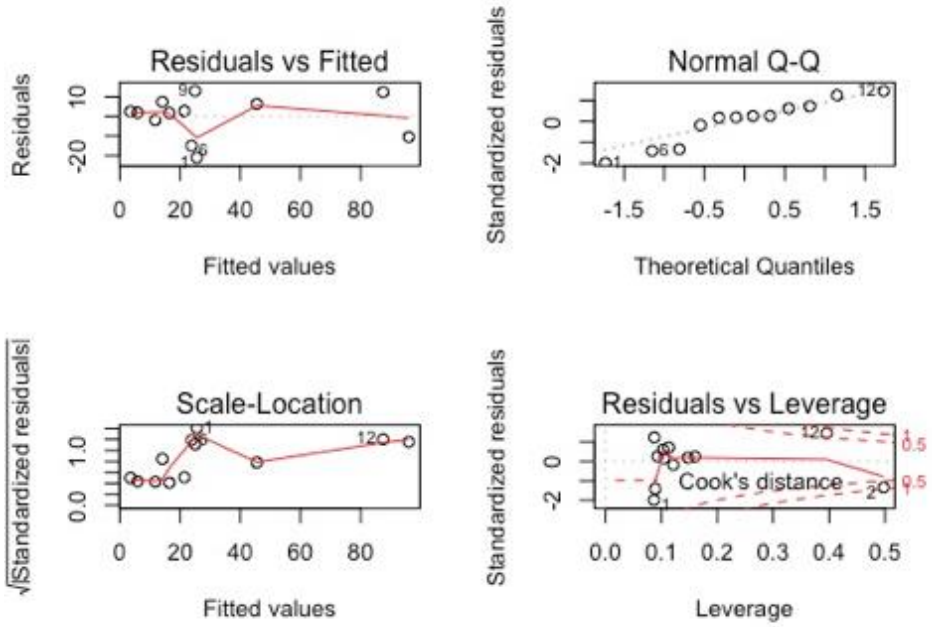


*Figure 4.77 Plots of the residuals and analysis of the Linear regression from experimental data of Max Differential Temperature vs Power according to Equation 4.8. for PB Geometry*

The inaccuracy of the results is linked to the presence of two different composite materials – MF and MAF – in the same sample, the diversity of test conditions and the limited amount of recorded results. However, the refence model presented is an accurate approach thanks to its physical base with the newton's law of cooling.

Furthermore, in some test a phenomenon was observed for which a drop of current intensity could affect the differential temperature development, emphasising the difference of heat production at different locations of the sample and, even in some cases, inducing temperature drops, such as for the case of PA-MAF at $V_{excit}$ = 0.9V for 8 hours cycle. The first guesses related this drops to a change on the resistivity of the material due to the current flux generated through the sample.

Consequently, the correlation between current intensity and temperature variation was analysed, looking for a pattern that could explain such phenomenon. In order to perform this analysis, the data from the heating sequences of PA-MF at $V_{excit}$ = 0.7V for 8 hours cycles was taken, since it was quite close to the optimal behaviour expected.

First, the correlation coefficients between both data sets were computed with a value of 0.892, which indicates a strong positive relationship. Then, the range of the data was analysed using a boxplot presented below (see Figure 4.78.). In this boxplot, the data sample exhibits a lot of outliers at the lower bound of the sample, and a very concentrated data body with very little range.

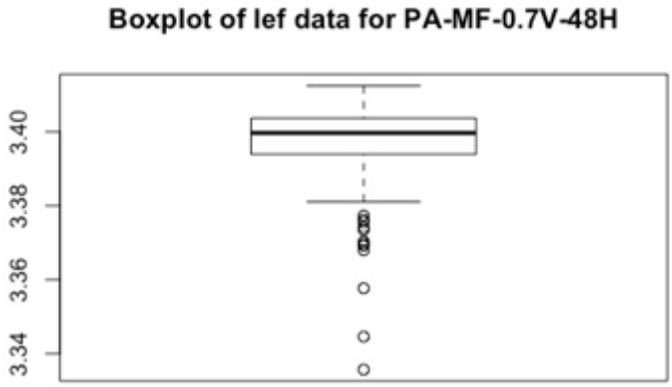


*Figure 4.78 Boxplot of the effective current intensity data from PA-MF at 0.7V for 48 hours cycles*

Consequently, a linear regression approximation was applied, with a result of a quite poor fitting to a straight line of slope 1.794e-03 with $R^2$ = 0.795, as shown in the figure below (see Figure 3.79.). This plot presents a lot of noise and an important quantity of outliers specially at the beginning, which influence the results.

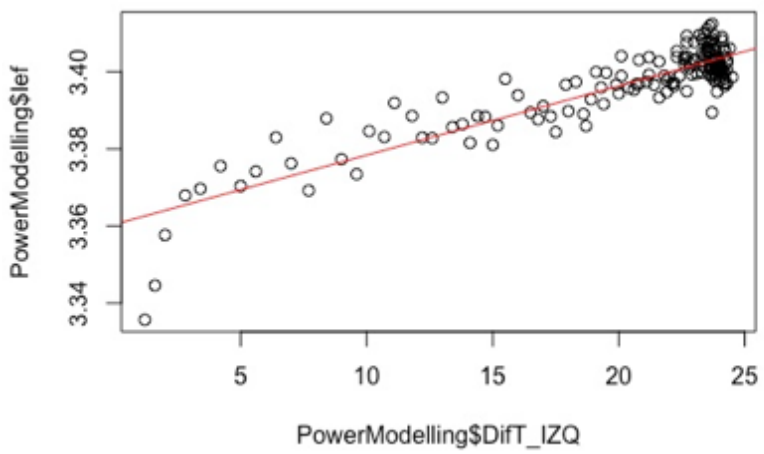


*Figure 4.79 Linear regression of the Differential Temperature developed at the left end against the Current Intensity*

Checking the residuals of the model, it was observed that, even though the linearity function fitted quite well and the errors presented a pronounced normal distribution, the presence of some big leverage for some residuals worsened the results of the regression. This can be observed in the set of plots below (see Figure 4.80.).

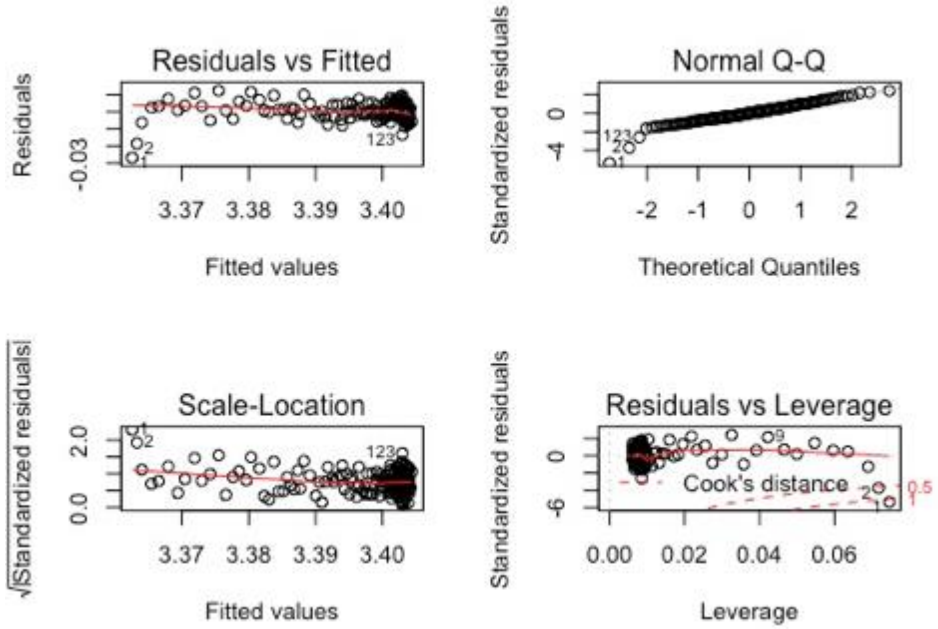


*Figure 4.80 Plots of the residuals and analysis of the Linear regression from experimental data of Differential Temperature and Current Intensity*

In order to improve the model of this data set, a "polifit" coding of Matlab was used, in order to evaluate its tendency with a polynomial function, recording an improvement of the $R^2$ accuracy coefficient up to 0.89 for a polynomial function of

degree 15, presented in the figure below, for both measurement locations along the sample (see Figure 4.81.).

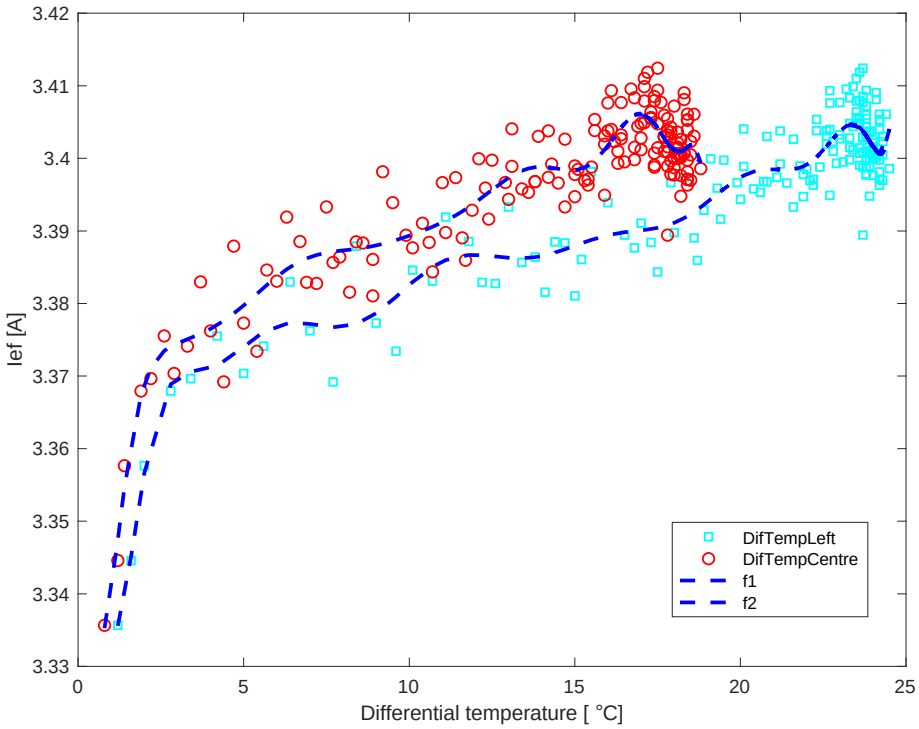


*Figure 4.81 Polynomial approximation of the Differential temperature against the Current Intensity experimental data from PA-MF at 0.7V for 48 hours*

Even thought, the modelling of the correlation between these two magnitudes did not provide many new information, we realised that when the intensity is kept constant, which would be the pursued objective, the temperature differential kips increasing gradually until reaching the thermal equilibrium, without requiring an increase of the electrical power supplied. Whereas, when the intensity decreases, the differential pf temperature stalls its increasing trend and reaches an intermediate plateau before reaching the thermal equilibrium and, if the decrease of intensity continues, the temperature differential and the temperature recordings start to decrease.

## 4.3. ANALYSIS AND CONCLUSIONS OF THE EXPERIMENTAL CAMPAIGN

Along this chapter, the results from the experimental campaign produced aiming at characterising conductive concrete samples with addition of recycled carbon fibre have been presented. Even though there are references to all kinds of characterizations, the research has mainly focused on the thermal characterization, although some other complementary studies were needed, such as conductivity and impedance

characterizations or consistency analysis, in order to understand properly the development of thermal properties and the effect of the carbon fibre addition to the UHPC concrete matrix.

The test series carried out evaluated on the one hand, the variation in content and nature of the carbonaceous material additions – MF and MAF –, looking for the most performant combination. On the other hand, the variation in thermal measurements between two different types of electrodes disposals – A and B – and, even, between two different types of sample geometries, with a heating test series performed using prismatic beam samples.

One of the main conclusions that obtained from the analysis of the results is that in most of the tests the MF dosage has performed much better than the MAF dosage, reaching higher temperature variations and overall temperature recordings and requiring lower excitation voltages than MAF.

In such a manner, the heat production of MF materials was significantly higher, such that for the same Vexcit values the MF materials reached much higher temperatures than MAF, even in some cases doubling the results.

Regarding the different carbonaceous addition materials, the CarbisoTM CT6/12 have a very remarkable performance, both for electrical properties, developing a significant increase in conductivity already for low content, such as the one used in this case of 0.5% just below percolation, and for thermal properties, generating large temperature differentials. Whereas, unlike the chopped recycled carbon fibre, the micronized carbon fibre consisting in very small natural graphite flakes did not develop rather small electrical conductivity recordings, and was determinant in the low thermal variations recorded for MAF materials, being the only difference between both types of conductive cement-based materials.

Nevertheless, it is important to remark that some aspects of the heating system should be improved, in order to provide a more homogeneous temperature distribution along the whole concrete element, avoiding the generation of temperature differentials between the centre of the samples and the ends, where the power inlet and outlet are located. This could be reduced improving the contact between the electrodes and the carbon fibres inside the specimen, avoiding the generation of areas with higher resistivity.

However, with regards to the overall results from heat production with a conductive concrete by means of the Joule effect, very significant temperature recordings have been achieved, which confirmed the possibility of using this material

for self-heating systems embedded to buildings or de-icing systems for outdoor urban furniture and concrete pavements, for cold environments.

# 5. CONCLUSIONS

After wide bibliographic research performed in this project, it can be observed that there is a very clear interest in the development of this type of materials. It evinces the possibility of developing a wide range of applications, that are emerging as promising solutions to problems that, nowadays, have either no solution or very inefficient solutions, such as the current snow removal technics in infrastructures.

With this research project, the addition of recycled carbon fibres as an alternative for the development of conductive concrete has been confirmed to be successful, with very satisfactory results.

From the production of different sets of tests using different dosages, it has been concluded that many factors influence the development of electrical and thermal conductivity, not only the conductive material addition, but also the homogeneity of the fibre's disposal throughout the concrete element, the electrodes disposal, the granular skeleton, the moisture content.

High conductivities up to 2 S/m were reached with high frequencies and relatively low voltages, for additions of conductive carbonaceous materials just below the percolation threshold. Furthermore, the correlation between impedance, conductivity and phase with respect to the frequency were modelled using power, logarithmic and polynomial laws, respectively, contributing to a better understanding of the relation between these magnitudes and their evolution for different voltages and frequencies.

The thermal behaviour test series revealed that the dosage of a relatively low percentage in volume of chopped carbon fibres of 0.4-0.5% vol. around the percolation threshold mixed with a UHPC is able to develop very significant temperature variations, confirming the possibility of using this material for self-heating systems embedded in buildings or de-icing systems for outdoor urban furniture and concrete pavements, for cold environments.

Furthermore, this project has introduced an added value in terms of sustainability by using recycled carbon fibre from industrial residues as an addition. This improved the economic viability of the material and reduced the environmental impact.

However, there are a few negative aspects that need to be reviewed and considered for further researches. The addition of micronized carbon fibre did not provide the expected results in terms of electrical and thermal behaviour. The electrical

conductivity developed by the samples containing this material were rather small compared to other types of carbonaceous conductive admixtures. But when it comes to the heat production, the temperature variations recorded for the MAF samples were much lower than only using chopped carbon fibre and, in some cases, bizarre phenomena related with temperature halts and drops related to intensity drops could be observed.

Aside from that, the heating tests revealed a pattern that indicated a heterogeneity of the temperature distribution throughout the samples, observable in nearly all the tests. This resulted in large temperature differences between the left end and the centre of the samples, which limits the performance of the heating system for these concrete elements. This might be generated by a deficiency on the connection between the electrodes and the conductive fibre, creating differential areas along the sample with much more impedance than in others.

After the research performed in this final bachelor research project, future investigations can be developed, such as:

- Carrying out an analysis of the conductive concrete elements by means of x-rays or other alternative methods, in order to verify the proper dispersal and uniformity of fibres through the cementitious matrix.

- Study new methods of manufacturing of conductive concrete samples more reliable, avoiding unequal fibre dispersions.

- Development of prototypes of urban furniture elements using the material developed in this research as an application to reality, suitable for the industrial scale production.

- Development of a self-sensing conductive concrete applied to structural health monitoring systems, creating a program that could transform the changes in resistivity into useful data, that could be ran through a software to work with it, having a fully integrated maintenance system of a structure.

# 6. BIBLIOGRAPHY


[1] T. M. W.-D. M. A. i. t. U.S, "The Weather Channel", 2018. [Online]. Available: https://weather.com/travel/news/2018-11-19-most-weather-delayed-major-us-airports.

[2] O. B. L. B. F. J. C. J. G. P. Galao, "Highly Conductive Carbon Fiber Reinforced Concrete for Icing Prevention and Curing", 2016.

[3] J. X. L. &. Z. Q. Zhang, "Investigation of carbon fillers modified electrically conductive concrete as grounding electrodes for transmission towers : Computational model and case study", *Construction and building materials,* no. 145, p. 347–353., 2017.

[4] A. A. A. C. H. K. S. S. S. M. S. G. K. …. A. H. Sassani, "Carbon fiber-based electrically conductive concrete for salt-free deicing of pavements", *Journal of cleaner production,* 2018.

[5] Q. Y. Y. C. W. C. T. Z. Y. &. L. H. Zhang, "Outdoor experiment of fl exible sandwiched graphite-PET sheets based self-snow-thawing pavement", *Cold Regions Science and Technology ,* vol. 122, pp. 10-17, 2016.

[6] Y. L. Y. &. M. D. Lai, "Automatically melting snow on airport cement concrete pavement with carbon fiber grille", *Cold Regions Science and Technology,* vol. 103, pp. 57-62, 2014.

[7] C. C. Q. F. H. &. C. J. Wang, "Heat conduction effect of steel bridge deck with conductive gussasphalt concrete pavement", *Construction and Building Materials,* vol. 172, pp. 422-432, 2018.

[8] M. W. S. W. H. &. Z. J. Chen, "Solar Energy Materials & Solar Cells Study of ice and snow melting process on conductive asphalt solar collector", *Solar Energy Materials and Solar Cells,* vol. 95, no. 12, pp. 3241-3250, 2011.

[9] Y. C. W. C. B. &. T. R. Bai, " Research on Electrically Conductive Concrete with Double- Layered Stainless Steel Fibers for Pavement Deicing", *ACI Materials Journal,* no. 114, pp. 935-944, 2017.

[10] J. G. O. G. V. Z. E. &. G. P. Gomis, " Self-heating and deicing conductive cement . Experimental study and modeling", *Construction and Building Materials,* no. 75, p. 442–449., 2015.

[11] T. V. D. H. M. &. H. M. Neumann, "Carbon fibre reinforced cement-based composites as smart floor heating materials", *Composites part B,* vol. 90, pp. 465-470, 2016.

[12] J. L. J. &. Y. F. Wu, "Three-phase composite conductive concrete for pavement deicing", *Construction and building materials,* vol. 75, pp. 129-135, 2015.

[13] C. DDL, Electrically conductive cement-based materials. Multifuctional cement-based materials, New York: Marcel Dekker Inc, 2004.

[14] R. T. C. L. B. &. X. A. Zhao, "Radiant heating utilizing conductive concrete tiles", *Building and Environment,* 2018.

[15] C. M. G. P. Pérez A, "Electromechanical Extraction of chlorides from reinforced concrete using a conductive cement paste as an anode", *Corrosion Science,* no. 52, pp. 1576-81, 2010.

[16] G. O. A. C. C. M. G. P. del Moral B, "Usability of cement paste containing nanofibres as an anode in electrochemical chloride extraction from concrete", *Materiales de construcción,* no. 63, pp. 39-48, 2013.

[17] G. O. Z. E. G. P. Baeza FJ, "Multifunctional cement composites strain and damage sensors applied on reinforced concrete (RC) structural elements", *Materials,* no. 6, pp. 841-55, 2013.

[18] G. Z. H. Y. Z. T. Wang B, "Electromagnetic wave absorbing properties of multi-walled carbon nanotube/cement composites", *Construction and building materials,* no. 46, pp. 98-103, 2013.

[19] L. R. Z. M. L. W. Sun M, "Development of the cement-based strain sensor for health monitoring of ultra high strength comcrete", *Construction and building materials,* no. 65, pp. 630-7, 2014.

[20] U. F. D. A. Materazzi A, "Carbon nanotube cement-based transducers for dynamic sensing of strain", *Cementitious concrete composites,* no. 37, pp. 2-11, 2013.

[21] E. O. A. B. P. R. K. M. Heymsfield, "Feasibility of Anti-Icing Airfield Pavements Using Conductive Concrete and Renewable Solar Energy", 2013.

[22] Z. E. A. E. G. O. A. L. Garcés P, "Mechanical properties and corrosion of CAC mortars with carbon fibers", *Construction and building materials,* vol. 34, pp. 91-96, 2012.

[23] Z. E. B. F. B. A. G. P. Galao O, "Effect of carbon nanofiber addition in the mechanical properties and durability of cementitious materials", *Materiales de construcción,* vol. 62, pp. 343-357, 2012.

[24] T. Y. N. &. E. A. B. Manzur, "Effect of Carbon Nanotube Size on Compressive Strengths of Nanotube Reinforced Cementitious Composites", *Journal of Materials,* 2014.

[25] A. A. A. D. U. F. K. S. L. S. &. S. C. Downey, " Novel nanocomposite technologies for dynamic monitoring of structures : a comparison between cement-based embeddable and soft elastomeric surface sensors", *Smart materials and structure,* vol. 23, 2014.

[26] X. &. H. H. Tian, "Test and Study on Electrical Property of Conductive Concrete", *Procedia Earth and Planetary Science,* vol. 5, pp. 83-87, 2012.

[27] L. L. Y. &. B. Y. Shi, "Mechanical and electrical characterisation of steel fiber and carbon black engineered cementitious composites", *ScienceDirect ,* vol. 188, pp. 325-332, 2017.

[28] B. &. Z. L. Han, Smart and Multifunctional Concrete Toward Sustainable Infrastructures, Singapore: Springer, 2017.

[29] A. S. E.-g. M. A. A.-r. M. A. H. S. E. &. N. A. El-dieb, "Multifunctional electrically conductive concrete using different fillers", *Journal of Building and Engineering,* 2017.

[30] A. C. H. K. S. G. K. A. A. &. T. P. C. Sassani, " Influence of mix design variables on engineering properties of carbon fiber-modified electrically conductive concrete", *Construction and building materials,* vol. 152, 2017.

[31] B. L. B. G. Y. L. T. L. Z. &. L. Z. Chen, "Investigation on electrically conductive aggregates produced by incorporating carbon fiber and carbon black", *Construction and building materials,* vol. 144, pp. 106-114, 2017.

[32] G. M. N. F. K. H. K. &. L. H. K. Kim, "Heating and heat-dependent mechanical characteristics of CNT-embedded cementitious composites", *Composite Structures,* vol. 136, pp. 162-170, 2016.

[33] W. Y. X. G. M. &. C. L. Yu, "State of the art and practice of pavement anti-icing and de-icing techniques", *Sciences in Cold and Arid Regions,* vol. 6, no. 1, pp. 14-21, 2014.

[34] X. Y. S. L. L. &. B. D. Jianchao, "Experimental study on the electrothermal effect of concrete reinforced with hybrid carbon and steel fiber", *Applied Mechanics and Materials,* vol. 491, pp. 94-98, 2014.

[35] R. W. H. W. H. T. C. Y. &. Y. M. Rao, "Models for estimating the thermal properties of electric heating concrete containing steel fiber and graphite", *Composites Part B,* 2018.

[36] Z. Hou, Z. LI and J. Wang, "Electrically Conductive Concrete for Heating Using Steel Bars as Electrodes", *Journal of Wuhan University of Technology-Mater,* no. June, 2010.

[37] W. Y. J. Xu, "Current distribution in reinforced concrete cathodic protection system with conductive mortar overlay anode", *Construction and building materials,* vol. 23, no. 6, p. 2220–2226, 2009.

[38] R. Polder, "Electrochemical techniques for corrosion protection and maintenance", *Corrosion in Reinforced Concrete Structures*, Cambridge, Woodhead Publishing, 2005, p. 215–241.

[39] L. Westhof, "Field experience with a conductive cement-based composite as anode for the cathodic protection of reinforced concrete structures" , *Proceedings of the 2nd International Conference on Concrete Solutions*, Watford, 2006.

[40] S. e. w.-a. c. b. o. l.-s. g. a. c. n. films, "www.nature.com/scientificrepots" 2017. [Online]. Available: https://www.ncbi.nlm.nih.gov/pmc/articles/PMC5443822/.

[41] K. E. YU X., "Carbon Nanotube Based Self-sensing Concrete for Pavement Structural Health Monitoring", University of Minnesota Duluth for U.S. Departmen of Transportation, 2012.

[42] C. Y. X. L. Q. G. T. J. T. Wang, "Preparation and performance of conductive gussasphalt concrete", *Transportmetrica A: Transport Science,* vol. 15, no. 1, pp. 55-70, 2019.

[43] W. C. B. C. R. T. Ying-hua Bai, "Research on Electrically Conductive Concrete with Double-Layered Stainless Steel Fibers for Pavement Deicing", *ACI Materials Journal,* no. 114, pp. 935-944, 2017.

[44] L. H. Zhang Q, "Experimental investigation of road snow-melting based on CNFP self-heating concrete", *Behaviour and Mechanics of Multifunctional Materials and Composites,* March 2011.

[45] H. W. Z. W. S. Z. J. C. G. Zhao, "Concrete pavement deicing with carbon fi ber heating wires", *Cold Regions Science and Technology,* vol. 65, p. 413–420, 2011.

[46] C. F. &. L. C. &. A. Kline, " Snowplow operator driving time: survey of state and local practices : final report", 2016.

[47] H. R. S. H. t. E. from, "blogs.ei.columbia.edu", 2018. [Online]. Available: https://blogs.ei.columbia.edu/2018/12/11/road-salt-harms-environment/.

[48] J. G. P. Alcaide, "Caracterización de morteros con adición o sustitución de diferentes materiales carbonosos", 2007.

[49] X. Huang, "Fabrication and Properties of Carbon Fibers", *Materials,* 2009.

[50] I. Diéguez, "Fibra de carbón", 2012.

[51] S. Pickering, "Recycling technologies for thermoset composite-current status", *Composites: Part A 37,* pp. 1206-1215, 2006.

[52] G. Gardiner, "Recycled carbon fiber: Comparing cost and properties", *Composites Technology,* 2014.

[53] S. Pimienta, "Recycling carbon fibre reinforced polymers for structural applications: technology review and market outlook", *Waste Management ,* 2011.

[54] D. CHUNG, "Carbon materials for structural self-sensing, electromagnetic shielding and termal interfacing", *Carbon,* vol. 50, pp. 3342-3353, 2012.

[55] O. Galao, "Matrices cementicias multifuncionales mediante adición de nanofibras de carbono" Departamento de Ingenieria de la Constrcción, Obras Públicas e Infraestructura Urbana. Universitat d'Alacant , Alicante, 2012.

[56] L. A. Z. H. Y. D. Q. H. S. LU, "Expermimental study on conductive asphalt concrete using steel slag as aggregate", in *1st International Conference on Microstructure Related Durability of Cementitious Composites*, Nanjing, China, 2008.

[57] C. Tuan, "De-icing technology", *Concrete,* vol. 50, no. 6, pp. 46-49, 2016.

[58] s. Wen and D. Chung, "Double percolation in the electrical conduction in carbon fibre reinforced cement-based materials", *Carbon 45,* pp. 263-267, 2007.

[59] C. P. d. Hormigón, "Anejo 14: Hormigón con fibras. Nueva versión de la Instrucción de Hormigón Estructural (EHE). Borrador 0", 2007.

[60] M. C. G. C. D. M. F. &. A. M. A. Leone, "Fiber-reinforced concrete with low content of recycled steel fiber : Shear behaviour", *Construction and Building Materials,* vol. 161, pp. 141-155, 2018.